EFFECTS OF INTERFACIAL STRUCTURE ON FILM CONDENSATION

by

James John Barry

A thesis submitted in partial fulfillment of
the requirements for the degree of

DOCTOR OF PHILOSOPHY
(Nuclear Engineering & Engineering Physics)

at the
University of Wisconsin-Madison
1987

EFFECTS OF INTERFACIAL STRUCTURE ON FILM CONDENSATION

by

James John Barry

A thesis submitted in partial fulfillment of
the requirements for the degree of

DOCTOR OF PHILOSOPHY
(Nuclear Engineering & Engineering Physics)

at the
University of Wisconsin-Madison
1987

A B S T R A C T

EFFECTS OF INTERFACIAL STRUCTURE
ON FILM CONDENSATION

James John Barry

Under the supervision of Professor Michael L. Corradini

Film condensation in the presence of a noncondensable gas is expected to be strongly affected by the presence of interfacial structure. An experimental program was undertaken to simultaneously measure a set of parameters for the interfacial waves and the condensation heat transfer coefficient. Experiments were performed in a square test section 100 mm by 100 mm and 1.83 m long. The heat transfer surface was formed by the last 610 mm of the bottom wall. Mass ratios of air to steam could be varied from about 1 to 15. Water films could also be injected to simulate thicker films.

An isothermal air-water series was conducted in which air was blown over a flowing film. The experimental techniques for wave characterization were developed during these tests. Film thickness and wave amplitude, frequency, and celerity were measured. Wavelengths were computed using the measured values. There was good agreement with those observed visually.

Two sets of heated tests were conducted. The first set utilized an injected film. Film and wave parameters were measured using the methods developed in the isothermal runs. The data showed an apparent suppression of the waves by the bulk flow of steam to the interface as was anticipated. Heat transfer data were also taken but were marred by problems with heat balance corrections for the injected film. The second set of heated tests did not use an injected film. Wave parameters were not measured, but visual observations were noted. Heat transfer coefficients compared well with the results of the previously developed theoretical model of M. H. Kim.

A C K N O W L E D G E M E N T

I would like express my sincere thanks to my advisor, Prof. Michael Corradini for his support and encouragement throughout the course of this work. His patience during the lengthy construction period was greatly appreciated.

I would also like to thank Dr. M. H. Kim for laying so much of the groundwork for this research and for the use of his CWNG code. A special thanks to go to Dr. Faustino Gonzalez and Dr. Timothy Bartel for their advice, computing expertise, and friendship.

The advice and machining skill of Mr. Sol Walsh were greatly appreciated. The construction of the apparatus would have been impossible without him. Thanks are also due to Mr. Steve Matesuwic for his assistance with plumbing and his seemingly limitless supply of distilled water.

I would also like to express my heartfelt appreciation to my wife, Libby, for her love, sacrifice, and constant support. I also cannot thank my parents enough for the love and support they have given me.

I gratefully acknowledge the financial support provided by the Westinghouse Electric Corporation. This research was performed under appointment to the Nuclear Engineering and Health Physics Fellowship program administered by Oak Ridge Associated Universities for the U.S. Department of Energy.

TABLE OF CONTENTS

L I S T O F T A B L E S

L I S T O F F I G U R E S

N O M E N C L A T U R E

a	:	constant in hot-wire curve fit
A	:	wave amplitude
A_p	:	area of heat transfer plate
A_{ts}	:	cross sectional area of test section
b	:	constant in hot-wire curve fit
c	:	celerity
C	:	tabulated orifice coefficient
C_p	:	specific heat
d	:	diameter of orifice
D	:	diameter of pipe (orifice meter)
E	:	hot-wire anemometer bridge voltage
f	:	fraction of time boiler heaters are on
f_{avg}	:	spectrum average frequency
f_{peak}	:	frequency of spectrum peak
f_{obs}	:	observed wave frequency
f_{true}	:	true wave frequency
f_{wave}	:	wave frequency
g	:	gravitational acceleration
h_{avg}	:	average heat transfer coefficient (from CWNG code)
h_{cool}	:	heat transfer coefficient from coolant to the back of heat transfer plate
h_{mean}	:	mean heat transfer coefficient (from

heat flux meters)

$h_{overall}$: overall average heat transfer coefficient over heat transfer plate (from coolant measurements)

i_s : enthalpy of steam

i_{vap} : heat of vaporization

k : thermal conductivity of aluminum plate

K : constant in orifice flowmeter fit

m : mass flow rate of film

m_a : mass flow rate of air

m_s : mass flow rate of steam

n : power in hot-wire calibration curve

N_s : number of samples

N_w : number of waves

OHR : hot-wire overheat ratio

P : boiler power

P_{boil} : boiler pressure

P_c : probability of contact

P_{crest} : probability of contact corresponding to crest of wave

P_s : partial pressure of steam in test section

$P_{preheat}$: preheater power

P_{tot} : total pressure (atmospheric)

P_{trough} : probability of contact corresponding to trough of wave

q	:	heat flux (without film if there is one)
q_{film}	:	heat flux (including film)
$q_{overall}$	:	overall heat flux (average over surface of plate)
Q_{cool}	:	volume flow rate of coolant
Q_{film}	:	volume flow rate of film
R	:	mass ratio (air/steam)
R_{cold}	:	cold resistance of hot-wire sensor
Re_f	:	Reynolds number of the film (based on δ)
Re_g	:	effective Reynolds number of the gas for comparison to duct flows
R_{op}	:	operating resistance of hot-wire sensor
T_{back}	:	temperature of back surface of heat transfer plate
$T_{exhaust}$	:	temperature of film at exhaust
T_{inlet}	:	temperature of film at inlet
T_{mix}	:	temperature of air-steam mixture
T_{sink}	:	temperature of coolant (heat sink)
T_{stm}	:	temperature of steam at orifice
T_{surf}	:	temperature of front surface of heat transfer plate
v	:	velocity in hot-wire calibration curve
v_{app}	:	apparent velocity of waves (with respect to stationary observer)
v_{film}	:	average velocity of film

v_g : air-steam mixture velocity

v_{hi} : high mixture velocity computed based on boiler timing

v_{lo} : low mixture velocity computed based on boiler timing

v_{orif} : mixture velocity computed from orifice measurements of steam flow

v_{pitot} : mixture velocity computed from Pitot tube measurements

v_{rel} : relative velocity of waves with respect to film

W : width of test section

x : distance from leading edge of plate

y : height above heat transfer plate

β : diameter ratio of orifice meter (d/D)

δ : film thickness

Δi : enthalpy change from feedwater to saturation

Δp_{orif} : pressure difference across orifice

Δp_{pitot} : Pitot tube pressure difference

Δt : delay time between wave crossings of sensors in wave speed measurement

Δt_s : sampling interval

ΔT_{film} : film temperature change across plate

ΔT_{hfm} : temperature difference across thermocouples in heat flux meter

ΔT_{cool}	:	temperature difference across coolant manifolds
Δx	:	separation distance of celerity sensors
Δx_{hfm}	:	thermocouple separation distance in heat flux meter
λ	:	wavelength
λ_c	:	critical Taylor wavelength
ρ	:	auto or cross correlation coefficient
ρ_a	:	density of air in test section
ρ_g	:	density of saturated steam
ρ_l	:	density of saturated water
ρ_{mix}	:	density of air-steam mixture
ρ_s	:	density of steam in test section
ρ_{stm}	:	density of steam at orifice
σ	:	surface tension
σ_A	:	error (standard deviation) in A
θ	:	angle of inclination of test section

1. INTRODUCTION

Condensation heat transfer has been the subject of both theoretical and experimental research for over 50 years. During this time considerable progress has been made in understanding many of the mechanisms and in developing models for prediction of heat transfer coefficients. Most of this work has been centered on condensation processes occurring under conditions similar to those found in steam condensers in thermal power plants. These are typically conditions in which steam containing small concentrations of noncondensable gas (usually air) flows over banks of small horizontal tubes at low (partial vacuum) pressures. The dominant mode of condensation is normally film condensation.

A very different set of conditions have been identified in post-accident studies of nuclear reactor containment performance. Following a loss-of-coolant-accident (LOCA), the containment atmosphere will be primarily made up of large quantities of both steam and air. In addition to the active systems, such as containment sprays, there are passive mechanisms, such as condensation onto cold walls and structures, which can reduce the pressure rise. This condensation occurs under condi-

tions of large concentrations of noncondensable gas, large surface areas, and relatively large total pressures. Some experiments in this regime have been attempted, but these have been primarily integral experiments aimed at overall containment behavior rather than at the separate effects that govern the fundamentals of the heat and mass transfer characteristics.

One important factor in determining the condensation rate is the structure of waves which occur on the condensate film. In pure vapor condensation, the film provides essentially the entire heat transfer resistance. Hence, turbulence or mixing in the film due to interfacial structure strongly affects the heat transfer coefficient. This same effect is also expected to be present in condensation in the presence of a noncondensable gas, but the interfacial structure also affects the heat transfer rate by another mechanism. In condensation in the presence of a noncondensable gas, the primary resistance to heat transfer is located in the gas/vapor boundary layer along the film surface. This is because condensation becomes a gaseous diffusion-limited process in this case. Interfacial structure may cause mixing and/or turbulence in the gas/vapor boundary layer as well as in the film. The effect of interfacial structure on heat transfer is therefore important again.

The purpose of the present research was to investigate the structure of the interface and its effects on the condensation rate. An experimental program was undertaken to couple interfacial structure characterization with heat transfer measurements. By directly observing the effects of interfacial structure on the heat transfer coefficient in film condensation, a more complete understanding of the fluid mechanics and heat transfer phenomenon could be gained.

In order to observe the interfacial effects, a set of measurement techniques was required. Previously investigators have primarily used electrical conductivity and light transmission methods to quantify the interfacial structure in isothermal air-water flows. These methods were not suitable for use with simultaneous heat transfer, so a different methodology was needed. The use of thermal anemometry in the recent work of Akai et al. [1,2] was identified as a promising starting point. The development of these measurement techniques was begun with a set of isothermal air-water tests. Using isothermal tests was not only more straightforward than using heated tests, it also allowed direct comparison to the data in the literature.

The heated tests using air/steam flows were then undertaken. Two sets of tests were done here. The first

set utilized an injected film. The measurement of the interfacial structure was accomplished using the methods developed in the isothermal tests. The second set of tests did not use an injected film. In this case the condensate films generated were too thin to measure using the hot-wire anemometry techniques. The heat transfer results were, however, quite useful since they were obtained under known, controlled conditions of large concentrations of noncondensable gas. Direct comparison could also be made to the CWNG code developed previously [3] in this research group.

The remainder of this thesis is organized in the following way. Chapter 2 contains a survey of the previously published literature on condensation and on interfacial structure measurement. The experimental apparatus and facilities are described in Chapter 3. Results of the testing of these facilities and equipment is discussed in Chapter 4. Chapter 5 reviews the isothermal tests and development of the interfacial wave measurement methods. The heated test series both with and without film injection are presented in Chapter 6. Finally Chapter 7 delivers conclusions and suggestions for further research.

2. LITERATURE SURVEY

2.1 INTRODUCTION

There are a variety of parameters affecting the condensation heat transfer rate. These include the vapor being condensed, the mode of condensation, the molecular weight and properties of the noncondensable gas, the noncondensable gas concentration, the Reynolds numbers of the gas/vapor bulk flow and the liquid film, and the absolute pressure. A large body of literature has been devoted to measuring and predicting the effects of these parameters. A complete review is, therefore, be attempted and the following survey is limited to the works that apply directly to the current research.

Previous work on condensation heat transfer may be categorized according to the parameters listed above. The two common modes of surface condensation are dropwise and filmwise. In dropwise condensation, the vapor does not form a continuous film but flows on the surface as individual droplets. This is a highly efficient method of heat transfer, but requires care to achieve and maintain because at high condensation rates the droplets tend to coalesce and form a film. This is then called filmwise condensation. A heat transfer resistance is caused by the

film and usually increases with film thickness. The majority of experimental and theoretical work has dealt with film condensation since it is the more common phenomenon and is generally more amenable to analysis. This work will also deal with filmwise condensation.

The most common vapor-noncondensable gas system treated by previous authors is the steam-air system. This system has been selected since it is the one which is commonly encountered in applications and because it is a convenient one to work with experimentally. This is also the system which will be considered in the present research.

Another large and separate body of work in two-phase flow deals with the interfacial characteristics of stratified two-phase gas-liquid flows. At low Reynolds numbers of the gas and liquid phases the interface remains smooth and unrippled, but at sufficiently high values of the Reynolds numbers of the phases, ripples and waves appear. The transition is marked by a large increase in the pressure drop and heat and mass transfer coefficients of the flow. As the object of the current investigation is to investigate the effects of interfacial structure on condensation heat transfer, literature pertinent to the study of interfacial structure and its effects will also be reviewed.

2.2 EXPERIMENTAL WORK IN CONDENSATION

2.2.1 Natural Convection - Pure Vapor.

The condensation of a pure vapor in natural convection has been studied extensively by many authors over a great number of years. Their results were usually compared to the predictions of Nusselt's classic analytical solution (see section 2.3.1), but often with rather poor results [4]. These differences can be attributed to several problems in their experimental methods:

1) significant forced convection,
2) presence of noncondensable gas,
3) waves, ripples, or turbulence in the condensate film,
4) departure from filmwise condensation mode.

Recently, however, several investigators [5-7] have achieved results which agree well with the Nusselt theory by taking special care to avoid the presence of the above effects.

2.2.2 Forced Convection - Pure Vapor.

The effect of vapor velocity on pure vapor condensation heat transfer has been studied extensively. Large vapor velocities cause the condensate film to become thinner due to the large interfacial shear stress and also

cause the film to develop interfacial structure (waves) and to become turbulent. As the film represents essentially the entire heat transfer resistance, the heat transfer coefficient is increased substantially. Much of this work has dealt with the case of flow over a horizontal tube or a bank of horizontal tubes [8-11]. This geometry is, of course, selected due to its use in condensing equipment in industrial situations. Condensation of methanol and acetone was done in a horizontal tube by Rosson and Myers [12]. The data were correlated as a function of angle with limited success. Goodykoontz and Dorsch [13,14] have run experiments in flow condensation in tubes at high vapor velocities.

Several experiments have also been conducted on the ubiquitous vertical flat plate [15-18]. The results of these experiments are, in general, fairly well correlated by their authors' own models. Choi's [19] experiment on condensation within vertical tubes used strong electric fields to induce surface instabilities. The presence of these instabilities or waves increased the heat transfer significantly.

Another grouping of experiments has dealt with condensation onto subcooled liquids with an adiabatic wall condition. Experiments by Linehan, Petrick, and El-Wakil [20] and Lim, Tankin, and Yuen [21] have dealt with cocur-

rent steam-water flows in flat plate geometries. M. Takahashi et al. [22] have recently investigated condensation heat transfer to the free surface of a developing turbulent film in an inclined channel. Segev, Flanigan, Kurth, and Collier [23] have investigated countercurrent steam-water flows in flat plate geometries. Kim and Bankoff [24,25] have also conducted countercurrent experiments in planar apparatus. Condensation of quiescent steam onto various turbulent pools has been observed by Thomas [26].

2.2.3 Natural Convection - Vapor with Noncondensable Gas.

The case of natural convection condensation of a vapor in the presence of a noncondensable gas has also been extensively investigated over a period of many years. The presence of a noncondensable gas significantly reduces the heat transfer coefficient by the following mechanism. As steam condenses at the interface with the condensate film, the noncondensable gas concentration in the vicinity of the interface increases. The presence of this layer of noncondensable gas poses a resistance to the diffusion of steam to the interface and hence reduces the heat transfer coefficient. This is illustrated in Figure 2.1.

Research into this regime began with Othmer [8] and continued with the work of Meisenburg et al. [27] and

Akers and Crawford [28]. Theoretical studies were also undertaken by a number of investigators. Unfortunately the above experiments failed to correlate well with the theoretical results. This is thought to be due primarily due to significant forced convection effects. The condensation of a vapor with a noncondensable gas is very sensitive to forced convection effects since gas may be swept away from the interface. This reduction in the concentration of noncondensable gas at the interface reduces the heat transfer resistance afforded by the gas-rich layer. Consequently, one would expect that in experiments where special care was not taken to preclude forced convection that heat transfer coefficients would be larger than expected. This is exactly the case in the above experiments.

Several more recent experiments have been conducted in which special care was taken to eliminate forced convection. The experiments of Mills and Seban [5] and Slegers and Seban [6] were only partially successful at reducing forced convection, but the experiments of Al-Diwany and Rose [7] enjoyed greater success and their results correlate well with theoretical models. This outcome indicates that forced convection effects were the culprit in the earlier investigations as previously thought.

DeVuono and Christensen [29] completed experiments in

which they correlated the condensation rate with the total pressure. They found a small but significant pressure dependence, but their correlation did not agree with previous data. This was thought to be due to the significantly higher pressures used in their work.

2.2.4 Forced Convection - Vapor with Noncondensable Gas.

The presence of forced convection significantly reduces the deleterious effects of a noncondensable gas on the condensation heat transfer coefficient. The majority of experiments in forced convection gas/vapor condensation have been done with horizontal tube or tube bank geometries. In experimental studies of condensation in the presence of a noncondensable gas on a horizontal (or nearly horizontal) tube, Othmer [8] and Henderson and Marchello [30] did not measure the velocities of the bulk gas/vapor flow and hence their results are of limited benefit in forced flow situations. Rauscher, Mills, and Denny [9] also conducted their experiments over a horizontal tube at relatively low but measured velocities. Their pure steam results were in excellent agreement with a theory for a horizontal tube which includes a vapor drag correction as well as with the Nusselt horizontal tube theory. The data obtained in air-steam runs agreed favorably with the theoretical analysis of Denny and South

[31]. More recently, Lee and Rose [11] conducted experiments for forced convection film condensation on a horizontal tube with and without noncondensable gases. Their results for both pure vapor and gas/vapor flows agreed well with their own theory and with previous data.

Few experiments have been conducted to date in flat plate geometries. This is significant due to the important effect of the bulk flow pattern of gas/vapor on the heat transfer. Asano, Nakano, and Inaba [18] recently completed experiments in forced convection gas/vapor condensation on a vertical flat plate. Their test section is shown in Figure 2.2. Their results show significant scatter when compared to their theory. They note that this may be due to the size of the thermocouple they used relative to the size of the thermal boundary layer. The condition of the interface between the film and the gas/vapor was not reported, but in the range of Reynolds numbers in which data was taken, waves and interfacial structure would be expected. Turbulence in the film or gas/vapor boundary layer might also have occurred, but is not considered either. Both of these effects may have had an important influence on the heat transfer rate.

Dallmeyer [32] also reported results of forced convection gas/vapor condensation experiments. In this work, a mixture of air and carbon tetrachloride vapor were con-

densed on a vertical flat plate. The condensate film was removed from the plate surface by suction in order to prevent the film from becoming wavy or turbulent. At the same time the gas phase boundary layer was maintained in a fully turbulent condition. These experiments were well predicted by the analytical work of Jones and Renz [33].

2.3 THEORETICAL DEVELOPMENTS IN CONDENSATION

2.3.1 Stationary Pure Vapor.

The original classic analysis of pure vapor condensation was done by Nusselt [34]. His analytical solution required the following assumptions:

1) laminar flow of condensate film,
2) constant fluid properties,
3) subcooling of condensate neglected,
4) momentum changes through film neglected,
5) no shear stress at vapor interface,
6) heat transfer by conduction only.

The solution begins with a force balance on a fluid element which yields the velocity profile in the film. This is shown in Figure 2.3. This profile is integrated to give the total mass flow rate as a function of film thickness. The heat transfer is then calculated by simply

computing the conduction through the film. The complete analysis is shown in detail in many books (eg. Collier [35]) and will not be repeated here.

The Nusselt model has formed the starting point for many other analyses of condensation. Bromley [36] considered the effects of subcooling within the condensate film. Rohsenow [37] allowed for convective heat transfer within the film. Dukler [38,39] utilized a simple set of differential equations to describe condensation in vertical falling film systems.

Sparrow and Gregg [40] used similarity transformations of the boundary layer equations to treat the condensate film. Their method allowed them to include inertia forces and convection terms for the film in the analysis. Koh, Sparrow, and Hartnett [41] have also used a boundary layer treatment with similarity transformation. Their work included the effect of interfacial shear stress, but it should be noted that the bulk velocity of the vapor was still zero. Chen [42,43] also examined the effect of interfacial shear stress, but he used an integral boundary layer formulation. Poots and Miles [44] have used a boundary layer treatment to examine the effects of variable physical properties.

2.3.2 Moving Pure Vapor.

The bulk motion of the condensing vapor will create an added shear stress at the vapor-liquid interface which can have significant impact on the value of the condensation heat transfer coefficient. Rohsenow, Webber, and Ling [45] accounted for the effect of vapor shear using an integral method for both laminar and turbulent films. Cess [46] used a boundary layer approach to model the moving vapor case in the absence of a body force (eg. horizontal flow). He also neglected acceleration terms in the film and thermal convection effects in deriving his approximate solution. Shekriladze and Gomelauri [47] have used a similar approach to examine the effects of interfacial shear on the film. They have also computed solutions for flow over a horizontal tube.

Mayhew et. al. [15-17] have developed a simple theory to account for the drag of the vapor on the film. Their approach [15,16] is to use an interpolation of the two asymptotic situations: where the drag is due to vapor friction on the film only and where the drag is due to momentum transfer of the condensing vapor. In later work [17], an adjustable parameter was suggested to match the experimental data. South and Denny [48] also suggested an interpolation formulation for estimating the interfacial momentum transfer. Their results showed good agreement

for both flat plate and stagnation point flows.

Jacobs [49] developed integral solutions for combined body force and nonzero bulk vapor velocity conditions. His results show good agreement with previous work in both the body force only and vapor velocity only asymptotes. Significant errors (up to 17%) were shown to occur by neglecting either effect. Fujii and Uehara [50] used the method of Jacobs but corrected an erroneous boundary condition. Their results for free, forced, and mixed convection agreed with previous analysis and with experimental data within certain temperature difference and Nusselt number limits. The authors attribute discrepancies outside these limits to turbulence in the film.

Soliman, Schuster, and Berenson [51] present an analytical model for annular flow condensation in tubes which includes the effects of friction, momentum, and gravity terms. Agreement with available data is satisfactory.

2.3.3 Stationary Vapor with Noncondensable Gas.

The presence of a noncondensable gas significantly impairs the heat transfer in stationary gas/vapor conditions as was described in section 2.1.3. and as shown in Figure 2.1. Due to the coupled nature of the problem, a simultaneous solution of the mass, momentum, and energy

equations in both the condensate film and gas/vapor layer is generally required. Several treatments of this situation have been made.

Sparrow and Eckert [52] and Sparrow and Lin [53] used a similarity transformation to solve the conservation equations for the laminar case. Sparrow and Eckert considered only the drag of the stationary gas/vapor mixture while Sparrow and Lin also included the free convection effects associated with composition differences. Minkowycz and Sparrow [54] also included free convection associated with temperature differences. Superheating was found to be a significant effect. The additional effects of interfacial resistance, thermal diffusion, and property variation were found to be of second order importance.

Rose [55] developed an approximate integral method due to the computationally intensive nature of the methods of Sparrow et. al. [52-54]. Assumed velocity and concentration profiles are used and a simple model results which gives good results when compared to the results of Minkowycz and Sparrow [54].

2.3.4 Moving Vapor with a Noncondensable Gas.

The deleterious effect of a noncondensable gas on heat tranfer is mitigated by bulk motion of the gas/vapor mixture. This phenomenon has been studied by Sparrow,

Minkowycz, and Saddy [56] using a similarity transformation and the boundary layer equations. They neglected inertia and convection in the liquid film and assumed the streamwise velocity component to be zero at the interface in the computation of the gas/vapor layer velocity field. A reference temperature method was used to account for variable properties. Koh [57] and Fujii et. al. [58] also solved this problem but removed the assumptions of Sparrow et. al. except for uniform properties. Their results showed good agreement with the earlier work.

Denny, Mills, and Jusionis [59] and Denny and Jusionis [60] also considered forced convection condensation in the presence of a noncondensable gas. Numerical solution of the conservation equations was done without use of a similarity transformation. Variable properties in the film were treated using a reference temperature technique while those in the gas/vapor layer were treated exactly. Results for a variety of vapors, velocities, mass fractions of air, and temperatures were generated.

Jones and Renz [33] used Prandtl mixing length models and two-equation (k-ϵ) turbulence models to predict turbulent condensation of carbon tetrachloride/air mixtures on a vertical plate. More recently Renz and Odenthal [61] also used a k-ϵ turbulence model to predict condensation of the same mixtures. Both analyses compared their

results to the data of Dallmeyer [32] with good agreement. Renz and Odenthal [61] also note that comparisons become increasingly poor due to waves on the film which increase the gas/vapor layer turbulence level.

In conjunction with their experiments, Asano, Nakano, and Inaba [18] developed a model which treated the film and gas/vapor boundary layer separately. A Blasius type similarity transformation was used in the gas/vapor layer and the shear stress at the interface was assumed to be about the same as for a flat plate boundary layer. They showed results which compared well with the results of Denny et. al. [59].

Rose [62] devised an approximate method based on analogies to flow over a flat plate with suction. The model was designed to correct for the asymptotic cases of zero and infinite mass transfer rates. The results were compared with the more exact solutions of Sparrow et. al. [56], Koh [57], and Fujii et. al. [58]. The agreement is quite good. Lee and Rose [63] have discussed various methods for calculating the mass transfer resistance associated with the presence of a noncondensable gas.

More recently, Corradini [64] and Kim [3] have developed simple models for condensation in the presence of noncondensables. Their work is based on analogies between heat and mass transfer. Kim also has included

methods for modelling countercurrent flows, bulk flows not parallel to the condensing surface, and waves on the condensate film.

2.4 CONDENSATION IN A REACTOR CONTAINMENT BUILDING

One important application of studies of condensation in the presence of a noncondensable gas is that of condensation of steam on cold walls and structures following a postulated nuclear reactor accident. This particular application is somewhat unique due to the set of conditions which would be expected. Relatively long length steam runs agreed favorably with the theoretical analysis of scales of the order of metres or tens of metres would be involved. The concentration of noncondensable gas would be high with mass ratios (air/steam) ranging from 1 to 20 or more. This application is also characterized by pressures that range from 1 atmosphere up to a few atmospheres. Typical conditions in a process condenser, by way of contrast, are characterized by very low concentrations of noncondensables, relatively small length scales, and partial vacuum pressures. Length scales would be typically of the order of the size of the tubes or a few centimeters. The mass fraction of air in steam would be of the order of a few percent. Pressures of a tenth of

an atmosphere would be typical.

A number of research efforts over the years have been aimed at understanding condensation phenomena within a containment building due to the fact that other condensation literature was of questionable applicability. A very brief review of some of the specialized literature pertaining to condensation in containment buildings is warranted. It should be noted that condensation phenomena related to other aspects of nuclear reactor safety can be found in the review of Bankoff [65].

Experimental studies in containment condensation phenomena have, in general, been integral tests in geometries which attempt to approximate those of typical containment buildings. Jubb [66] used a large boiler as the containment vessel and used a second boiler to inject steam. The period in which steam was injected was thought to model the blowdown phase in which forced convection would be present and the period following injection would simulate the long term natural convection phase. The instrumentation and experimental facility were so extremely crude and the data so scattered that the utility of the results is negligible.

Koflat [67] also conducted experiments in which steam was injected into a large steel vessel. Unfortunately, the data was only reported as a heat transfer coefficient

as a function of time. These results also have no real use since no scaling relationship is known for extrapolating to a full size containment.

The results of Uchida [68] and Tagami [69] represent some of the most quoted data in containment analysis. Their experiments took place inside a large structure where an instrumented test surface was placed. The authors themselves note that applying their results to different scales and different geometries is on unknown theoretical ground.

The Carolinas Virginia Tube Reactor (CVTR) experiment [70] was a large integral test of an actual containment. Steam was injected into the building and heat transfer to the wall was measured. The measured heat transfer coefficients exceed those predicted by the Tagami correlation.

Recently, a number of containment simulations have been conducted in the Federal Republic of Germany [71-75]. The Battelle-Frankfurt tests were conducted on a 1/64 scale model of the Biblis A PWR plant. The HDR experiments have been conducted on a much larger scale. The experiments of Schwan and Aust [76], also in the FRG, were conducted in a large scale pressure suppression test facility to simulate the conditions present in a break compartment. Large heat transfer coefficients were present despite the high concentrations of noncondensable

gas.

One of the problems present in all of the above experiments is that little or no information on the steam flow patterns and velocities is available. Generally, only heat transfer coefficients are measured and analysis of the results requires assumptions or numerical predictions of the flow patterns and velocities. With the possible exception of the recent German experiments, very little is known about the effects of scale either. This has hindered much of the detailed modelling of the condensation phenomena that has taken place.

In spite of these difficulties, considerable analytical modelling has been attempted. The models of Corradini [64] and Kim [3] all utilize various forms of the analogies between heat, mass, and momentum transfer. Carbajo [77] uses a Nusselt analysis modified for the presence of noncondensables by the method of Sparrow, Minkowycz, and Saddy [56] or Henderson and Marchello [30]. All show varying degrees of agreement with integral experiments such as those of Tagami or those in CVTR.

2.5 CHARACTERISTICS OF INTERFACIAL WAVE STRUCTURE

2.5.1 Overview.

The interfacial wave structure of stratified two-phase

flow has been studied from a variety of points of view. Mathematical stability and growth analyses of waves have been a popular research topic for many years and continue to be so today. There is also a large body of literature related to the predictions of ocean waves and the associated effects on meteorology, erosion, et coetera. This research also continues on in the present. Chemical, mechanical, and nuclear engineers have also studied interfacial wave structure due to its profound effect on pressure drop, mass and heat transfer coefficients. As the object of the current research is to study the effects of interfacial wave structure on the combined heat and mass transfer processes of condensation in the presence of a noncondensable gas, the latter point of view is most appropriate. The literature review will be further restricted to those studies which treat relatively thin films and in which both film and gas are in motion relative to the solid wall. General reviews of literature on film flow and interfacial wave structure include those of Fulford [78] and Dukler and Wicks [79].

2.5.2 Vertical Film Flows.

Vertical falling films exhibit interfacial wave structure at all but the smallest Reynolds numbers with or without a parallel gas flow. In the absence of gas flow,

these waves are due to gravity and may show some periodic character at low film flow rates. Measurements show, however, that the periodicity is soon lost at higher flow rates or at some distance from the entrance. Hence theoretical approaches which seek to find solutions to the classical wave equation are limited in effectiveness [80]. Krantz and Goren [81] conducted experiments on planes at high angles of inclination in order to examine the validity of linear stability theory. The details of small amplitude two-dimensional waves were predicted successfully at extremely small Reynolds numbers. A more successful approach for flows of more reasonable Reynolds numbers has been to try to characterize the waves statistically. Several workers have attempted this approach.

Telles and Dukler [80] conducted experiments in which conductivity measurements were used to determine the instantaneous film thickness. Their results indicate the interface has a random character and behaves as a "two-wave" system. This two-wave system consists of large waves containing a significant portion of the mass flow which occur infrequently and much smaller ripples on a substrate which are more abundant. This system is illustrated in Figure 2.4. The relative dominance of the two types was found to be dependent on the gas flow rate (interfacial shear) rather than on the film flow rate.

Their work also shows quite clearly that the behavior of horizontal and vertical films are markedly different. Vertical waves appear to be driven by gravitational forces whereas waves in horizontal films seem more dependent on interfacial shear and hence on the flow rate of the gas. Their work also yields useful methods for extracting the desired statistical quantities from the experimental data.

Chu and Dukler [82,83] have examined the behavior of the two-wave system model in more detail. In their study of the substrate layer on which the small waves travel, Chu and Dukler [82] developed methods for deriving characteristics of the substrate from their experimental data. The substrate wave structure (small ripples) were found to be nearly independent of interfacial shear. An attempt was also made to apply published theories for the substrate waves since it appeared that these analyses would readily apply. The results were very poor, however, and indicated that a new approach would be required to accurately predict the wave structure.

In their second paper, Chu and Dukler [83] examined the structure of the large waves and their interaction with the gas phase flow. The wave amplitude spectra, see Figure 2.5, exhibited a transition from a unimodal to a bimodal character at a specific liquid Reynolds number (in the absence of gas flow). This indicates that the large

waves have more than one characteristic size. Frequency spectra and wave celerity (speed relative to film) were also measured. Again the results do not correlate well with any of the theories. They attributed this to the use of a few terms of a Fourier series to describe the waves when measurements show a very distinct asymmetry. Measurements also show that the large waves make only a small contribution to the overall shear stress and that the small ripples and wavelets on the substrate tend to govern momentum transfer. Large waves, on the other hand, control the hydrodynamic behavior in the film.

Extensive measurements of downward cocurrent annular flows of air and water in vertical tubes have been obtained by Webb and Hewitt [84]. The interfacial characteristics, including wave frequency and velocity, were extensively examined using the conductance probe method. Data on local pressure fluctuations and liquid entrainment were also recorded. Attempts at correlating local pressure variations with film thickness variation were not successful. New flow regime maps including the effects of interfacial structure were proposed.

Brodowicz and Dyakowski [85] have also conducted measurements in vertical film flows. They have used hot wire anemometry to characterize the turbulence in the gas phase in the vicinity of the liquid interface. Although

their data and analysis are limited, their work clearly shows an increase in gas phase turbulence when a liquid film is present. This turbulence level does not appear to strongly depend on the liquid Reynolds number however. No information on the details of the interfacial structure are given.

The effects of longitudinal distance were studied by Takahama and Kato [86]. Their experiments were conducted on flow down the outer surface of a vertical cylinder without concurrent gas flow. The results show that the critical Reynolds number for transition from laminar to turbulent films is dependent on the longitudinal distance. Similar findings were made regarding wave velocity and amplitude. As in earlier works, the waves appeared to be statistically distributed and thus theoretical solutions of the wave equation were not appropriate. The type of statistical distribution function which fit the data was used to classify wave characteristics in a modified flow regime map.

Mancini and Andreussi [87] have recently published results of their study of wave structure in vertical annular flow. They have developed a different method for statistically differentiating between ripples and large waves. They conclude that the bimodal amplitude spectra found by Chu and Dukler [83] does not refer to two

dominant sizes of large disturbance waves but only to the ripple amplitude and the large wave amplitude. In other respects, their data agrees reasonably well with the results of previous experiments. Andreussi [88] has also published results on the droplet entrainment regime in which it is suggested that entrainment is due to Kelvin-Helmholtz instabilities.

2.5.3 Horizontal Stratified Flow.

The interface in horizontal stratified flow may be smooth at low flow rates. This behavior differs from that of vertical falling films for which the surface is nearly always wavy. As the gas flow rate is increased, the interface becomes rough and wavy. Eventually entrainment of the liquid phase occurs when wave crests are torn off. The behavior of the interface in horizontal stratified flow had been modelled by a number of people over many years using mathematical techniques, but detailed experimental observations were not available until the late 1950's.

The pioneering work in interfacial structure measurement was that of Hanratty and Engen [89]. They studied flows of thin liquid films of water with cocurrent flow of air in horizontal flat plate geometries using Pitot tubes to map the velocity profiles. The following flow regimes

were identified in their work:

1) smooth interface,
2) two-dimensional waves,
3) three-dimensional waves (pebbled or squall waves),
4) roll waves,
5) dispersed flow and entrainment.

Smooth interfaces are generally present at low gas phase flow rates. Hanratty and Engen observed that the transition to two-dimensional waves (small waves spanning the channel) occurred at about the same point as the transition to a turbulent gas phase. They were, however, able to attain a fully turbulent gas flow with a smooth interface and conversely a wavy interface without fully developed turbulence in the gas phase.

Two-dimensional waves existed over only a small range of the variables investigated (gas flow, liquid flow, and liquid film thickness) before the transition to squalls, later called three-dimensional waves, occurred. The transition did depend on the properties of the liquid film. The squall surface persisted over a fairly wide range of gas flows, but eventually roll waves appeared at sufficiently high rates of flow. Roll waves are large high-speed waves which travel through the three-dimensional waves. Dispersed flow and entrainment occur

only at extremely high flow rates. In this regime droplets are torn from the liquid surface. Later work by Woodmansee and Hanratty [90] indicate that this phenomenon is due to Kelvin-Helmholtz instability. This last regime is of limited interest in the current research.

Hanratty and Engen compared their results to the predictions of many theories on transition to wavy flow and found little agreement. Similarly, their data on wave speed and wavelength were not predicted by theoretical models. They also measured velocity profiles in the gas with an impact tube and found the maximums were skewed towards the top of the test section indicating an increased shear stress at the wavy interface.

Ellis and Gay [91] conducted experiments quite similar to those of Hanratty and Engen. Their measurements also consisted primarily of Pitot tube readings which were used to estimate the pressure drop and the interfacial shear stress. The data is in good agreement with that of Hanratty and Engen.

Another early experiment was that of Van Rossum [92]. Measurements of film thickness were made with a conductivity cell. A Pitot tube was also used for measuring velocity profiles in the gas. Theoretical predictions of film thickness were found to deviate substantially from measured values. The data show only moderate agreement

with that of Hanratty and Engen [89]. Correlations were also developed for the onset of atomization (entrainment).

Lilleleht and Hanratty [93] used a method of measuring film thickness in which a beam of light was attentuated by dye dissolved in the liquid film. This allowed them to measure both the mean film thickness and the root mean square fluctuations due to the wave structure. The frequency spectrum was also determined. Lilleleht and Hanratty [94] also attempted to correlate the interfacial shear stress with wave height using an equivalent sand roughness approach. They compared their data to the sand roughness experiments in pipes conducted by Nikuradse. The correlation was not good and indicated that the sand roughness approach was not appropriate.

Hanratty and Hershman [95] studied the roll wave transition in more detail. Satisfactory agreement was found with the theoretical model of Jeffreys [96] for the case of water, water-glycerine, and water-butanol solutions with concurrent air flow. Poor agreement with theory was found when surface-active agents were introduced into the water. The reasons for this were unknown.

Cohen and Hanratty [97] used the model of the gas flow proposed by Benjamin and Miles [98-102] to calculate shear stress and pressure variations over the wavy surface. These variations were thought to be responsible for the

interfacial structure transitions. This method was found to agree well with their experimental measurements. Further experiments by Cohen and Hanratty [103] sought to explore sand roughness modelling of the wavy interface. It was found that velocity profiles in the gas were different than for flow over roughened surfaces and that the most important parameter involved was the amplitude of the waves.

The experiments of Craik [104] on very thin liquid films was accompanied by mathematical stability analysis. The work was conducted on very thin (less than 0.5 mm) liquid films of water with concurrent air flow. It was shown that thin films are not necessarily more stable than slightly thicker ones and that a fundamentally new instability arises at the low thickness limits.

Linehan [105] conducted experiments on stratified air-water flow in a two-dimensional geometry. Steam-water tests were also conducted. Conductance and needle contact probes were used to measure average film thickness. Correlations for the interfacial shear stress in both the one-component and two-component situations were derived from analytical models and were compared to experimental data. It was found that interfacial shear stress was a linear function of the film Reynolds number only and was augmented by the effects of condensation.

Narasimhan and Davis [106] studied the effects of surface active agents on surface waves. Experimental data show that for contaminated films (with surfactant) that the wavelength of two-dimensional waves is greatly increased. This implies that the mechanism through which disturbances are damped is not surface tension. It was also noted that even trace amounts of surfactant greatly alter the wave characteristics. This makes the prediction of waves in contaminat fluids very difficult.

More recently, Akai et. al. [1,2] have performed experiments on air-water and air-mercury flows. Akai, Inoue, and Aoki [1] measured the structure of the wavy interface of air-water flows using thermal anemometry in conjunction with a correlation and probability analyzer. Measurements of the velocity profiles and turbulence levels were also made in both phases. Some of their results are shown in Figure 2.6. They attempted to achieve all combinations of laminar/turbulent liquid flows with laminar/turbulent gas flows, but were unable to obtain the laminar liquid with turbulent gas flow situation. Their results clearly show that the "wave effect depth" spans the entire liquid flow field, but that it only penetrates about one wave amplitude into the gas phase. The eddy diffusivity in the vicinity of the interface in the gas phase was also shown to be much larger

than the value in single phase turbulent gas flow.

Akai, Inoue, Aoki and Endo [2] conducted air-mercury experiments using similar instrumentation. The observed flow patterns were nearly the same as those observed for air-water systems, but some important differences were reported. In some situations a discontinuous mercury film was observed. Results on pressure drop and turbulence in the gas phase were also reported.

A computational modelling effort was also undertaken by Akai, Inoue, and Aoki [107]. A two-equation turbulence model is used in conjunction with the Navier-Stokes equations to predict the results of their air-mercury experiments. Use of a smooth interface boundary condition produced somewhat poor results. Good agreement with experimental profiles was obtained when a boundary condition based on experimental results was used. The wavy interface was modelled as a source of turbulent kinetic energy in the liquid phase and as a flow separation in the gas phase.

Chang, Plate, and Hidy [108] conducted measurements of turbulent air flow over water waves. They used a unique arrangement of a thermal anemometry probe that was mechanically moved so as to maintain a constant distance from the water surface. Their work indicated separation of the air flow occurs behind the wave which supports the

sheltering theory of Jeffreys [96]. It should be noted that the experiments were attempting to simulate ocean waves in deep water rather than thin liquid films.

2.5.4 Heat and Mass Transfer with Interfacial Structure.

The effect of interfacial structure on heat and mass transfer coefficients is of vital interest in many areas of engineering. In chemical engineering apparatus, both falling films and horizontal stratified flows are used for mass transfer. This mass transfer may take place between the film and the gas or the film and the solid surface. Studies of mass transfer between liquid films and solid surfaces are clearly of little interest in the present research. Mass transfer between films and gases is also of limited applicability since the primary mass transfer resistance is in the film and relates to mixing phenomenon and alteration of the concentration gradients. In condensation in the presence of a noncondensable gas, the primary resistance to heat transfer is in the gas/vapor boundary layer. Furthermore, the majority of mass tranfer work has been either protypical in nature or pertained to situations in which the flow characteristics were dissimilar to the ones of current interest (eg. two-dimensional waves on stagnant pools of liquid). Finally, the details of the interfacial structure were seldom, if

ever, measured. The experimental results, in general, show greatly increased (to 100% or more) mass transfer coefficients when wavy films are present. Frisk and Davis [109] review some of the work in mass transfer.

An early experiment in heat transfer in falling films was that of Bays and McAdams [110]. Films of oils and water were used and the heat transfer coefficient was measured. Apparently no direct observation of the interface was conducted and the authors relied on being below the critical Reynolds number (2000) in order to assure streamline (laminar) flow. A marked effect of viscosity and temperature difference were observed.

Chand and Rosson [111] also conducted heat transfer measurements with a vertical falling film. Using a dynamic heat flux meter, they were able to measure the variation in the heat transfer coefficient as individual ripples on the film passed by. At low heat fluxes, little effect on the heat transfer coefficient is caused by the ripples. Oscillations in the heat transfer coefficient were measured, however, in cases with high heat fluxes. The amplitude of these fluctuated was typically of the order of 10% of the mean. The frequency of the oscillations was about the same as that of the surface ripples.

Experiments with aqueous sugar solutions were conducted by Fedotkin and Firisyuk [112] in inclined planar

geometries. An assessment of the effects of evaporation over the heated length of the channel was made. No measurements of interfacial structure aside from casual visual observation were conducted.

Takahama, Fujita, Kodama, Kuribayashi, and Aiso [113] have studied countercurrent air-water flows with heat transfer in a vertical planar geometry. The effects of air and water flow, inlet air humidity, and inlet water temperature were measured. Interfacial structure was characterized qualitatively from photographs. Good success was achieved by correlating pressure drop, heat and mass transfer by using the relative velocity between the phases. A marked increased in all transport processes was found in the presence of waves.

Davis et. al. [109,114,115] have done several studies of the effect of interfacial structure on heat transfer. Davis and Cooper [114] studied thermal entrance effects. Under smooth interface conditions, their model showed good agreement with experiment. Waves greatly enhanced the heat transfer and reduced the thermal entry length so greatly that the primary problem was the prediction of the fully developed temperature profiles.

Frisk and Davis [109] conducted further experiments on the effects of interfacial structure. They found that the presence of two-dimensional waves had little or no effect

on the heat transfer as compared to wavy films. Theoretical predictions showed good agreement here. Three-dimensional and roll wave regimes showed increases of about 100% on the heat transfer coefficient. In order to make a direct comparison, a surfactant was used to inhibit wave formation so that the heat transfer coefficient could be compared at the same liquid and gas flow rates for both smooth and wavy films. It was found that it was the presence of the interfacial structure that caused the increase in the heat transfer. When the waves were suppressed, the heat transfer could be directly predicted by smooth film theory. This result is shown in Figure 2.7. It was also observed that for Gr/Re(liquid) greater than 1., that Rayleigh-like instabilities due to buoyancy became significant.

Davis, Hung, and Arciero [115] applied the von Karman analogy to prediction of heat transfer with interfacial structure. Their results indicate that the primary effect of the gas velocity is in the indirect effect on the film thickness. It is also stated that this indicates that the film substrate (described by Dukler et. al. [82,83]) is the predominant resistance to heat transfer. The apparently different hydrodynamics of the large wave structure at different gas flow rates does not seem to affect the heat transfer coefficient strongly. Reasonably good

agreement between the von Karman analogy and the experimental results is noted.

2.6 SUMMARY AND CLOSING REMARKS

The preceding survey has shown the large quantity and variety of research which has been devoted to both condensation phenomena and the study of interfacial structures. Despite the abundance of literature references, however, a dearth of information exists with regards to condensation research under conditions of moderate pressures and high concentrations of noncondensable gas. The few integral experiments that do exist do not furnish adequate information about the flow field. Consequently comparison with separate effects tests or theoretical models is often difficult.

There has been little or no effort made to characterize the effects of interfacial structure on the condensation heat transfer coefficient experimentally in spite of the fact that it is thought to strongly influence the structure of the gas/vapor boundary layer. The majority of the experiments, in fact, go out of their way to eliminate waves from the films so that theoretical analysis can be more readily applied. In many applications of interest, however, this waveless situation does

not exist and currently no data exists which includes interfacial structure information. Simultaneous measurement of the heat transfer coefficient and the interfacial structure is needed in order to evaluate the models which have been proposed.

The use of thermal anemometry is also comparatively rare in the study of interfacial wave structure in thin films. It has been used occasionally in isothermal flows, but no use in a heat transfer or condensation experiment has been found. Data on film thickness and wave spectra are common since they can be easily acquired using conductivity cells or needle contact probes. Thermal anemometer probes can be used like needle contact probes for determining film thickness and wave spectra, but can also measure wave speed and turbulence parameters in the vicinity of the interface. In applications in which the film controls the heat or mass transfer rate such turbulence data is of little utility, but in condensation in the presence of a noncondensable gas the gas/vapor boundary layer becomes the dominating influence and such data is of primary importance.

Consequently it can be seen that deficiencies do exist in the understanding of condensation in the presence of a noncondensable gas, particularly regarding the subject of interfacial structure. These deficiencies can be sum-

marized as follows:

1) little work done in condensation in the presence of large concentrations of noncondensable gas at moderate pressures;
2) no simultaneous measurements of interfacial waves and condensation heat transfer coefficients;
3) little measurement of turbulence parameters in the vicinity of a wavy interface in isothermal flows;
4) no measurement of turbulence parameters in condensing flows;

The current research program was addressed towards remedying these deficiencies. Condensation was studied under conditions of large concentrations of noncondensables and experimental techniques were developed for measurement of interfacial wave parameters in both isothermal and condensing flows.

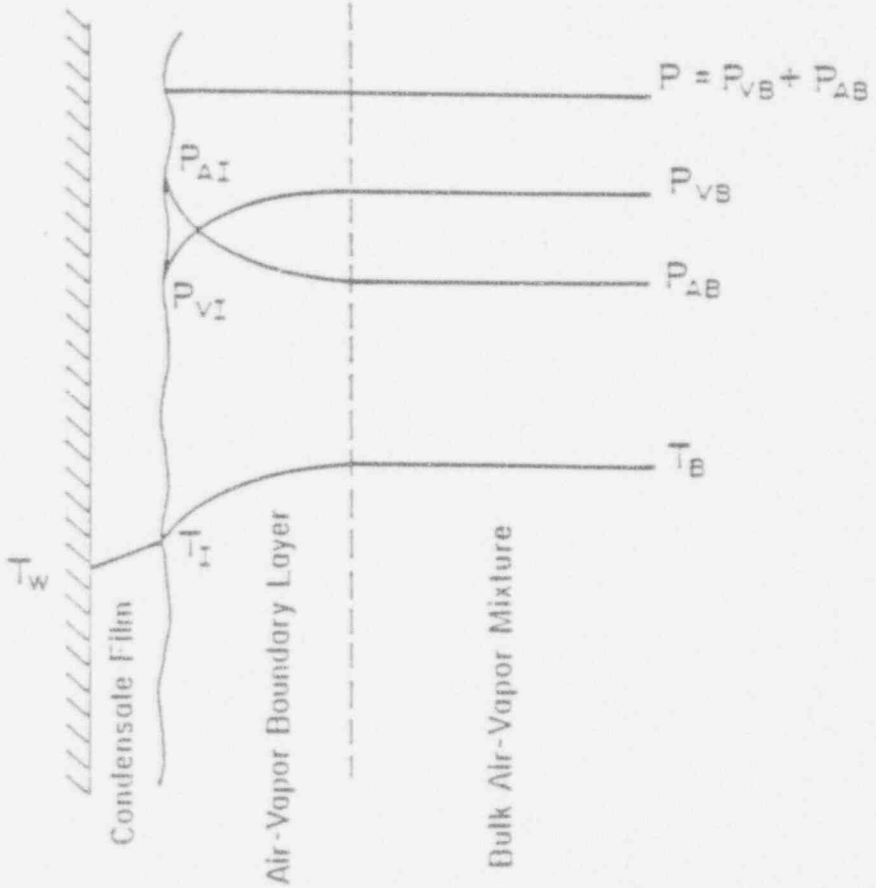

Figure 2.1 Condensation in the Presence of a Noncondensable Gas

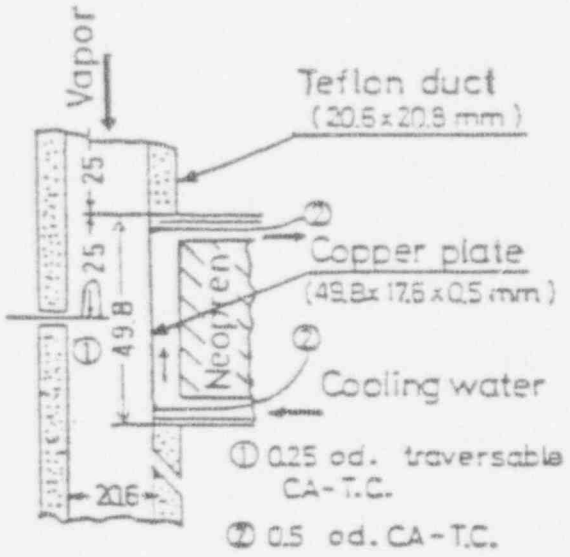

Figure 2.2 Test Section of Asano et al.

from Asano et al. [18]

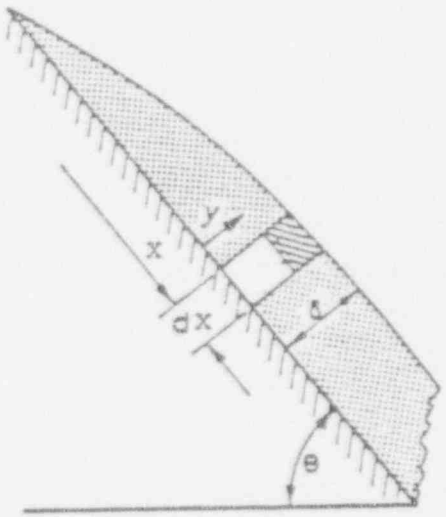

Figure 2.3 Nusselt Film Analysis

from Collier [35]

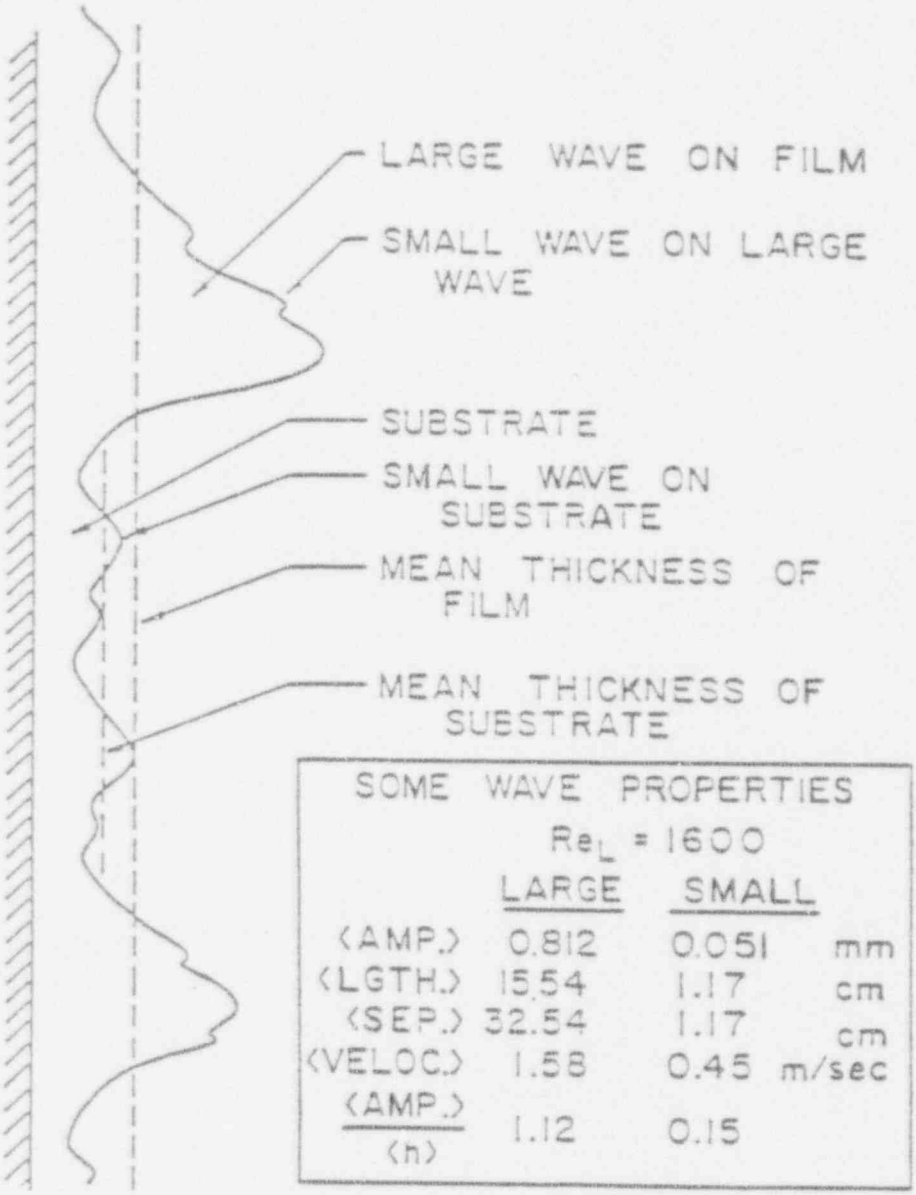

Figure 2.4 Two-Wave System of Dukler et al. from Chu and Dukler [83]

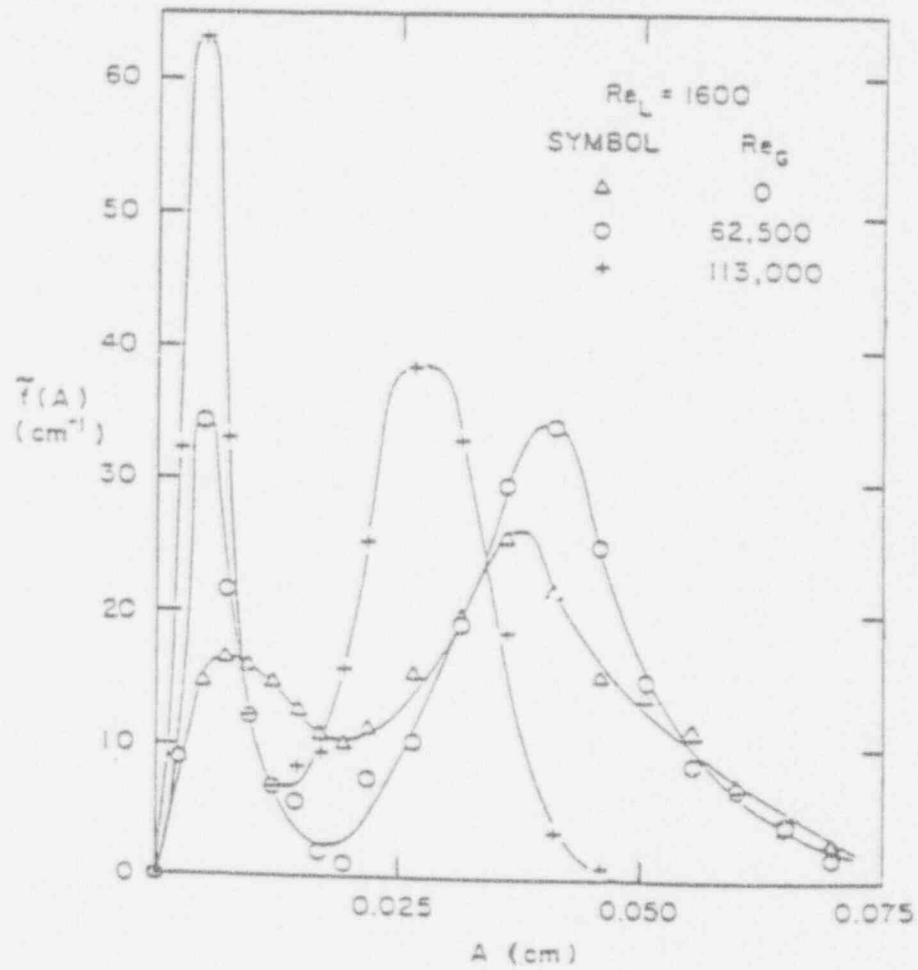

Figure 2.5 Bimodal Wave Amplitude Spectra from Chu and Dukler [83]

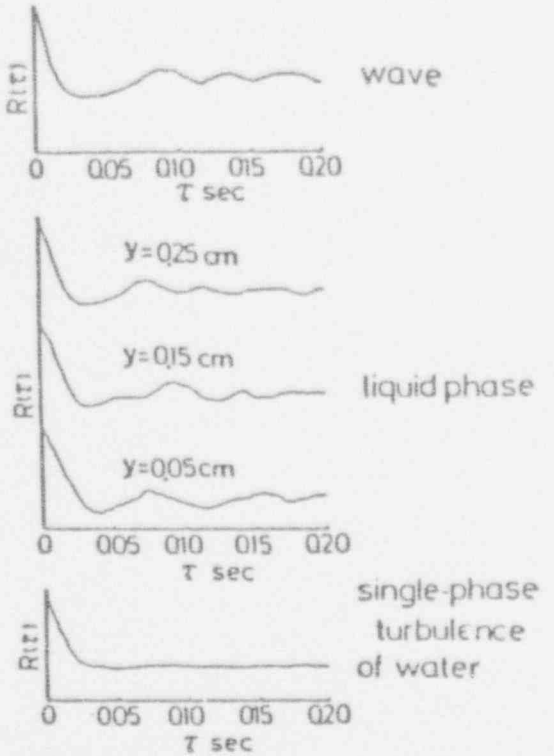

Typical Autocorrelations
of Wave and Liquid Phase Velocities

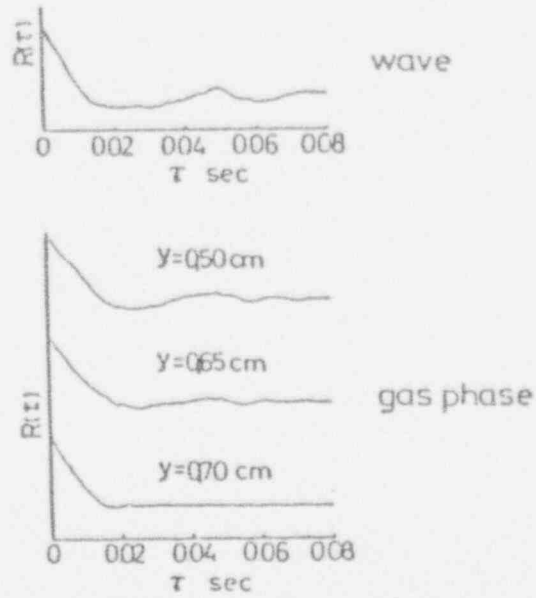

Typical Autocorrelations
of Wave and Gas Phase Velocities

Figure 2.6 Sample Results of Akai et al. [1]

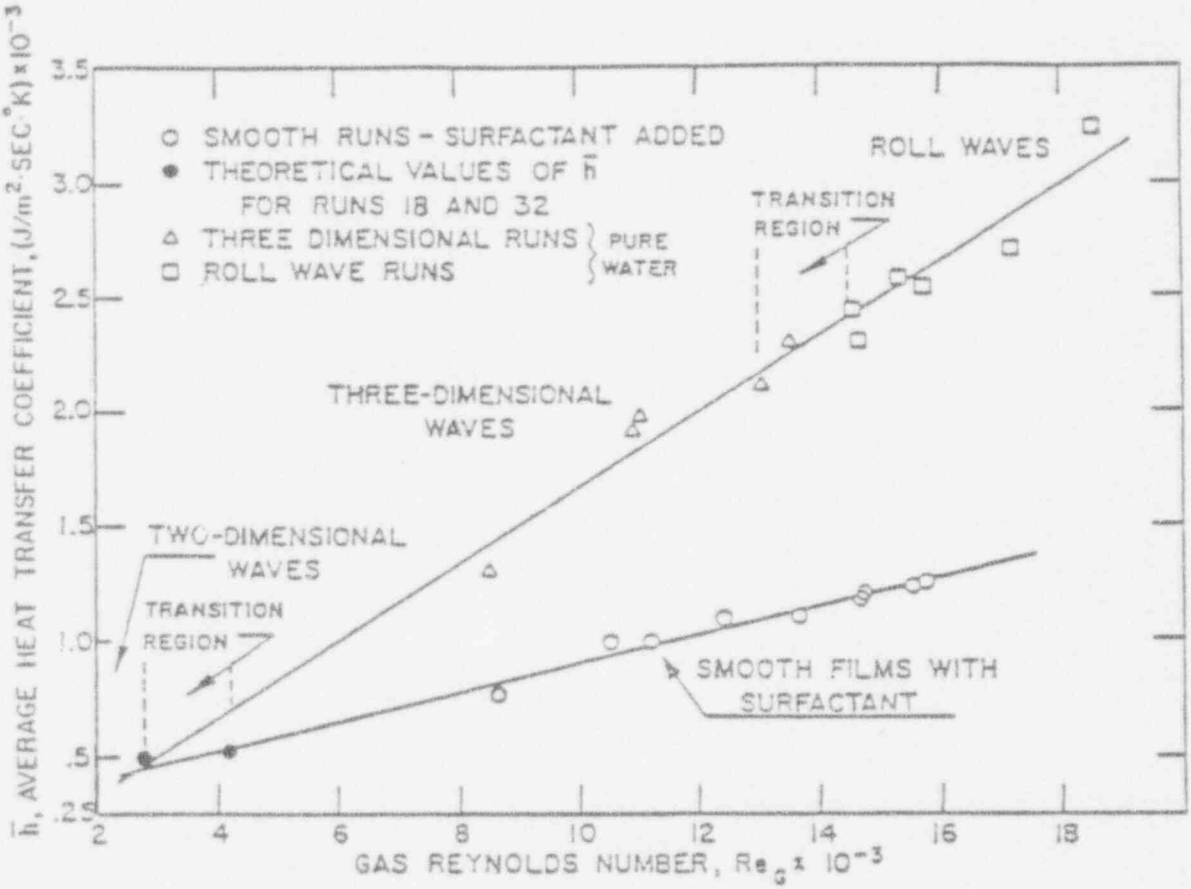

Figure 2.7 Heat Transfer Coefficient showing Effect of Interfacial Waves from Frisk and Davis [109]

3. DESIGN AND CONSTRUCTION OF EXPERIMENTAL FACILITIES

3.1 INTRODUCTION

The following sections discuss the design and construction of the experimental facilities which were used in the experimental program. Prior to the start of the research none of these facilities existed. This even included the laboratory in which the experimental apparatus was erected. The procurement and fabrication of the test section, support equipment, and instrumentation as well as the development of operating procedures and software was all included in this effort. For this reason, the design and construction are reviewed in some detail. This should aid future research which is performed using these facilities.

3.2 TEST SECTION

The test section in which all the fluid mechanics and heat transfer measurements were to be made was designed to accomplish the following goals:

1) approximate two-dimensional planar geometry,
2) allow for local heat flux measurements to the wall,
3) provide visual access to the flow,

4) allow access for thermal anemometry probes,
5) provide a variable angle of inclination,
6) provide the desired flow conditions,
7) prevent substantial facility degradation under the desired flow conditions.

In addition to the above goals, the design also had to be reasonably inexpensive to construct and of a scale such that support equipment could be relatively simple and inexpensive.

A variety of flow conditions were desired for the various experiments anticipated. Achievement of this variety of configurations in a single multipurpose test section required compromise on several of the flow parameters.

The design was made primarily on the basis of satisfying the needs for the conditions of forced convection film condensation on a wall or structural surface. Under these conditions, the film conditions are important primarily for the effects on the gas/vapor boundary layer. A large aspect ratio section and fully developed flow is undesirable. What is preferred is a situation in which the boundary layers on the surfaces of the duct are thin enough so that they do not interact. In general the largest cross section possible is desired. Since forced

convection conditions with substantial steam or steam/air velocity were desired, however, the size of the cross sectional area was directly proportional to the amount of steam and air that must be supplied. Hence, a compromise on the size of the experimental section was necessary based on the amount of steam and air that could be supplied and the velocities that would be attained. The initial design conditions are listed in Table 3.1. It should be noted that these were calculated based on boiler capacity limits alone and, therefore, do not account for the limited capacity of the air blower. The results which were actually achieved are discussed in section 4.6.3.

Experiments in characterization of the interfacial structure of air-water flow typically utilize a large aspect ratio geometry and long entrance lengths in order to achieve fully developed flow. Unfortunately, these features are inconsistent with the design of the test section for the condensation measurements. Consequently, the type of measurements which were made in the Isothermal Air-Water Test Series were adapted. This did not become a serious problem since the primary purpose of the isothermal series was to develop the experimental methodology and to observe the features of the flow near the interface.

The test section, as built, is shown in Figure 3.1. The section is a square duct 102 mm on a side and 1.83

metres long. It consists of three pieces: a U-shaped channel and two floor sections. The second (downstream) floor section is made of an aluminum plate to allow for heat transfer to the floor. The first (upstream) floor section and the U-shaped channel are constructed of clear polycarbonate plate to allow for visual observation of the flow. The test section is mounted on a Unistrut carriage which is in turn mounted on a large Unistrut structure which allows the entire carriage to be pivoted to various angles of inclination with the horizontal. Due to the movable nature of the test section, supply of water, steam, and air is made by flexible hose.

The air and steam are admitted to the test section by an aluminum inlet duct. This duct is shown in Figure 3.2. Air enters the duct and passes over three finned strip heaters. These heaters provide the preheating necessary to avoid condensation of the steam by the cooler incoming air. Steam enters the duct via two pipe diffusers. A copper screen is located just downstream of the diffusers to assist in mixing of the air and steam flows. The mixture then passes through a reducing section and into the test section.

In the air-water test series, air entered the test section at the upstream end. The water film was injected through the bottom of the plate just downstream. No

cooling water was circulated through the cooling plate in these tests. Water and air were exhausted at the downstream end of the section.

In the air/steam-water series the air/steam mixture entered the test section at the upstream end of the entrance length. Condensation took place at the downstream end of the test section on a cooled plate which forms one of the walls of the duct. A water film was injected well upstream of the cooled plate. This was sometimes done to augment the film formed by the condensing steam. Due to the low heat transfer rates sometimes encountered in condensation in the presence of large quantities of noncondensable gas, the film formed by the condensing steam alone was sometimes extremely thin and/or not continuous. Air, steam, and water were exhausted into the secondary condenser hotwell at the downstream end of the section.

3.3 SUPPORT EQUIPMENT

3.3.1 Steam Supply System.

It was recognized early in the design of the experimental facility that a substantial steam supply would be required in order to achieve the conditions of moderate steam velocities over a relatively large cross sectional

area.

The use of the building steam supply was investigated first. The mass flow rates available were more than adequate for any reasonable test section size, but the steam was treated with a variety of chemicals to inhibit corrosion, etc. in the supply system. The interfacial structure of a film has been shown to be very sensitive to the presence of contaminants such as surfactants [106] and thus the building supply steam was not considered satisfactory. Consideration was given to local construction of a boiler, but it was decided that from manpower, economic, and safety points of view that it would be better to purchase a package unit.

An electric steam boiler was purchased from Reimers Electra Steam in Alexandria, Virginia. The 36 kilowatt unit is rated at 56.8 kg/hr of saturated steam at 100 C. This was estimated to allow velocities of pure steam in the test section in excess of 2.5 m/sec. Mixtures of air/steam could achieve substantially higher velocities (4 m/sec for a mass ratio of 1). These velocities were well within the experimental range desired. The boiler is equipped with a high-pressure feedwater pump and fully automatic controls. Two Honeywell Pressuretrol pressure controllers are used. One is used as an over-pressure trip with manual reset and is factory set for about 8 bar (100

psig). The second is a differential pressure control. The operating pressure setpoint can be adjusted from approximately 0.7 bar to 8 bar (10 - 100 psig). The differential can be adjusted from approximately 0.35 to .85 bar (5 - 12 psi). Boiler level is maintained by a McDonnell and Miller controller which includes a low water level trip. Complete specifications are listed in Table 3.2.

Steam leaving the boiler is routed from the boiler outlet valve to the orifice flow metering section by 1 inch pipe. The flow is then run from the end of the metering section to the steam throttle valve via 3/4 inch ID Goodyear Plicord steam hose. Another length of steam hose then connects to the inlet piping of the steam diffusers.

A 25 litre can filled with room temperature water is used as a catch tank for steam or hot water released if the boiler's safety relief or blowdown valves are actuated. Flow is routed from the boiler using 1 inch diameter steam hose. The relief tank is fitted with a dump valve which empties the contents of the tank into a floor drain.

3.3.2 Air Blower and Preheater.

An air supply was also required in order to provide the flow rate desired for both the air-water and air/steam

water test series. Initially use of the building compressed air supply was contemplated, but the flow rates achievable were too low and the outlet pressure much larger than required. In addition, the noise level from the outlet nozzle due to choked flow would have been deafening.

A centrifugal blower powered by a 1/4 horsepower electric motor was salvaged from a natural gas-fired furnace for use as an air supply. No blower rating was available but air velocities of 12.19 m/sec were attained. These velocities were of the order of the maximum required.

The blower was connected to the test section by two masonite reducing ducts and a length of 8 inch diameter Fedflex hose. Since the blower and motor were single speed units and flow control was required, a flow control shutter was installed in one of the masonite ducts. The control available with this method was rather crude.

Following initial testing with the secondary condenser system in place, it was found that the pressure drop had increased substantially and that the flow velocities had diminished accordingly. In addition, the flow control provided by the shutter was imprecise and only provided a very limited flow range. For these reasons, a 1/3 horsepower motor equipped with a variable speed control was

installed. With this motor, air velocities could be adjusted between approximately 1 to 12 m/sec. The speed control was also much more precise and repeatable.

Preheat of the inlet air was necessary to prevent condensation of the steam during mixing of the two gas streams. Calculations indicated that approximately 1.5 kW of heat addition, in conjunction with moderate steam superheat, would provide the energy necessary to achieve all of the desired experimental conditions. Three Chromalox Finstrip finned electrical strip heaters of 475 W each were mounted in the inlet section. Heater power is controlled by a Superior Electric variable autotransformer.

3.3.3 Film Injection System.

The film injection system was designed to inject a continuous liquid film into the test section. Preliminary calculations indicated that in order to achieve a film thickness of approximately 5 mm, a flow rate of 30 litres/min would be required for a vertical configuration. Angles of inclination less than vertical would require substantially smaller flow rates. The system was designed to achieve the worst case (vertical) flow rate.

The film injection system, as built, is shown in Figure 3.3. A fitting was machined from aluminum to allow

injection of the film into the test section. A constant head tank is used to provide a stable film flow rate. This tank delivers water to a pair of rotameters through a set of metering valves via 3/4 inch Goodyear Plicord steam hose. Originally a Dwyer VFC-151 rotameter was used, but was later replaced by a set of Omega FL-2 and FL-3 rotameters operating in parallel. Another length of hose leads from the flowmeter to the film injection fitting. The film exits the test section at the downstream end and flows into the secondary condenser hotwell.

The water in the secondary condenser hotwell is pumped back up to the constant head tank via 3/4 inch aluminum pipe and steam hose by a 1/12 horsepower Grundfos pump. The level in the tank is maintained by controlling a Parker Gold Ring solenoid valve with an Anderson Flotec level switch. In order to allow the pump motor to run continuously, a bypass line is located just upstream of the solenoid valve. The bypass line returns water to the condenser hotwell by spraying it over the incoming air/steam mixture to assist in the condensation of excess steam. The bypass line can be seen in Figure 3.5.

3.3.4 Plate Cooling System.

A large aluminum plate assembly forms a 610 mm length of one wall of the downstream end of the duct. The as-

sembly is shown in Figure 3.4. Inside the plate are five spiral channels machined into the aluminum. Water is circulated through these channels to provide the cooling. The spiral geometry is designed to assure a uniform heat flux on the surface of the aluminum plate.

Cooling water is provided by a Neslab HX-150 Refrigerated Heat Exchanger capable of removing 4500 watts of thermal energy from the coolant. This translates to an ability to handle a test plate heat flux of about 75,000 W/m^2. The heat exchanger circulates water at a rate of approximately 20 l/min with a temperature stability of +/- 0.1 C.

As cold water leaves the heat exchanger it passes through a Dwyer VFC-151 rotameter then is routed to the inlet manifold by 3/4 inch Goodyear Contender hose. The inlet and outlet manifolds are mounted on the test section carriage and are constructed of 2 inch pipe. Five gate valves are mounted on the inlet manifold to allow for control of the flow in each cooling channel. Flow is then routed via 1/4 inch stainless tubing to the channels. The coolant then is returned to the outlet manifold by additional stainless tubing and finally back to the heat exchanger by another length of hose.

3.3.5 Secondary Condenser System.

The condensing surface inside the test section is not capable of condensing all the steam in the flow stream, hence a second condenser is required to condense the remaining steam, allow the air to escape, and to store the water until it is pumped back to the boiler or the constant head tank.

The secondary condenser system, which is shown in Figure 3.5, works in the following way. Water and the air/steam mixture enter the hotwell through one end and pass through the film injection bypass spray. Water collects in the lower portion of the hotwell. As the steam and air travel upward into the stack portion of the system, an array of pipes spray cold water downward on the rising steam and air, condensing much of the steam. The water and condensate drain back into the hotwell. The air and remaining water vapor flow up through a dehumidification heat exchanger on which the most of the remaining vapor condenses.

The hotwell is connected to the downstream end of the test section by a length of 6 inch diameter Fedflex hose. The hotwell is constructed of 120 litre tank which is normally about half full of water. The hotwell water inventory is cooled by two coils of 3/8 inch copper tubing in which cold tap water is circulated. The spray and film

injection system pumps take their suction from the end of the hotwell nearest the cooling coils.

A Grundfos Model CP2-30KU 2-stage 3/4 horsepower centrifugal pump is used to supply water from the hotwell to the spray array. This pump also supplies water to the suction side of the boiler high-pressure feedwater pump. The spray pump delivers approximately 20 l/min of flow at a pressure of 3.5 bar. Water is routed to the spray header by 3/4 inch copper tubing. The spray piping is constructed of 1/2 inch PVC pipe. The dehumidifier heat exchanger is constructed of a Harrison radiator salvaged from a 1964 Chevrolet. It is cooled by cold tap water.

3.4 INSTRUMENTATION

3.4.1 Heat Flux Measurement.

A variety of strategies can be utilized in computing the condensing heat flux. Many previous investigators have used overall global mass and energy balances to determine the heat transfer coefficient. Typically, the condensing surface is cooled on the back side by circulating water or a refrigerant. The flow rate and temperature rise of the coolant is then used to compute the total heat transferred and the average heat transfer coefficient. Alternatively, the amount of vapor condensed is weighed or

metered and the total heat transfer computed from the heat of vaporization. These global methods have the advantage of being relatively simple, but have the following disadvantages:

1) overall average rather than local heat transfer coefficients are determined;
2) potential for error exists due to poor insulation of the test section or other losses;
3) accurate temperature measurement is required due to small temperature differences.

Nearly equally popular strategies also exist which employ the use of the local measurement of the heat flux by determining the local temperature gradient through one wall of the test section. Thermocouples are normally inserted into small holes drilled into a copper block. Using the temperature profile from these thermocouples both the heat flux and surface temperature can be calculated. The disadvantages here are:

1) precise emplacement of the thermocouples is required for accuracy in determining the profile;
2) precise calibration of the thermocouples is necessary since small temperature differences are being measured.

Both global heat balance and local temperature

gradient techniques have been used successfully. The local temperature gradient technique has been selected for the current work. Heat balance measurements on the cooling loop were also used both as a check and as a backup. This choice was made for a variety of reasons. Early on in the design it became clear that measurements of the amount of vapor condensed would be impractical due to the large flow rate of the injected film. The quantities of vapor condensed would be relatively small in relation to the total flow rate. In addition, overall heat transfer coefficients might be suspect due to the heat capacity of the film. Finally, all the methods require the determination of the wall surface temperature. The global heat balance methods entail the use of wall mounted thermocouples which have sometimes proved inaccurate. The surface temperature is automatically provided, on the other hand, by the local temperature gradient method.

The steady development of improved local temperature gradient method techniques has been achieved by Rose et al. [7,116-119]. One of their recent developments [118] used a set of thermocouples accurately cast in a thin epoxy (Araldite) strip. This strip was then placed in a thin slot machined into the back of their heat transfer plate. The advantages of this method were that it allowed very precise measurement of the postion of the ther-

mocouples and that the front surface of the plate remained smooth and unmarred.

This technique was used with minor changes in the current research. Approximately 1.6 mm (1/16 inch) slots were machined into the back of the test plate to a depth of 25.4 mm. A mold was fabricated from two pieces of aluminum bar stock. A piece of aluminum sheet of the same thickness as the slots (1/16 inch) was used to maintain the correct separation of the mold. The mold was mounted on a board and clamps were added to hold the thermocouple wires taut during molding. The thermocouple emplacement is shown in Figure 3.6.

The molding procedure began with welding of the thermocouples. The thermocouples were made from 0.254 mm E-type wire. All thermocouples in each strip were made from the same spool of wire for consistency. The mold was then prepared. Each mold surface was sanded with fine emery cloth to remove any traces of epoxy, then polished with 400 grit paper. The surfaces were then cleaned with soap and water. Finally, the surfaces were cleaned with acetone and a mold release was applied by spraying.

Four thermocouples were placed into the mold for each strip approximately 5-6 mm apart. The thermocouples were clamped in place. High-strength epoxy was then mixed and poured into the mold. The mold was then clamped tightly

shut. At least 8 hours were allowed for hardening, then the clamps were removed and the mold broken open. The strip was removed and the precise location of the thermocouple junctions was recorded. Then the strips were placed into the machined slots of the test plate. Thermocouples were connected directly to the thermocouple input boards of the data acquisition system to eliminate errors due to connectors.

3.4.2 Pressure, Temperature, and Composition Measurement.

The pressure, temperature, and mass ratio of air to steam must be measured in order to properly correlate the data. Although the experiment was designed to operate at approximately atmospheric pressure, pressure in the test section was measured using a Dwyer 424-5 inclined-vertical manometer and the static taps of a Dwyer 3.175 mm miniature Pitot tube. The barometric pressure in the lab was known hence the total pressure in the test section was determined. It was found during initial testing, however, that the pressure differences had a negligible effect on the results and they were not included in the later tests.

A total of 29 thermocouples were used during the experiment. These are summarized in Table 3.3. Nineteen of the thermocouples were used in the epoxy strips to measure heat flux and wall temperature. The temperature

of the injected film was measured at the film injection fitting. Two thermocouples were used to measure the inlet and outlet temperatures of the coolant in order to determine the global average heat transfer coefficient. One thermocouple was used to measure the steam temperature in the orifice meter. A thermocouple was also used to monitor the temperature in the hotwell.

Five thermocouples were used to monitor temperatures in the test section. The inlet thermocouple was used to monitor the temperature of the air/steam mixture at the beginning of the entrance length. Similarly an exhaust thermocouple was placed at the exit end of the test section. A traversing thermocouple was used to measure temperature profiles in the test section. During many of the experimental runs, the traverse and exhaust thermocouples were also used to indicate the temperature of the water film.

The final two thermocouples were located in the psychrometric probe. This probe was used to assure that a saturated mixture of steam in air was present. The psychrometric probe utilized two small diameter thermocouples, one of which was immersed in a wick. The wick was connected to a small reservoir of distilled water. During the experiment the steam flow and air preheat were adjusted so that the wet and dry bulb temperatures were

the same, hence a saturated mixture existed. After initial testing, precalculation of the correct preheat setting was found to be satisfactory and was used throughout the experimental test series.

3.4.3 Thermal Anemometry.

Hot wire and hot film anemometry have been used for taking velocity, turbulence, and interface measurements in these experiments. Although the use of thermal anemometry in determining velocity and turbulence parameters in air and water flows is common and well documented, its use in characterizing wavy interfaces and in steam flows has been rare. Akai et al. [1,2] has made use of hot wire/film probes in studies of horizontal cocurrent air-water and mercury-water flows. Brodowicz and Dyakowski [85] have used hot wires/films to measure the "pulsations" in the air along a vertical falling film. Reviews of the principles and use of hot wire/film anemometers are located in many references [120,121].

A TSI IFA-100 thermal anemometer was used throughout the current research. This anemometer is a modular, microprocessor-controlled, multichannel system capable of frequency response of up to 200 kHz depending on the probe and flow. The current system has two anemometer modules and two matching signal conditioning modules.

A variety of probes were used in the different test series. A standard TSI wire probe was used in the test section qualification (AIR) series. The 1210-T1.5 probe utilizes a 4 micron tungsten wire which provided very high frequency response in air flows. In the air-water isothermal test series, standard hot wire and film probes were initially used. The experimental conditions were well within the standard operating envelope of the probes. The 1210-T1.5 probe was again used to measure velocity and turbulence in the air. Two hot film probes, a 1212-60W and a 1218-60W, were used to take measurements of the wave amplitude and film thickness.

Although hot film probes are relatively rugged, the repair cost of replacing the sensors is high. The measurement of wave speed was also difficult with the factory probes. The wave speed measurement requires determining the time it takes for a wave to travel from one sensor to another. Due to the probe and sensor geometry required, none of the standard two-sensor TSI probes could be used. Using two separate probes to make the measurement was also not workable. Hence, special home-made probes designed for the wave speed measurement were required. Upstream probes for amplitude and film thickness measurements were then also constructed locally.

The probe bodies were constructed of 3/16 inch stain-

less steel tubing. The sensor supports were made out of plated brass pins. The supports were held in place by wire wraps then cemented into position on the body with high-strength epoxy. The sensors themselves were made from a spool of TSI platinum-iridium wire 12.7 microns in diameter. The configuration of the probes is discussed further in sections 5.2 and 5.4 and is illustrated in Figures 5.1 and 5.7.

The use of home-made probes made fast and inexpensive repair possible. Due to the materials with which they were constructed, the probes were also capable of functioning in steam environments. This capability was previously a subject of some concern with the TSI probes [122].

Calibration of thermal anemometry probes is an important aspect of their use. The calibration depends on a large variety of parameters including temperature, pressure, and composition. This calibration entails use of a primary standard (or known velocity) under conditions similar to those in which measurements will be taken. This fact is frequently one of the primary obstacles to use of thermal anemometry.

The demands of the current research for precise calibration were, fortunately, reasonably modest. The primary interest here was in the structure of the

interface. The measurements of the interfacial wave structure actually required no calibration whatsoever. The output signal levels were radically different depending on whether the probe was in the liquid or gas phase due to the large difference in heat transfer. The correlation of those large changes in signal levels, not the details of the individual signals was what gave an indication of the wave structure. The detailed methods used to conduct these measurements will be discussed later.

Some calibration of the probes was necessary for the air and air-water tests. The calibration of hot wire or hot film probes in air streams is simple and was used successfully. A Dwyer 3.175 mm miniature Pitot tube and Dwyer model 424-5 Inclined-Vertical Manometer were used as the velocity standard. The probes were calibrated using the usual King's Law form.

$$E^2 = a + b\,v^n \qquad (3.1)$$

where E = anemometer bridge voltage
v = gas velocity
a, b & n are experimentally determined coefficients

The HWCAL program written to generate the coefficients given a set of E and Δp_{pitot} (Pitot tube manometer reading) pairs. The Δp_{pitot} values were converted to velocity

using the known temperature and pressure in the lab. For a given value of the exponent n, a and b were computed from a least squares linear fit. The value of n was determined by an interative false position method.

The use of thermal anemometry requires quality support in the form of computer-based, high-speed data acquisition and reduction. This support has been procured and is described in detail in the Data Acquisition and Processing section.

3.4.4 Steam Flow Meter.

The velocity of the air/steam mixture is one of the primary variables on which the condensation heat transfer coefficient depends. Hence, its measurement was important to the success of the experiments. Use of the Pitot tube for such measurements is not usually considered reliable due to the problems associated with condensation inside the narrow passages of the tube and the small differential pressures which are measured. It was therefore necessary to measure the mass flow rate of the steam. Knowing this and the temperature of the air/steam mixture, one can relatively easily compute the velocity of the gas mixture.

There are many types of mass flow meters available, but the simple orifice meter was selected due to its ease of construction and wide application in steam flows. The

meter was designed following ISO standards using a standard flowmeter handbook [123]. The metering section was constructed of 51 mm (2 inch) diameter stainless steel tubing, welded to 102 mm diameter stainless flanges. Flange pressure taps were used. The square edge orifice plate was machined from 4.1 mm thick stainless. The orifice was 12.7 mm in diameter. The details of the meter's construction are shown in Figure 3.7.

The metering section was installed just downstream of the boiler in a vertical position with steam flowing downwards as recommended [123]. A Dwyer Model 4025 Capsuhelic differential pressure gauge was used to measure the pressure drop across the orifice. This gauge has a 1-25 inch water column scale and 3% of full scale accuracy. The gauge is connected to the metering section via a condensate trap. The trap also allowed for equalization and purging which prevented the accumulated condensate from blocking the lines and giving erroneous readings.

3.5 DATA ACQUISITION AND PROCESSING

3.5.1 Hardware.

A computer-based, high-speed data acquisition system is virtually required for detailed studies of turbulence and interfacial structures. In addition, automated data

collection and reduction from less demanding instruments was also desirable. An IBM PC-based system was selected for economy, versatility, and compatibility with existing equipment. A PC-based system is somewhat less powerful than the typical system used in thermal anemometry, but met the needs of the current research quite well.

The computer was a rack-mounted IBM PC equipped with the following equipment:

1) 640 kilobytes of memory,
2) 20 megabyte external hard disk system,
3) two 360 kilobyte floppy disk drives,
4) dot matrix printer,
5) color/graphics adapter,
6) RGB monitor,
7) Centronics parallel port,
8) two serial RS-232C ports,
9) 8087 NDP.

This system was interfaced to a Keithley Series 500 data acquisition and control system. The Series 500 is a modular system utilizing a 10 slot external mainframe cabinet into which input modules, signal conditioners, and analog-to-digital converters can be placed. This system uses bus extension architecture to allow high-speed data transmission from the external modules to the computer.

The mainframe uses its own shielded dataways to exchange data and signals internally. The configuration of the Series 500 is listed below:

1) AMM1 master analog input module including signal conditioning and A/D converter; 8 differential inputs are supported;
2) AIM7 analog thermocouple input module (includes automatic cold junction compensation); 16 channels are supported;
3) AIM7 (a second module with 16 additional channels)
4) DIO1 digital input/output module.

The Series 500 requires an adapter which is mounted in the PC. It includes a complete software library of BASIC-callable assembly language routines.

The Series 500 system is capable of data acquisition at rates up to 31.4 kHz for a single channel. Data rates for multiple channel acquisition are reduced. The maximum sampling rate for 10 channels, for instance, is approximately 1 kHz. The maximum sample size is limited by available memory in the PC. A built-in amplifier is available for acquisition of low-level signals such as thermocouples. Multiplexing allows a large number of channels to be connected.

The Series 500 was only marginally capable of handling

the high frequency turbulent fluctuations that are of interest in some of the expected flow situations. In order to extend the frequency range of the measurements and to increase the flexibility of the data acquisition system, a Nicolet digital oscilloscope was also used. The scope uses the model 4094A mainframe with model 4562 plug-ins. This scope is capable of sampling at speeds of up to 2 MHz on from 1 to 4 channels. A maximum of 15,872 data points total is available for all channels. The primary limitation in the use of the Nicolet is the long time required to transfer the data to the computer. A 9600 bps serial line is used which requires several minutes to dump the entire memory (15,872 samples) of the Nicolet to the PC.

In addition to the data acquisition equipment described above, the TSI IFA-100 hot wire/film anemometer was also remote controllable from the computer. The computer has access to most of the features of the anemometer and signal conditioner modules. Certain settings, such as bridge selection and operating resistance, must be set manually.

3.5.2 Software.

A complete system of software called CADAR (for Computer-Assisted Data Acquisition and Reduction) was

developed to allow fast, flexible data acquisition and reduction. This system allows access to the Keithley Series 500 DAS, Nicolet 4094 digital scope, and TSI IFA-100 hot wire/film anemometer. The system was designed in a modular structure to facilitate future expansion to new equipment or applications. Details of system operation are given in the CADAR User's Guide [124]. In addition to the CADAR system itself, a great deal of software was written during the course of the experiments in order to automate the data acquisition and reduction process. Table 3.4 gives a list of all of the software written during the course of the research. This section will discuss the general CADAR software only. The software which was written for more specialized data reduction purposes will be discussed in the section on data analysis.

In the CADAR system, data acquisition and reduction are done in two major stages. These stages and the data flow are illustrated in Figure 3.8. The first stage (testing phase) involves instrumentation setup, data set acquisition, conversion of the raw data into engineering units using a calibration curve, basic statistics, simple plotting, and permanent storage on disk. The second stage (post-test phase) includes more numerically intensive reduction of the data such as computation of Fast Fourier

Transforms (FFT's) or autocorrelation functions. The natural breakdown into these two stages comes as a result of consideration of the experimental procedure and of the capabilities of the available software.

The experimenter normally requires a limited amount of detailed data analysis while he is running the experiment. Hence, long-running or numerically intensive reduction programs can usually be run at a later time. The primary need for the actual laboratory testing phase is for rapid data collection and storage along with some simple monitoring of the results.

The functions during each phase of data acquisition and reduction are also very dependent on the programming language used. A large variety of language software is available for use with the IBM PC and each has its own advantages and disadvantages. In particular, the execution speed when doing numerically intensive computations is critical and varies widely. The experimenter is hardly interested in waiting for the computer to finish its calculations when the test rig is up and running. Therefore, the functions which should be included in the testing phase software are those which could be expected to execute quickly.

The Keithley Series 500 DAS was furnished with a package of assembly language subroutines, SOFT500, call-

able from the BASICA interpreter. This is a very powerful subroutine library and enables the power of the Series 500 to be easily and quickly accessed. The use of assembly language and 8087 NDP support enables the SOFT500 routines to execute extremely quickly. Unfortunately, any routines which were not supplied with SOFT500 were coded in interpreted BASICA which is rather slow in execution speed and does not utilize the 8087 NDP. Hence, use of a monolithic program to do all of the data acquisition and reduction was not advisable. This was particularly true since very numerically intensive work such as FFT's was anticipated. The use of BASICA and SOFT500 as a front end for acquisition and simple computations during the testing phase was therefore the preferred route. The large (1400 line) DATAC program was written to provide these functions. The program granted the user a great deal of flexibility and power in conducting the data acquisition portion of the experiments.

Late in the experimental program, Keithley released a compileable version of its data acquisition subroutines called Quick500 designed to work with the Microsoft QuickBASIC compiler. This version would allow the portions of DATAC or other programs coded in BASICA to run much faster. The DATAC program was ported to the Quick500 environment, but the combination of Quick500 subroutines

and Microsoft QuickBASIC compiler proved to be incredibly bug-infested. A stripped down version of DATAC, QDATAC, was eventually run successfully, but required a loss of too many important features to be useful in the current research. Therefore, the BASICA/SOFT500 environment and the DATAC program were used throughout the experiments.

Communication to the Nicolet 4094 digital oscilloscope was provided by the DATRAN program written in BASIC. Since no software library is used with this program, the BASIC source code was compiled under 87BASIC, an 8087-supported BASIC compiler, to generate a very fast program.

A standalone program was also written for complete access to all remote controllable features of the IFA-100 anemometer. This program was written in BASIC (compilable under 87BASIC). Its routines were also incorporated into DATAC.

The second stage, or post-test stage, of the data reduction process is primarily concerned with time-consuming or noncritical computations. A variety of language products are available for use including 87BASIC, various C compilers, Microsoft FORTRAN, and Ryan-McFarland FORTRAN. This is in part possible due to the specification of an ASCII format for the intermediate data files. The use of ASCII is not only advantageous from a flexibility point of view, but necessary since binary

(random access) file formats for BASICA (with or without SOFT500) and 87BASIC are not the same. The use of ASCII files does require significantly larger amounts of disk storage space however.

Second stage data reduction is extremely flexible. This enables future users to devise their own programs to manipulate the data in any way they wished. The CADAR system includes programs of fairly general interest for computation of autocorrelation functions, cross correlation functions and FFT's. The other data reduction programs were of a more specialized nature and are not included in the CADAR system itself although they were written to use the same file formats. This was mainly done to keep the documentation simple. These specialized programs are discussed in the sections on data analysis.

The FFT is computed using the SSPak [125] routine FFT which uses the FORTRAN algorithm of E. O. Brigham [126]. This FFT algorithm uses all real input data and folds it into meshed real and pseudo-imaginary vectors which allow more efficient computation. A variety of windows can be applied to the input data to limit leakage. The Papoulis window [127] has been used throughout the current research due to its excellent leakage reduction characteristics.

The AUTO program, which computes autocorrelation functions, uses a brute force integration approach. This

simple method is rather slow when compared to methods which use FFT's. However, since the AUTO program was only used sparingly during the course of the experiments time was not spent converting to a speedier algorithm. The cross correlation program, CROSS, also uses a simple integration algorithm. CROSS was used quite extensively in computing the wave speed, but its speed limitations were not found to be restricting.

TABLE 3.1

TEST SECTION DESIGN FLOW CONDITIONS

P = 1.013 bar (1 atm)

mass ratio air/steam	Tsat (C)	maximum mixture velocity (m/sec)
0	100.0	2.1
1	86.7	3.4
10	52.3	13.9
20	40.4	24.3
50	23.7	large

TABLE 3.2

ELECTRIC STEAM BOILER SPECIFICATIONS

Model: RH-36

Manufacturer: Reimers Electra Steam
Clearbrook, VA

Boiler Horsepower	-	3.6
Maximum kW	-	36
Voltage	-	480
Phase	-	3
Number of Steps (controller)	-	1
kg steam/hr (100 C)	-	56.8
Operating Pressure Range (bar)	-	0.7 - 8
Dimensions (cm)	-	W 135
		L 117
		H 84
Weight (kg)	-	311

TABLE 3.3

THERMOCOUPLES

steam	steam temperature at orifice
inlet	mixture at entrance to test section
traverse	mixture at beginning of plate
	or film at beginning of plate
psychrometer dry	dry bulb of psychrometric probe
psychrometer wet	wet bulb of psychrometric probe
exhaust	mixture at exit of test section
	or film at end of plate
coolant-in	coolant inlet manifold
coolant-out	coolant outlet manifold
film-inlet	injected film inlet
hotwell	water in secondary condenser hotwell
hf-1a	heat flux meter #1 t/c a
hf-1b	b
hf-1c	c
hf-1d	d
hf-2a	heat flux meter #2 t/c a
hf-2b	b
hf-2c	c
hf-2d	d

table continued next page

Table 3.3 continued

hf-3a	heat flux meter #3 t/c	a
hf-3b		b
hf-3c		c
hf-4a	heat flux meter #4 t/c	a
hf-4b		b
hf-4c		c
hf-4d		d
hf-5a	heat flux meter #5 t/c	a
hf-5b		b
hf-5c		c
hf-5d		d

TABLE 3.4

DATA ACQUISITION AND REDUCTION SOFTWARE

ARCHIV	writes data into archive files
AUTO	autocorrelation function
AVG	averages multiple spectra
AVGFFT	determines spectrum average
CROSS	cross correlation function
DACON	data conversion and statistics
DATAC	data acquistion from Keithley 500
DATRAN	data transfer from Nicolet scope
FFT	Fast Fourier Transform
FILM	computes film thickness, amplitude
FLOW	steam flow rate through orifice meter
HTFLUX	heat flux and heat transfer coefficients
HTS	precalculation of test rig parameters
HWCAL	hot-wire anemometer calibration curves
PRODAT	hot-wire anemometer data conversion
QDATAC	Quick500-compatible version of DATAC
RECALL	recovers data from archived files

table continued next page

Table 3.4 continued

SMOOTH	smooths frequency spectrum
SPECTRA	computes autocorrelation & FFT
VEL	computes test section velocities
VTPRO	assembles velocity profiles
WAVE	FFT preceeded by autocorrelation
IFACP	IFA-100 remote control

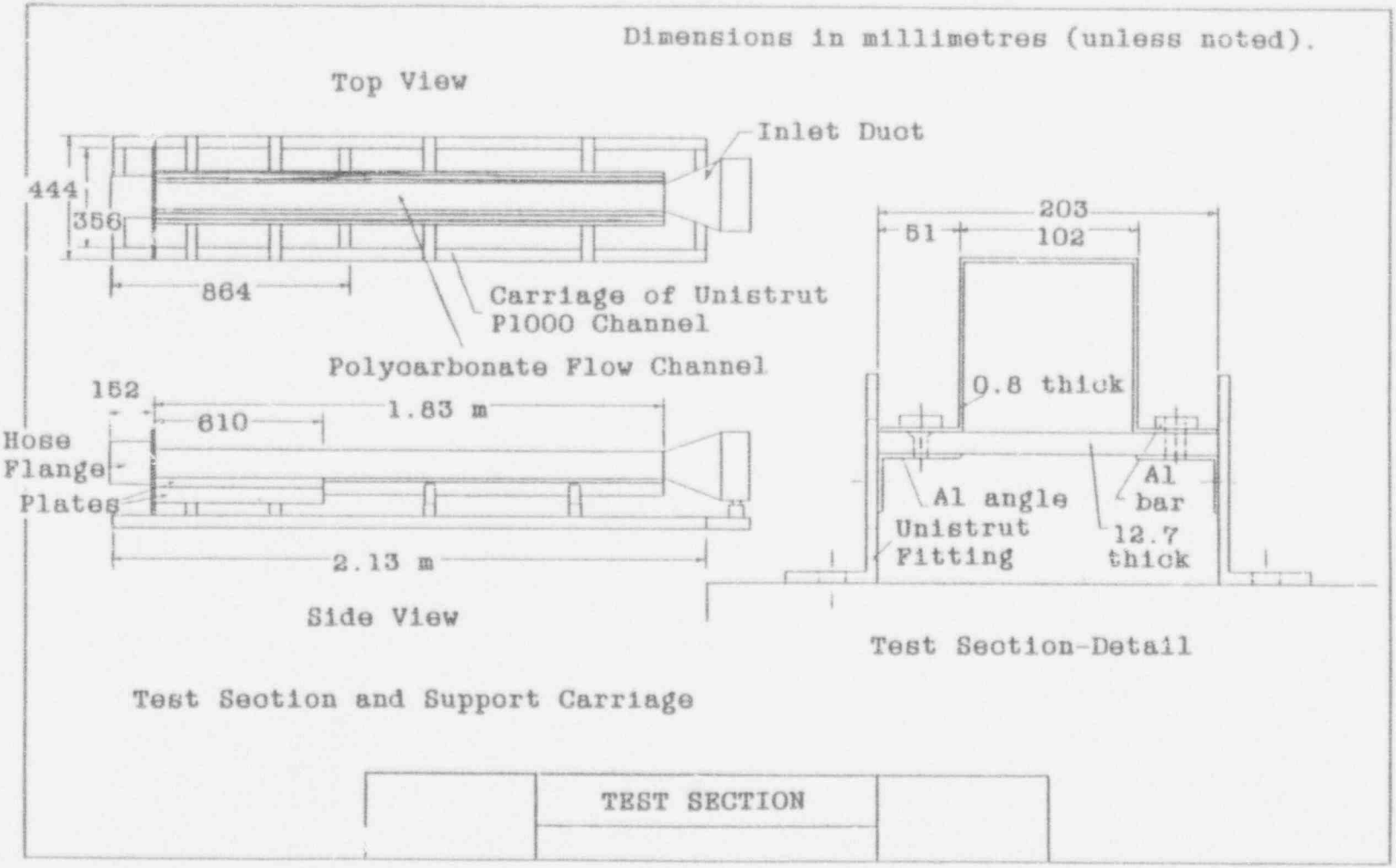

Figure 3.1 Test Section

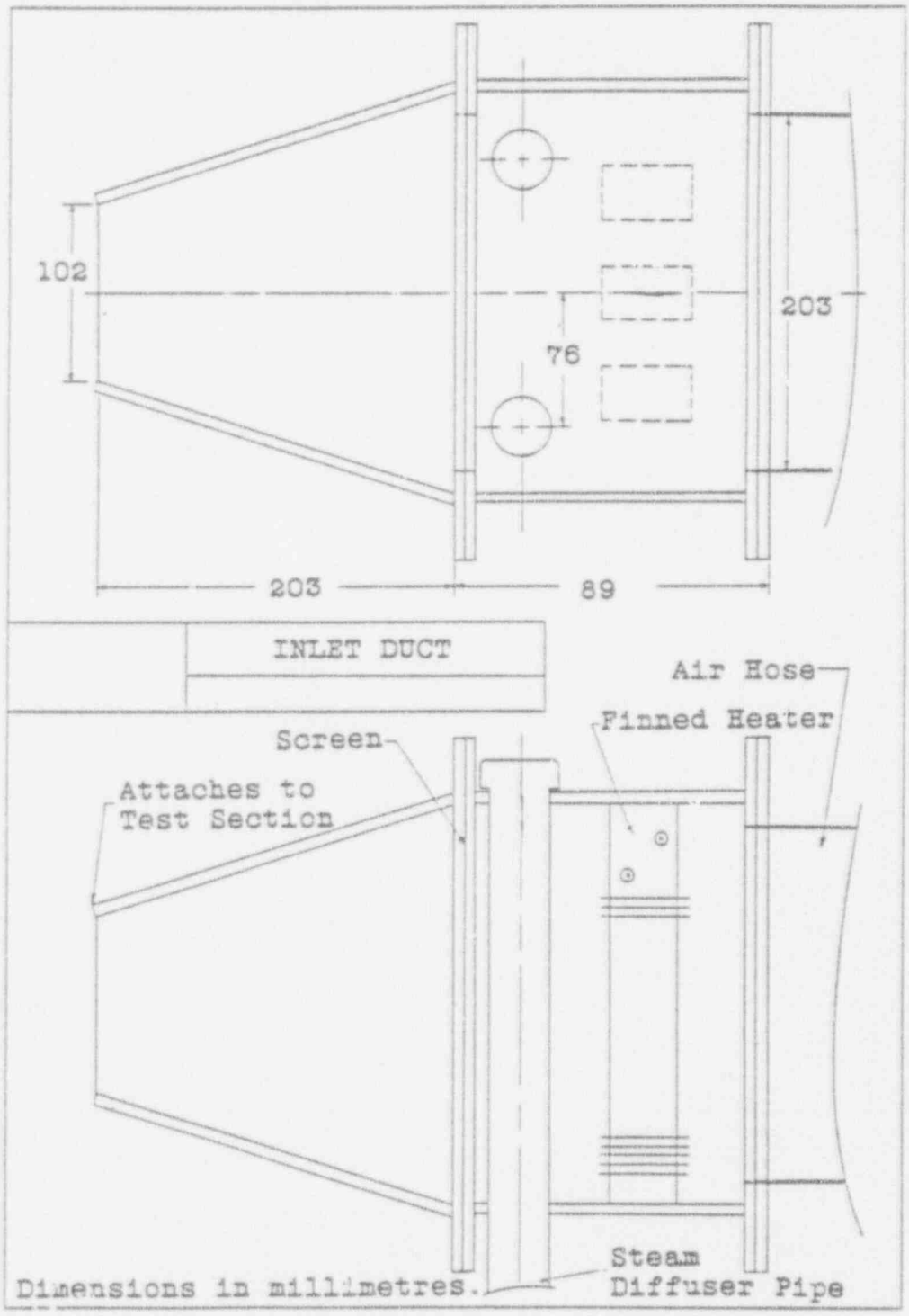

Figure 3.2 Inlet Duct

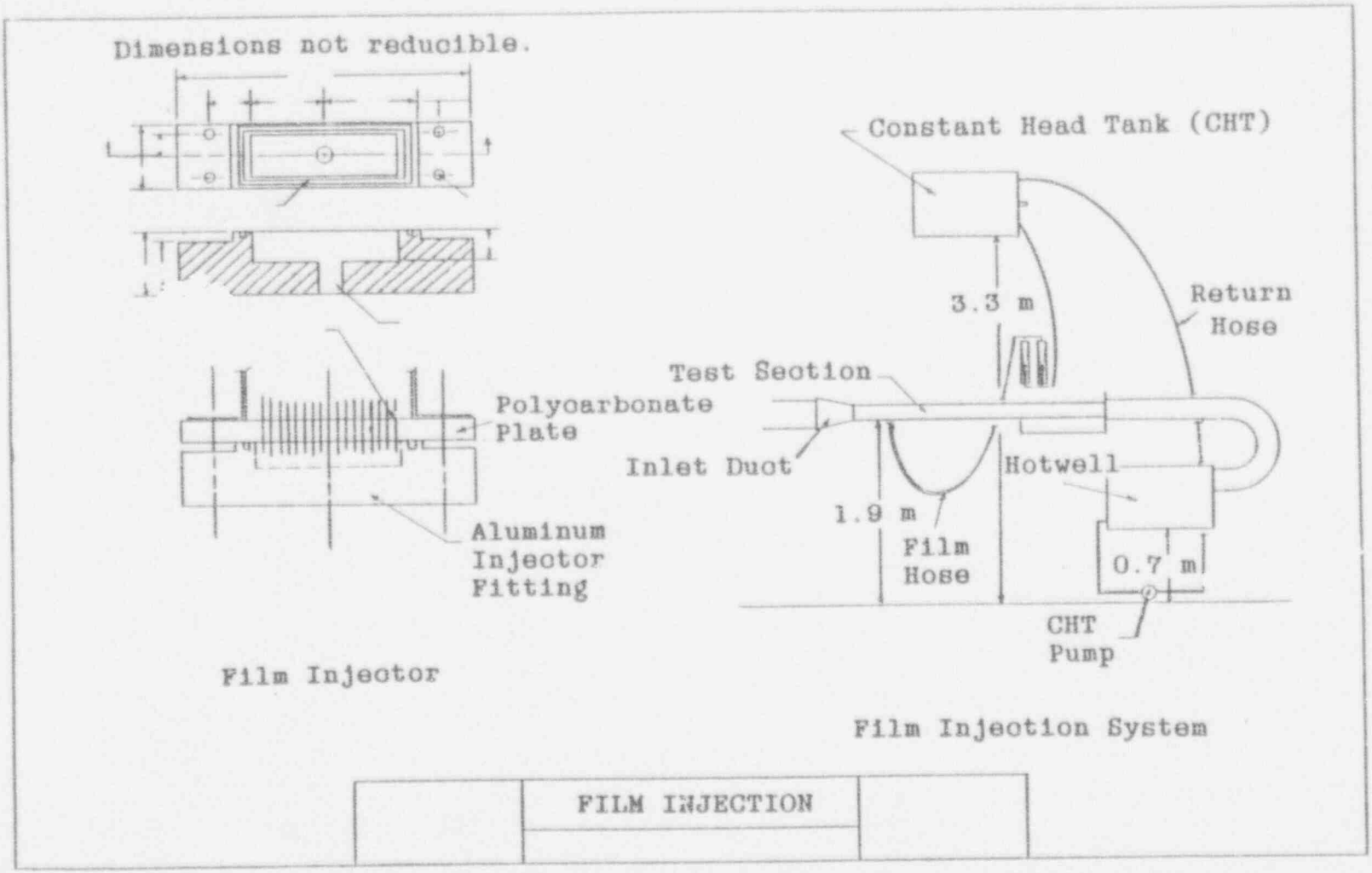

Figure 3.3 Film Injection System

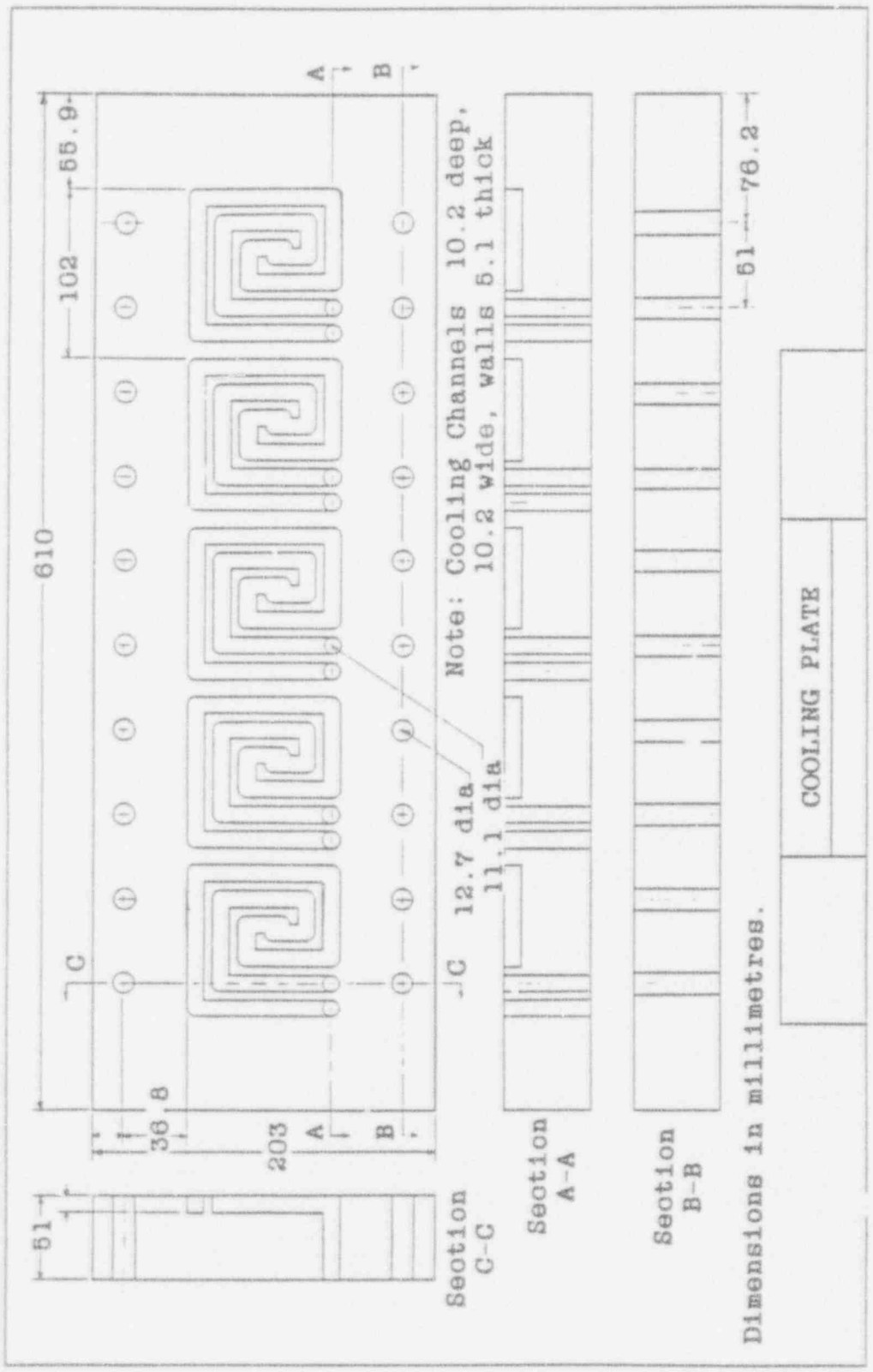

Figure 3.4 Cooling Plate

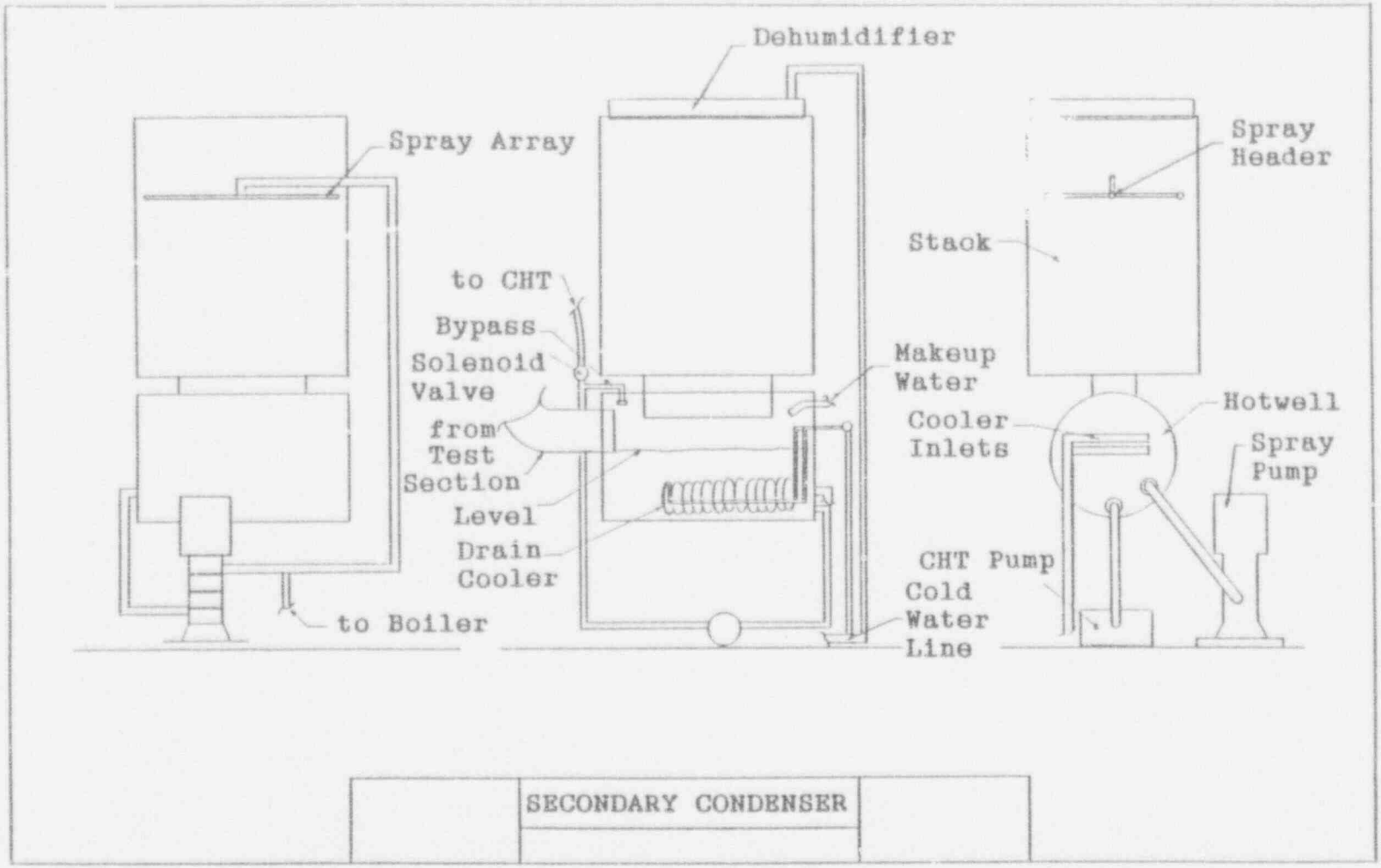

Figure 3.5 Secondary Condenser System

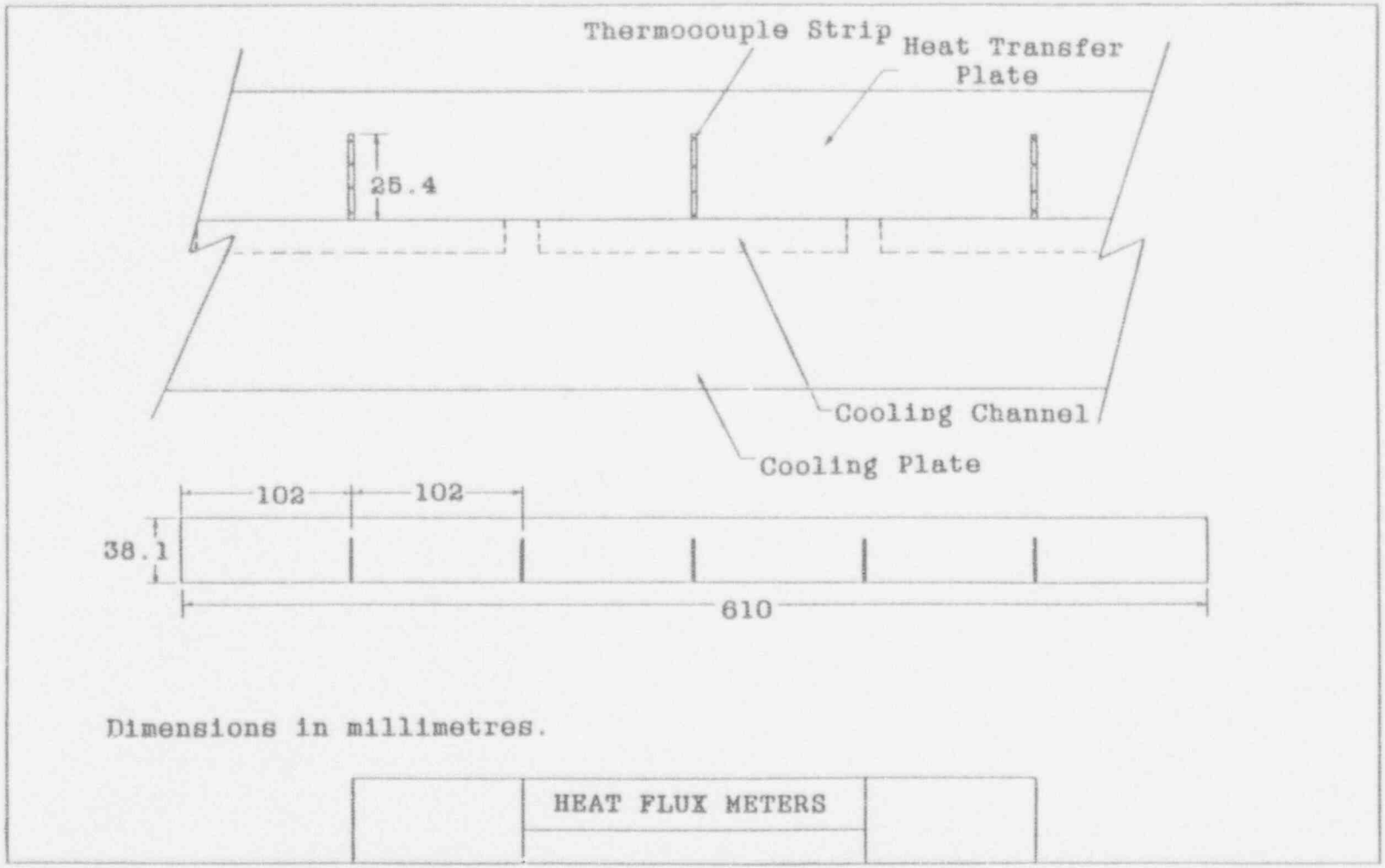

Figure 3.6 Thermoooouple Strip Emplacement

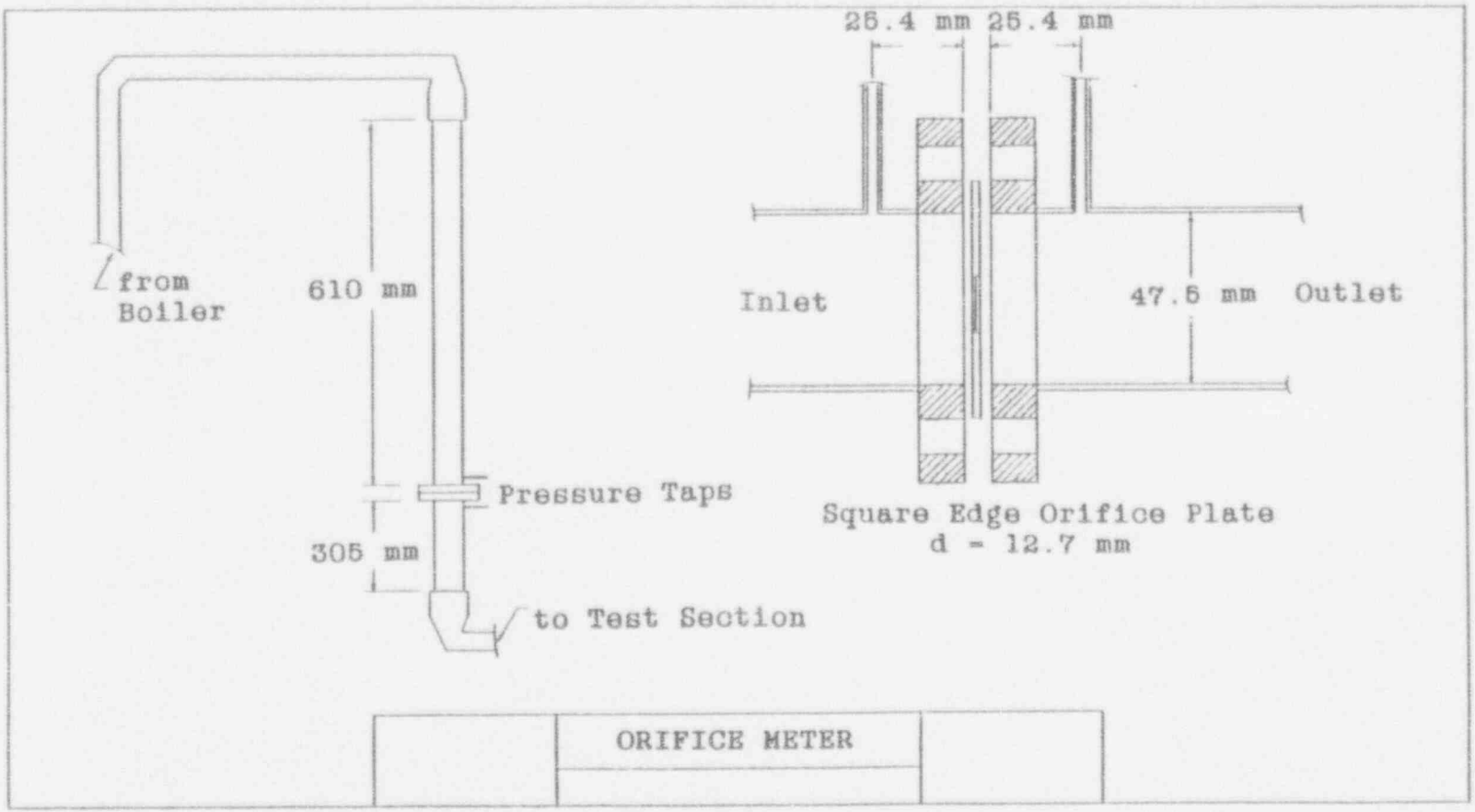

Figure 3.7 Orifice Flowmeter

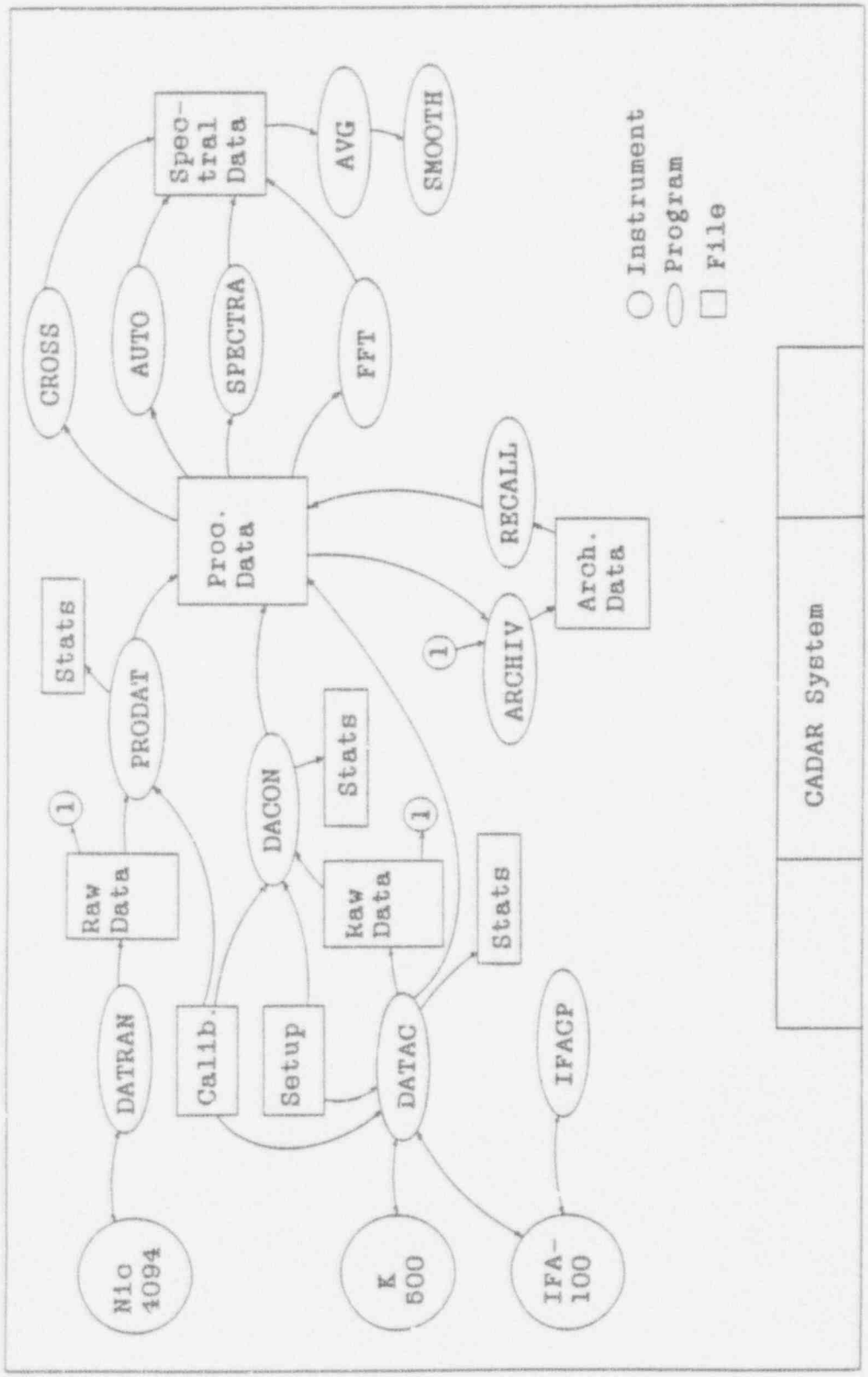

Figure 3.8 CADAR System

4. EQUIPMENT TESTING

4.1 INTRODUCTION

A great deal of both formal and informal testing of equipment was conducted during the course of the research. This was necessary because the experimental rig was completely new and no benchmark or operating characteristics were available as a guide. The following sections document some of the more important testing which occurred and which is considered important to the understanding and interpretation of the experimental results.

The information is also provided to assist future users of the experimental equipment in making efficient use of their time in design modifications and in planning experiments.

4.2 TEST SECTION

4.2.1 Air-Only Tests.

In order to become familiar with the characteristics of the test section and to assure that the basic design goals were met, a number of air-only tests were conducted. Both hot-wire and hot-film probes were used to conduct traverses of the test section to determine

velocity and turbulence intensity profiles. The probes were carefully calibrated against a Pitot tube throughout the range of flow velocities that were attainable in the test section. A typical calibration curve is shown in Figure 4.1.

Some measurements were taken with both hot-wire and hot-film probes. Velocity profiles taken with both probes looked essentially identical. The primary practical difference in the probes for these air measurements was that the 1210-T1.5 (wire) probe had a much higher frequency response than the 1218-60W (film) probe. This difference is evident in the turbulence intensity profiles shown in Figure 4.2. The film probe was unable to sense the high-frequency fluctuations that the wire probe detected. For this reason, the 1210-T1.5 probe was used for all of the following measurements.

The initial measurements were made before the addition of a second screen (located at the film injection fitting) and before the final inlet duct had been installed. Figures 4.3 and 4.4 shows typical velocity and turbulence intensity profiles under these conditions. The turbulence intensity is defined in the usual way (root mean square of the fluctuations divided by the mean). It was thought that the addition of the second screen might help reduce the "freestream" or centerline turbulence intensity. Such a

screen was added, but was attached only at the bottom. The test results then showed a slight reduction in turbulence intensity as well as a significant drop in the velocity. These results are also shown in Figures 4.3 and 4.4. The "for" and "cal" refer to the streamwise position. The "forward" and "calibration" stations were located about 120 mm and 460 mm, respectively, downstream from the leading edge of the cold wall.

During these latter tests however, it was noted that the screen seemed to be vibrating due to the fact that it was only held at the bottom. A power spectrum was generated which indicated a peak in the low frequency end of the spectrum at 12 Hz. A stroboscope was used to verify that this was the frequency of vibration of the screen. The turbulence intensity profiles also indicated an increased turbulence intensity towards the top of the test section. The screen was then clamped at the top and the tests were repeated to show that the frequency peak had been removed. This is shown in Figure 4.5. Another vibration at about 1200 Hz, which was believed to be due to the operation of the blower motor (1050 rpm) was also detected, but was easily damped. This is also well above the frequencies of interest during most of the measurements and was filtered out using the low pass filters of the anemometer signal conditioner.

The velocity and turbulence intensity profiles were again measured after the final inlet duct was installed. Figure 4.6 shows the velocity profiles at low and high speed. Both profiles show a relatively flat region in the center of the duct which indicates that the flow can be considered a reasonable approximation to flow over a flat plate. This is especially the case at lower speeds which is fortunate, as most of the heat transfer measurements were later taken at low to moderate velocities.

The turbulence intensity profiles are shown in Figure 4.7. Here it is important to note the relatively low centerline turbulence intensities as compared to those in the vicinity of the wall. This is certainly what one would expect and gives some assurance that heat transfer in the vicinity of the wall will not be strongly affected by the freestream turbulence values.

Traverses were also made during tests in which a 3 lpm film (Re = 490) was injected. The velocity, shown in Figure 4.8, behaves about as one would expect. The shear stress in the vicinity of the rough, wavy film is sharply increased. It is reassuring to note, however, that the flow in the rest of the channel remained very similar to flow without a film. This again indicates a reasonable approximation to a flat plate flow. The turbulence intensity in the vicinity of the film is also greatly in-

creased, as expected, also reaffirming that heat transfer to the film would be relatively insensitive to freestream turbulence levels. This is shown in Figure 4.9.

4.2.2 Air-Steam Test.

A test was conducted to assure that the air and steam had achieved reasonable mixing by the time the flow reached the heat transfer plate. The temperature profile in the test section was measured by traversing a thermocouple probe. This profile is shown in Figure 4.10. The conditions of the test were T_{mix} = 85 C and v_g = 3 m/s. There was no injected film. The profile shows a very uniform temperature profile across the test section which indicates that the mixing of the air and steam was indeed quite good.

4.3 COOLING CIRCUIT FLOW BALANCE

The five coolant circuits which cool the back of the test plate were tested to verify that approximately the same coolant flow was delivered to each circuit. In the current experimental configuration, only the average heat transfer coefficient over the entire plate can be measured by coolant measurements. The total coolant flow is measured by a rotameter. The temperatures of the inlet and

outlet coolant streams are measured at their respective manifolds. In these experiments, precise balancing of each individual cooling circuit to provide a specific boundary condition in the test section was not necessary. Nevertheless, an approximate knowledge of the flow rate in each circuit was desirable for interpretation of the data and for verification that the manifolds were working properly.

The flow in a circuit was measured by disconnecting the outlet tubing just before it entered the outlet manifold, while leaving all of the other circuits connected. The heat exchanger pump was then started and the time required to fill a container with 2 litres of coolant was recorded. The tubing was then reconnected and the operation was repeated with the next circuit. Duplicate measurements were made for three of the circuits and showed very good repeatability.

The results of the flow balance test are shown in Table 4.1. The tests showed that the #2 and #5 circuits were about 10% low and high respectively, with the other three circuits in very close agreement. The flow rates based on the time required to pump 2 litres were computed and totalled. The total flow of 18.5 litres/min (lpm) agreed quite well with the readings for the total flow taken from the rotameter.

No attempt was made to fine tune using the individual circuit valves. The measurements involved sufficient enough uncertainty that the results of such an effort would have been questionable. The measurement technique, although somewhat crude, did verify that there was no systematic change in the flow which depended on the position of the circuit in the manifold. This indicates that the manifold was working well and that the system could perform its function without detailed tuning.

4.4 ORIFICE FLOW METER

The orifice flow meter which was used to measure the steam flow was thoroughly tested in order to verify its accuracy. Measurement of the mass flow rate of steam was used to compute the gas mixture velocity in the test section, which was one of the primary independent variables in the experiments. Although the flow meter was constructed following the ISO/ANSI standards, independent verification was highly desirable.

Testing of the flow meter was difficult, however, since no other more reliable meter was available. The meter was therefore tested indirectly by two methods. In the first method, the gas mixture velocity in the test section was measured using a Pitot tube. The second

method involved performing an energy balance on the boiler.

Use of a Pitot tube to measure velocities in steam flows is not a very reliable method. The velocity pressures which were expected were of the order of hundredths to tenths of an inch water column. When one considers the possibility of steam condensing inside the tiny passages of the Pitot tube, substantial errors could clearly be generated in such pressure readings. Nevertheless, with care and a certain amount of good fortune, the Pitot tube was made to work.

In testing the orifice meter, the Pitot tube passages were blown clear of condensate prior to startup of the experiment using compressed air. The air preheaters and blower were then run for several minutes before the first introduction of steam to warm up the tube as well as the rest of the test section. Using these precautions, the Pitot tube results were sometimes acceptable, particularly at higher velocities where the higher velocity pressure was less sensitive to errors. Although certainly not a good standard, the Pitot tube results were still useful as an independent indication of steam flow rate.

A somewhat more robust method of testing involved a simple energy balance on the steam boiler. In this method, the percentage of time the boiler's electric

resistance heating elements were turned on was measured. Knowing the operating pressure and feedwater temperature of the boiler and therefore the heat required, the mass flow rate of steam could be computed. Typically the measurements were taken over about a 15 minute interval. At typical steam flow rates, the boiler pressure controller switched the heaters on and off on a 1-2 minute period. Hence the measurements were taken over the average of several periods.

One problem with this method, however, comes about due to the operation of the boiler level control. The deadband of the controller is fairly wide. Therefore feedwater is introduced to the boiler fairly infrequently, depending on the steam flow rate. The period of this controller was generally much longer and varied between about 2 and 10 minutes. Clearly the measurements would often not cover enough cycles of the level controller to provide a good average feedwater flow.

This problem was accounted for in the data by computing two estimates of the steam flow rate. The first estimate includes the sensible heat required to heat the feedwater to saturation temperature as well as the latent heat of vaporization. This is obviously the strictly correct estimate and the results should approach this if the measurements are rade over enough cycles of the feed-

water controller. This is called the low estimate. The high estimate simply ignores the sensible heat and computes the steam flow only using the latent heat of vaporization. Clearly the steam flow should not exceed this estimate. These estimates are listed below.

$$v_{lo} = \frac{f\ P}{\rho_s\ A\ (i_{vap} + \Delta i)} \qquad (4.1)$$

$$v_{hi} = \frac{f\ P}{\rho_s\ A\ i_{vap}} \qquad (4.2)$$

where f - fraction of time heaters are on

P - boiler heater power (36 kW)

ρ_s - density of steam at test section temperature

i_{vap} - heat of vaporization

Δi - enthalpy change from feedwater to saturation in boiler

The results of some of the orifice flow meter tests are shown in Table 4.2. Many tests were conducted throughout the course of the experiments since several changes were made in the design of the condensate traps and in the type of differential pressure gauge used in order to increase the accuracy and repeatability. By the end of the modification and testing period, the flow meter was found to give fairly consistent results and was used

with a reasonably high degree of confidence throughout the remainder of the heated test program.

One important benefit of testing the flowmeter was that there was a serious error found in the flowmeter handbook [123] that was used to design the metering section. Fortunately, the error did not affect the design of the section or orifice plate. The error was located in the calculation procedures and sample computer programs which are given in the handbook for calculating the steam flow rate from the differential pressure. Due to an initial lack of agreement between the orifice flowmeter results and those of the testing methods described above, the equations were rigorously rederived and cross-checked with several other references and the error was discovered.

4.5 HEAT FLUX METERS

The heat flux meters were tested to assure accuracy and repeatable results. The accuracy of these meters was important because they provided almost the entire heat transfer measurement capability. The meters were the primary source of heat flux measurement. In addition, the temperature profiles measured with the meters were used to determine the surface temperature of the heat transfer

plate.

Initially there were only two heat flux meters in use because there was only one AIM7 thermocouple input module for the Keithley data acquisition system. This limited the total number of thermocouple inputs to 16, which only was enough for two four-thermocouple meters plus the other necessary monitoring thermocouples. The tests of the these two heat flux meters also indicated that the thermocouples were placed too close together in the epoxy strip. This limits the accuracy of the meter and will be discussed further in the Limitations and Procedures section.

Shortly after these initial tests, a second AIM7 module was purchased. The two original thermocouple strips were also torn out. Five new thermocouple strips were constructed following the procedures which have been discussed in the Facilities section. These strips were made with the thermocouples spaced out as far possible and resulted in significantly better accuracy. The remainder of this section will discuss only the five "new-model" heat flux meters.

During installation of the thermocouple strips, the #3 strip was apparently cracked. This broke the 4th thermocouple (3d) in the strip. The break was not discovered until the test section had been completely reassembled, so

it was not repaired. The readings of the #3 meter were unexplainably out of line with the readings of the other four meters throughout the tests. The cracking of the epoxy may also have changed the positioning of the other thermocouples in the strip and caused this problem. For this reason, the results of the #3 meter are shown in this section to illustrate the problem, but were not used in the remainder of the research work.

The values of the heat flux generated by the meters were repeatedly compared to the overall heat flux computed from the coolant measurements throughout the course of the research program. A sampling of results for the overall heat flux as compared with the average of the heat flux meters is shown in Table 4.3. This comparison shows that the meters do appear to be generating accurate readings. The mean heat flux computed from 4 (excluding #3) and 5 (including #3) meters are included. Similar results can be seen in Table 6.5 for the heated runs without film. A plot of the typical temperature profile for one of the heat flux meters is shown in Figure 4.11. The linearity of the profile is clearly excellent.

The repeatability of the heat flux meters was also tested. Four sets of data were taken under the following test section conditions:

T_{mix} - 70 C

v_g - 3 m/s

T_{surf} - 25 C

Q_{film} - 0 lpm

The data is shown in Figure 4.12. The scatter of the data is clearly within the error bar on a single measurement.

The effect of two-dimensional heat flows in the heat transfer plate was shown to be negligible. The test section and cooling plate were well insulated with at least 5 cm of fiberglass. In addition, the average temperature of the heat transfer plate was usually in the range of 15-25 C. Using a typical room temperature of 22-25 C, a simple hand calculation of the heat flux through the insulation yielded a leakage heat flux of about 5-10 W/m^2. This is about three orders of magnitude smaller than than the condensation heat flux.

4.6 HEATED EXPERIMENTS - LIMITATIONS & PROCEDURES

4.6.1 Introduction.

The conditions which may be achieved in the test section are limited by many factors. These include the capacity of the steam boiler and air blower, the minimum differential pressure of the boiler pressure controller, the minimum accurate differential pressure on the orifice

meter pressure gauge, and the temperature resolution of the thermocouples. Unfortunately most of these effects are very interconnected and must be considered almost simultaneously in order to operate the experimental rig. The following sections try to break down the limitations by their source. The last section describes a computer program that was written to generate a set of operating parameters for a given set of desired experimental conditions. This was used throughout the heated experiments as a guide to setting up the test rig.

4.6.2 Materials.

The temperature at which the test rig may be operated is slightly limited by the materials which are used. As was mentioned in the design section, the polycarbonate material used to construct the test section was selected over acrylic for its resistance to temperature. No strict upper temperature is given by the manufacturer for the polycarbonate, but it is said to retain significant strength up to 120 C. This is well above any operating temperature contemplated here. There was, however, a good deal of warping of the polycarbonate channel due to stresses when the test section was heated above about 85 C.

Another temperature limitation was the large diameter

hoses which connected the test section to the blower and the secondary condenser hotwell. During operation of the apparatus at temperatures of about 90 C or greater, a black material was found in the inlet duct. Although no failures occurred and none of the material appeared in the test section, it appeared that runs above 90 C are ill advised, at least until the potential problem can be further explored.

Neither of these problems was considered to be detrimental to the experimental program since both occurred at temperatures above the range where most of the runs were planned.

4.6.3 Boiler & Blower Capacity.

The air/steam mixture velocities in the test section are limited due to the capacity of the steam boiler and air blower. Further limitations on the low velocity end of the spectrum are due to the boiler pressure controller and the orifice meter and will be discussed later.

In the section on the design of the test section, the maximum attainable velocities were computed based on the design capacity of the boiler. Table 4.4 lists a new set of maximum attainable velocities based on experience in operating the test rig. Although not all of these have been verified, they represent a good estimate of the

capabilities of the apparatus.

The limitations due to the boiler capacity are in the low mass ratio (high temperature) region above about 60 C. Here it was found that a maximum duty cycle of about 80% for the boiler heaters represented about the highest steam flow that could be maintained without large deviations from the desired pressure.

The air blower capacity limits are manifested in the high mass ratio (low temperature) region, below about 60 C. The maximum velocity achievable in the test section under air-only conditions was about 12 m/s. The velocities attainable under heated conditions were much less however due to the additional pressure drops of the secondary condenser sprays and to the backpressure of the steam injection. It is interesting to note that the maximum velocity at 50 C is less than the maximum achievable at 60 C. This somewhat anomalous result was noticed in testing. The velocity tended to rise again below 50 C however.

As a practical matter, it was found that operating at or near the maximum velocities was undesirable based on other problems as well. As the velocities were increased, for instance, the secondary condenser system was less and less able to recover excess steam from the flow. Makeup water was then required to be added at a larger than

normal rate. Under maximum velocity conditions, the test rig might consume as much as 18 to 20 litres per hour. Since distilled water from the Nuclear Reactor Laboratory still was used as makeup, such large flows were undesirable.

4.6.4 Pressure Controller and Pressure Gauge.

The limitations of the boiler operating pressure controller and the orifice meter's differential pressure gauge worked in a combined fashion to restrict the velocities on the low end of the range. These limitations worked in the following way.

The boiler's operating pressure control has an adjustable differential pressure band in which it tries to maintain the steam pressure in the boiler. Unfortunately, since the boiler was not designed for precision experimental use, the minimum differential pressure to which the controller can be set is about 5 psi. In other words, the boiler pressure would oscillate about 5 psi during normal operation. Therefore, in order to prevent large temperature oscillations in the test section, it was desirable to make the pressure oscillations small in comparison to the total pressure by maintaining a relative high boiler pressure.

The differential pressure gauge which was used to

sense the pressure difference across the orifice plate encountered a different problem. In order to minimize the effects of condensation in the lines, a relatively large differential pressure should be maintained. A differential pressure of about 15 inches of water (full scale is 25) was found to give good performance. In addition, a reading of about 20 in. H_2O generally corresponded to about the maximum desirable steam flow (80% of boiler capacity). Thus 15 in. H_2O was found to be an excellent target value.

The problem is that the two limitations (controller and gauge) were working in opposite directions. For a given set of test section conditions, if the boiler pressure was increased to reduce the controller oscillations, the steam flow and the differential pressure across the orifice plate would decrease. Unfortunately, the point at which the situation became a problem was located at test section conditions which were of interest. Table 4.4 shows the estimated minimum velocities.

This limitation could most easily be reduced by using a pressure controller with a smaller differential setting. This is being reviewed for use in future research.

4.6.5 Coolant Flow.

Limitations on the range of coolant flow are due

several factors, most of which were interrelated. The coolant flow rate available from the refrigerated heat exchanger ranges from about 0-20 lpm. The rotameter used to measure this flow has a 2-20 lpm range, but also has a 2% of full scale error. In order to be assured of limiting the flowmeter error, a minimum flow rate of 6 lpm was maintained in the cooling loop. This kept the error down to about 6.7%.

The coolant flow rate was also limited by the total amount of heat which was transferred. In order to determine the overall heat flux through the heat transfer plate, the flow rate and the temperature rise across the manifolds were measured. The thermocouples (coupled with the data acquisition system) used to measure the temperature in the manifolds have a maximum resolution of 0.08 C. In order to keep the error made in determining ΔT_{cool} below about 10%, the coolant flow rate was kept low enough so that ΔT_{cool} was greater than about 1.2 C. In some cases where the heat flux was sufficiently low, the coolant flow rate would have needed to be reduced to below 6 lpm. In these cases the flow rate was set to 6 lpm and the error in ΔT_{cool} taken into account.

The coolant flow rate also affects the heat transfer coefficient from the coolant to the back of the heat transfer plate. In some cases, therefore, the coolant

flow rate was also adjusted to assist in attaining the desired wall temperature boundary condition in the test section. This was because this boundary condition was controlled indirectly by the coolant temperature and the heat transfer resistances. This will be discussed in more detail in the section on the precalculation program.

4.6.6 Heat Flux Meters.

The contraints in the performance of the heat flux meters was also caused by the limited resolution of the thermocouples. The design of the heat flux meters utilized four thermocouples placed about 5 mm apart. Using the simple criteria that the temperature difference across the entire strip should be 1.2 C or better (for 10% error considering only two thermocouples), the minimum heat flux could be computed:

$$q = k \, \Delta T_{hfm} / \Delta x_{hfm} \qquad (4.3)$$

where q - heat flux

k - thermal conductivity

ΔT_{hfm} - total temperature difference

Δx_{hfm} - spacing of furthest thermocouples

For ΔT_{hfm} - 1.2 C and Δx_{hfm} - 20-21 mm, the value of the minimum heat flux, q, is about 8000-8500 W/m^2. This is a relatively large heat flux, particularly for the runs

which were undertaken without a film. Fortunately, since in reality there were four thermocouples per meter and the temperature gradient is determined by a least squares fit, the error is somewhat less than that which is given here. A complete error analysis was conducted for the heated tests.

4.6.7 HTS Program.

Due to the complicated interdependencies of the various variables used in setting up the test rig for a run, a computer program called HTS (for heated test series) was written. Using this program and some experience, the experimenter could achieve the test conditions desired with a minimum of wasted effort. The following will discuss the procedure used in HTS and in using its results to set up the test rig.

The temperature of the air/steam mixture (T_{mix}), the velocity of air/steam mixture (v_g), the temperature of the heat transfer surface (T_{surf}), and the Reynolds number of the film (Re_f) were the primary independent variables in the heated experiments undertaken. The parameters that the experimenter had under his control, however, were the boiler pressure (P_{boil}), position of the steam throttling valve, position of the air blower control, heat sink (coolant) temperature (T_{sink}), coolant flow rate (Q_{cool}),

film flow rate (Q_{film}), and air preheater power ($P_{preheat}$). This is summarized below:

Independent Variables:	T_{mix}
	v_g
	T_{surf}
	Re_f
Controlled Parameters:	P_{boil}
	steam flow valve
	air blower control
	T_{sink}
	Q_{cool}
	Q_{film}
	$P_{preheat}$

It was clearly necessary to relate the two sets of variables. For Re_f, the relationship with Q_{film} was simple and direct. For the others, however, it was usually not so simple. The film's effects on the other aspects of the problem were either negligible or unknown and were therefore ignored in the HTS analysis.

Using the desired values of T_{mix} and v_g, the steam flow and air flow could be calculated from the following equations.

$$\rho_s = \rho_g(T_{mix}) \qquad \text{(EOS)}$$

$$P_s = P_{sat}(T_{mix}) \qquad \text{(EOS)}$$

$$R = 1.611\ (P_{tot} - P_s)/P_s \tag{4.4}$$

$$\rho_a = R\ \rho_s \tag{4.5}$$

$$m_a = \rho_a v_g A_{ts} \tag{4.6}$$

$$m_s = \rho_s v_g A_{ts} \tag{4.7}$$

where ρ_s = density of steam

ρ_a = density of air

P_s = steam partial pressure

P_{tot} = total pressure

R = mass ratio of air/steam

m_a = mass flow rate of air

m_s = mass flow rate of steam

A_{ts} = cross sectional area of test section

The known steam flow was then used to compute the required Δp_{orif} if the boiler pressure was specified. The calibration curves for the orifice meter were generated by the FLOW program for several different P_{boil}. The pressure difference was then computed across the orifice.

$$m_s = K\ (\Delta p_{orif})^{0.5} \tag{4.8}$$

where $K = f(P_{boil})$ from FLOW

$$\Delta p_{orif} = (m_s/K)^2 \tag{4.9}$$

A simple energy balance was used to compute the preheat

power, then the conversion to the variac units (85 equals 1425 W full power) was made.

$$P_{preheat} = m_s(i_{s1}-i_{s2}) - m_a C_{pa}(T_2-T_1) \quad (4.10)$$

$$\text{variac setting} = 85\ P_{preheat}/1425 \quad (4.11)$$

where C_{pa} - specific heat of air

i_{s1} - steam enthalpy before mixing

i_{s2} - steam enthalpy after mixing

T_1 - air temperature before mixing

T_2 - air temperature after mixing

This concludes the first portion of the analysis.

The second portion of the analysis uses the known or predicted heat transfer resistances to calculate heat flux related values. The condensation heat transfer coefficient was first calculated using the CWNG code [3]. Then the flow rate of coolant was computed based on the limitation in temperature difference across the manifolds discussed earlier.

$$q = h_{avg}(T_{mix} - T_{surf}) \quad (4.12)$$

$$Q_{cool} = q\ A_p/(C_p \Delta T_{cool}) \quad (4.13)$$

where q - average heat flux

h_{avg} - condensation heat transfer coefficient (CWNG)

A_p - area of the heat transfer plate

The heat sink temperature remains to be computed. In order to determine it, the heat transfer coefficient from the coolant to the back of the heat transfer plate must be known. This was measured on several occasions by using T_{back}, or the temperature of the back surface of the plate, which was found from the least squares fit of the heat flux meter data. Initially a Dittus-Boelter form was selected which seemed to fit the data well.

$$h_{cool} = (Q_{cool}/18 \text{ lpm})^{0.8} 5000 \text{ W/m}^2\text{-C} \quad (4.14)$$

where h_{cool} - coolant heat transfer coefficient

This later was abandoned in favor of a constant value, h_{cool} - 2300 W/m^2-C. Neither value was entirely satisfactory, but further work on this was left to future users.

The above computation procedures were coded into the HTS program. The typical use of the program went as follows. The user first specified the values of the independent variables T_{mix}, v_g, and T_{surf}. The next step was to run the CWNG code to compute an estimate of the condensation heat transfer coefficient, h_{avg}. CWNG only requires the value of those three independent variables and the dimension of the heat transfer plate as input and

runs in a minute or two on an IBM PC. Therefore it was very handy for running these quick precalculations.

An input file for HTS was then edited. This file contained the values of the three independent variables and the heat transfer coefficient calculated by CWNG. The HTS program was then run. A menu of possible boiler pressures was displayed to the user. After selecting a P_{boil}, the code calculated Δp_{orif} and the preheat setting and displayed their values on the screen. The user then decided whether to select a different pressure or to complete the calculation with the previously selected pressure. The general rule of thumb which was followed was to select a fairly high P_{boil} as a start, and to reduce it until Δp_{orif} became about 15 in. H_2O. This frequently necessitated a compromise on the desired values. After the user had made a final selection of the boiler pressure, the program finished and a report was written. The report contained all of the input values as well as a complete listing of the output parameters in the appropriate engineering units.

When the experiment was run, the normal procedure was to set the preheat and cooling water flow rate to the figures in the report. Then the steam flow was adjusted until it matched the desired value of Δp_{orif}, then the air flow was adjusted for the correct T_{mix}. After this had

been done, T_{sink} was adjusted to give the correct T_{surf} using the heat flux meters and the HTPLUX program. This latter adjustment was very time-consuming due to the long (15-30 minute) time constants of the coolant loop and plate. The details of the operation of the test rig are given in the Condensation Heat Transfer Loop Operation and Maintenance Manual [128].

TABLE 4.1

COOLING CIRCUIT FLOW BALANCE

Circuit	Time (sec)			% Diff. from	
#	Trial 1	Trial 2	Mean	Overall Mean	Flow (lpm)
1	33.1		33.1	+2.2	3.6
2	29.3		29.3	-9.6	4.1
3	32.4	31.8	32.1	-0.9	3.7
4	30.7	33.4	32.1	-0.9	3.7
5	36.0	34.8	35.4	+9.3	3.4

Overall mean = 32.4 sec Total = 18.5 lpm

Resolution = 1 sec (3%)

TABLE 4.2

ORIFICE FLOWMETER COMPARISON

Test	T_{mix} (C)	Mass Ratio	metres/sec V_{orif}	V_{pitot}	V_{lo}	V_{hi}
therm-0a*	46.	14.2	9.4	9.8	-	-
therm-6 *	81.3	1.63	3.2	2.1	2.8	3.6
therm-8 *	68.1	4.01	5.6	6.3	4.8	5.7
therm-10*	70.4	3.52	5.4	6.1	5.4	6.4
therm-12*	45.8	14.2	10.8	9.4	8.6	10.1
therm-23*	71.4	3.31	3.9	6.3	5.0	5.9
therm-25	68.7	3.92	4.9	-	5.2	6.2
therm-26	67.9	4.12	5.1	-	5.2	6.2

* Denotes tests performed before differential pressure gauge was in final configuration.

TABLE 4.3

HEAT FLUX METER COMPARISON

(W/m^2-C)

Test	$h_{overall}$	$h_{mean}(4)$	$h_{mean}(5)$
therm-32	970	864	916
therm-33	953	977	1001
therm-34	655	646	676
therm-37	531	494	521
therm-38	796	784	822
therm-45	205	160	168
therm-46	233	165	169
therm-58	203	157	160
therm-59	206	160	165

Note: (4) excludes the defective #3 heat flux meter

(5) includes the defective #3 heat flux meter

TABLE 4.4

MINIMUM & MAXIMUM VELOCITY

T_{mix}(C)	R	v_{min}(m/s)	v_{max}(m/s)
40	20.5	7.0	≈ 10.0
50	11.6	4.5	7.0
60	6.6	3.0	8.4
70	3.6	2.0	5.5
80	1.8	1.3	3.7
90	0.7	0.9	2.6

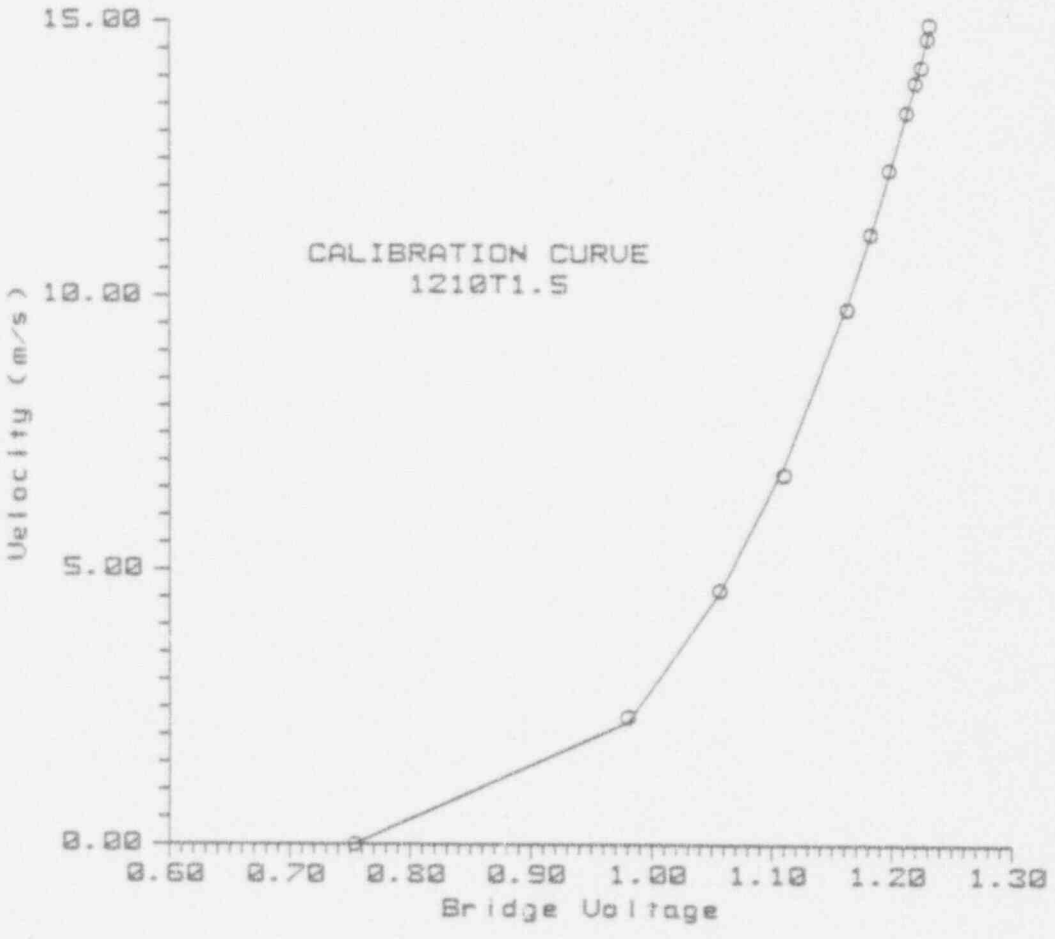

Figure 4.1 Typical Calibration Curve

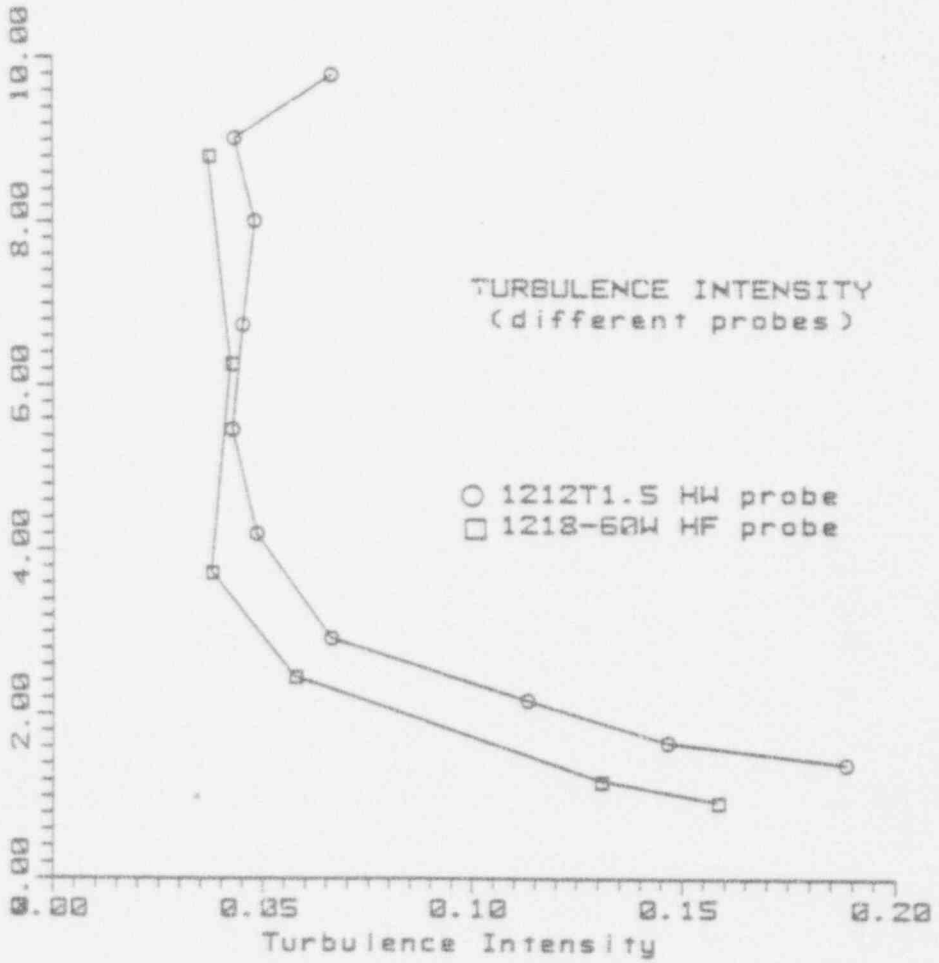

Figure 4.2 Comparison of Probe Response to Turbulence

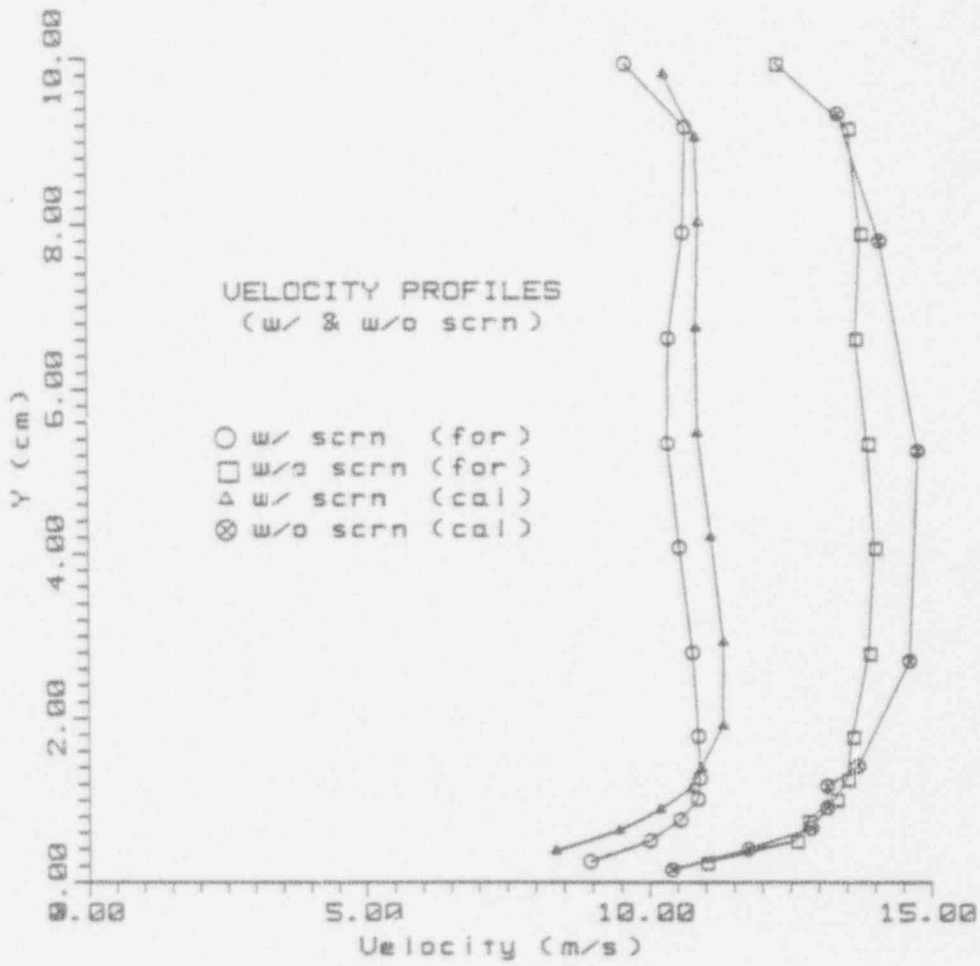

Figure 4.3 Velocity Profile-With and Without Screen

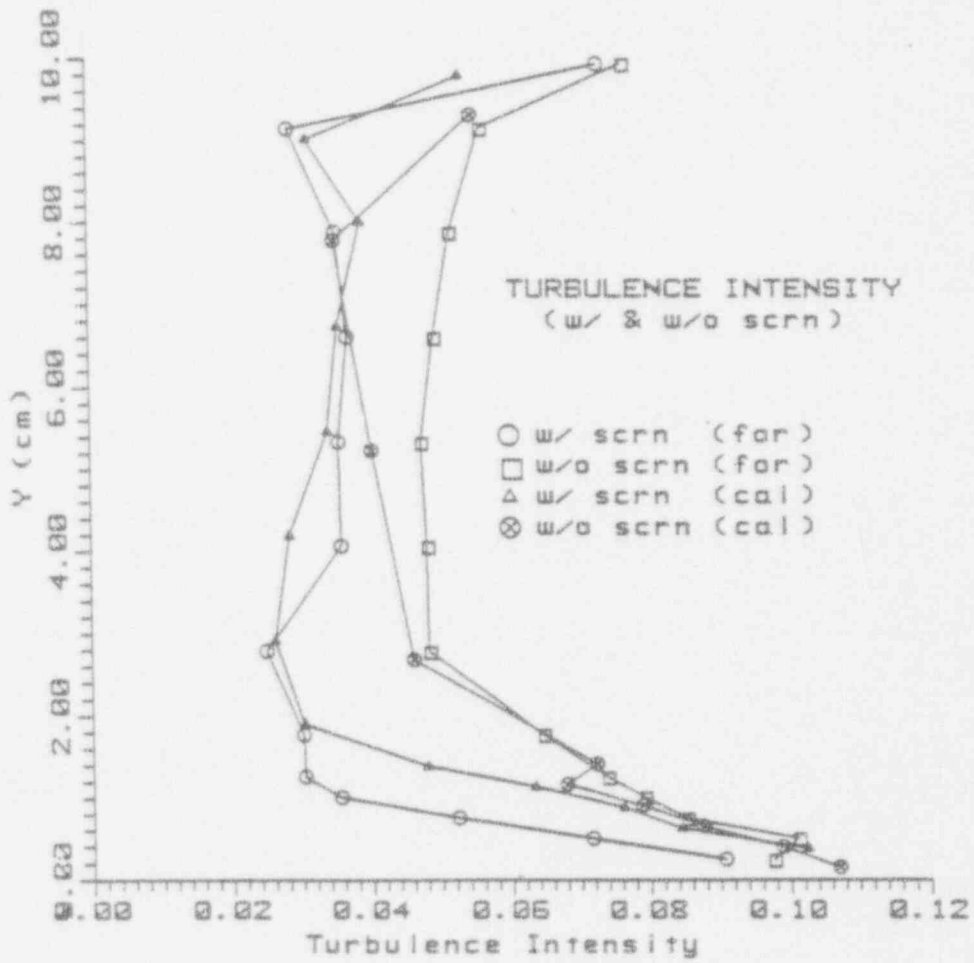

Figure 4.4 Turbulence Intensity Profile-
With and Without Screen

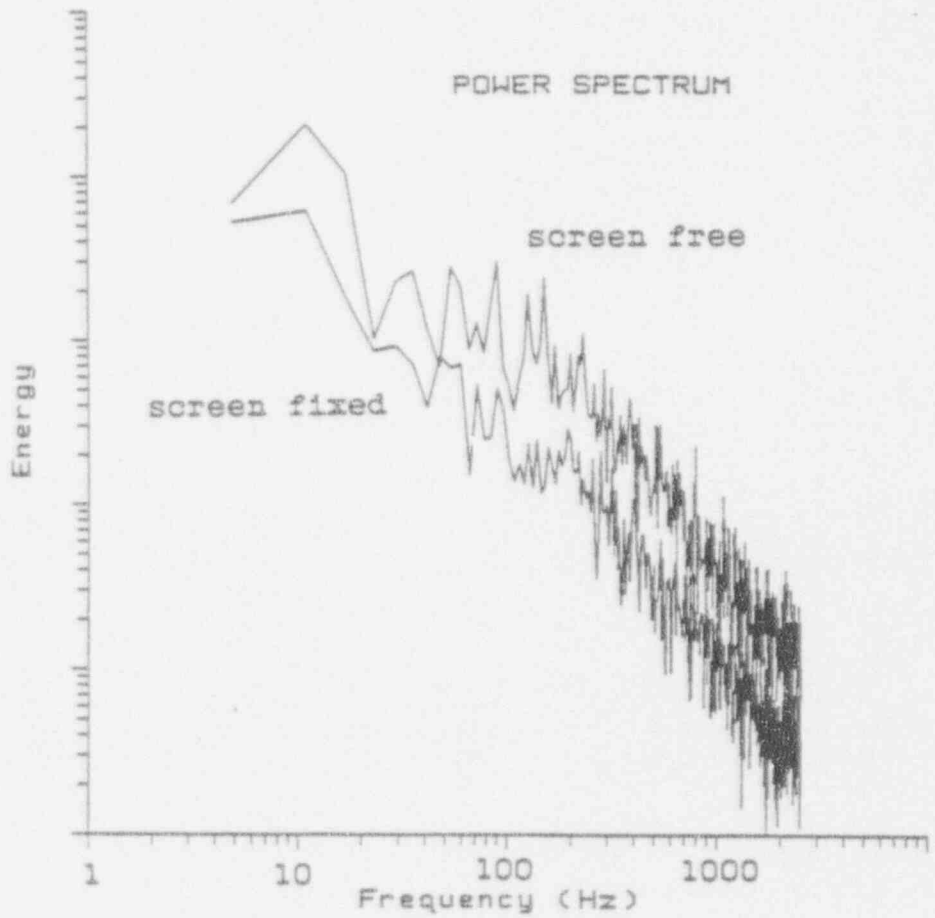

Figure 4.5 Frequency Spectra-With and Without Screen Fixed

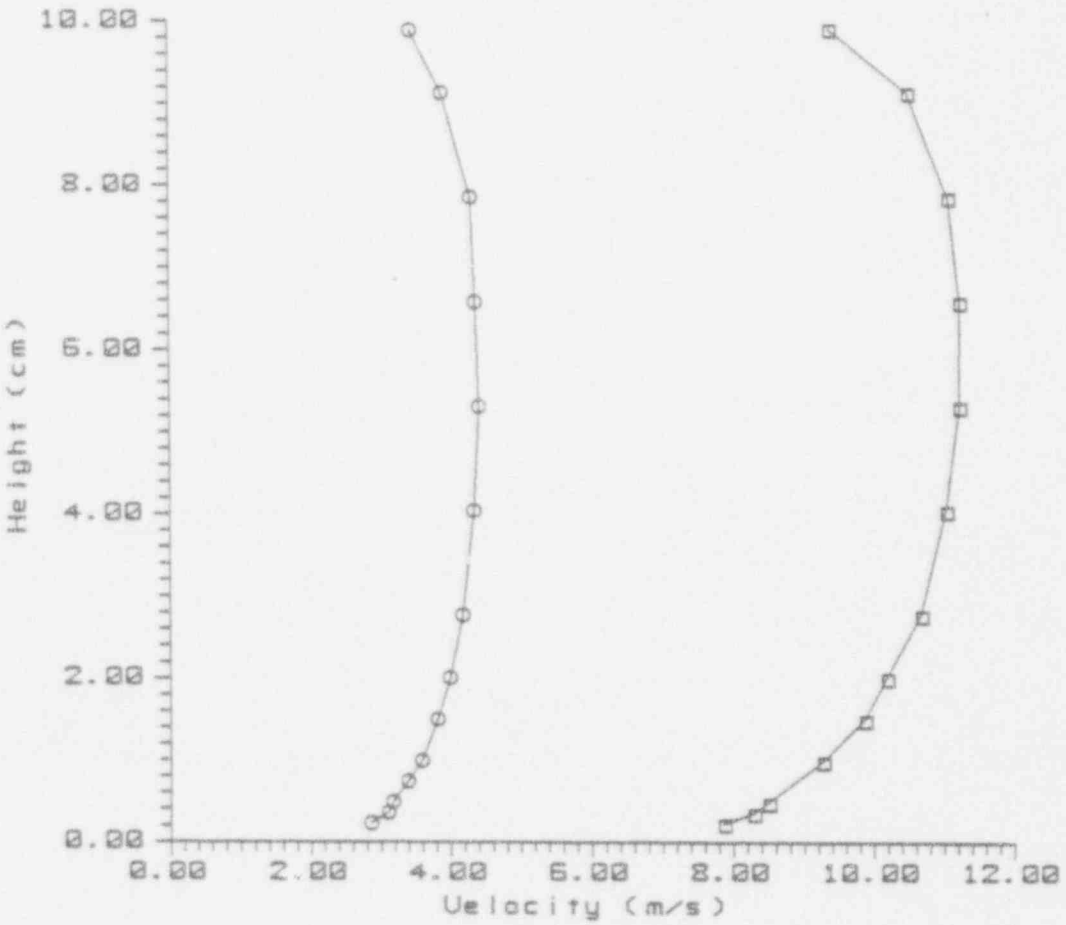

Figure 4.6 Velocity Profiles-Final Configuration

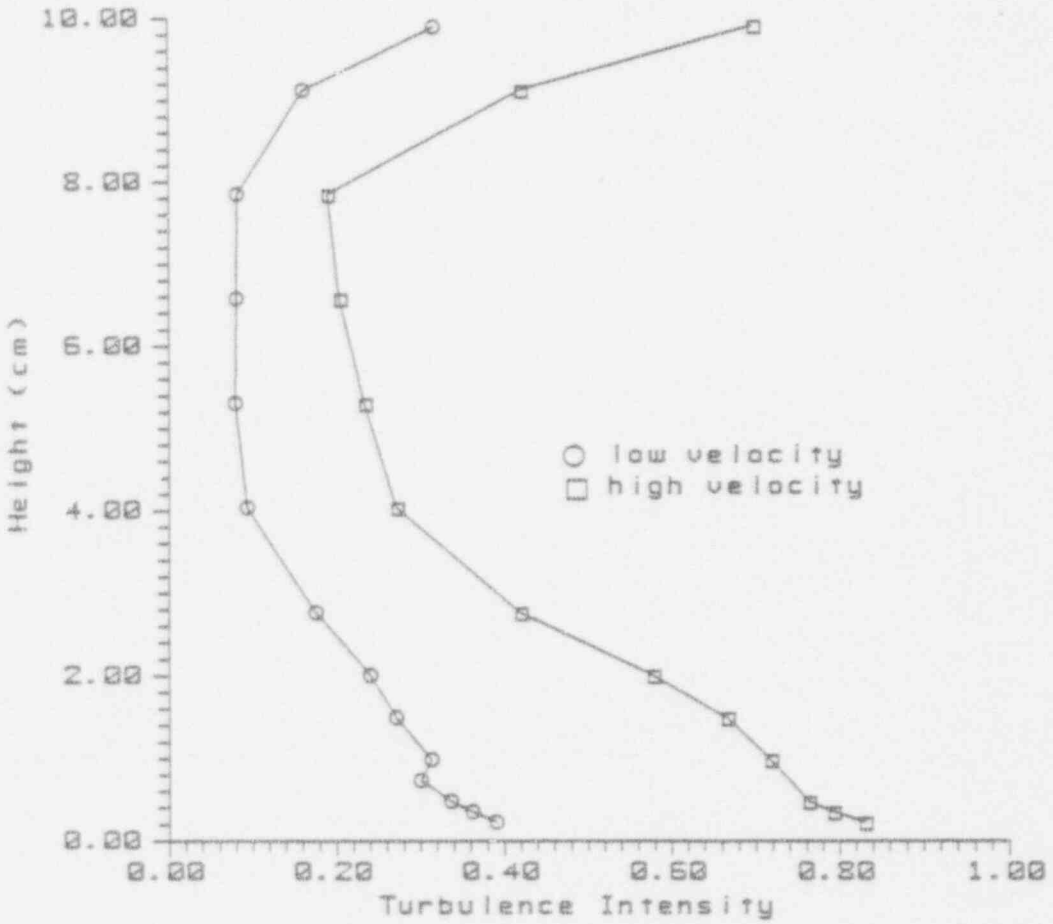

Figure 4.7 Turbulence Intensity Profiles-
Final Configuration

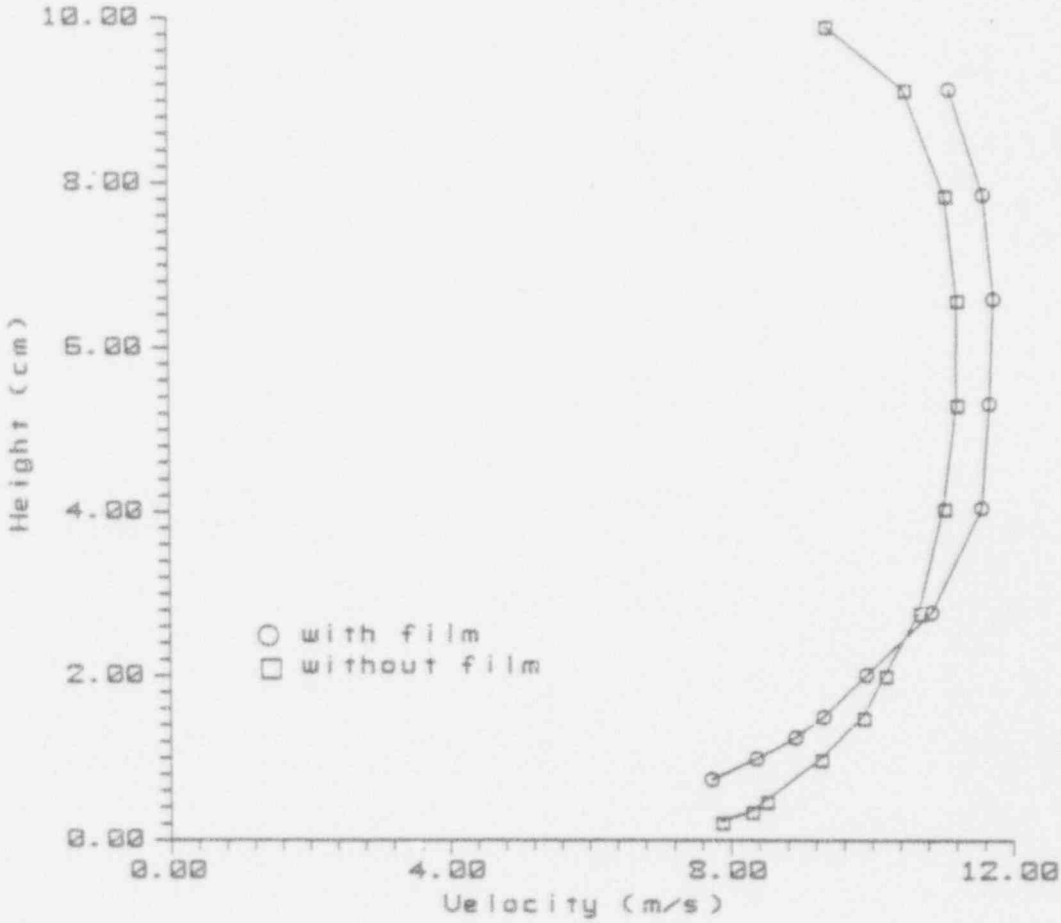

Figure 4.8 Velocity Profile with Film

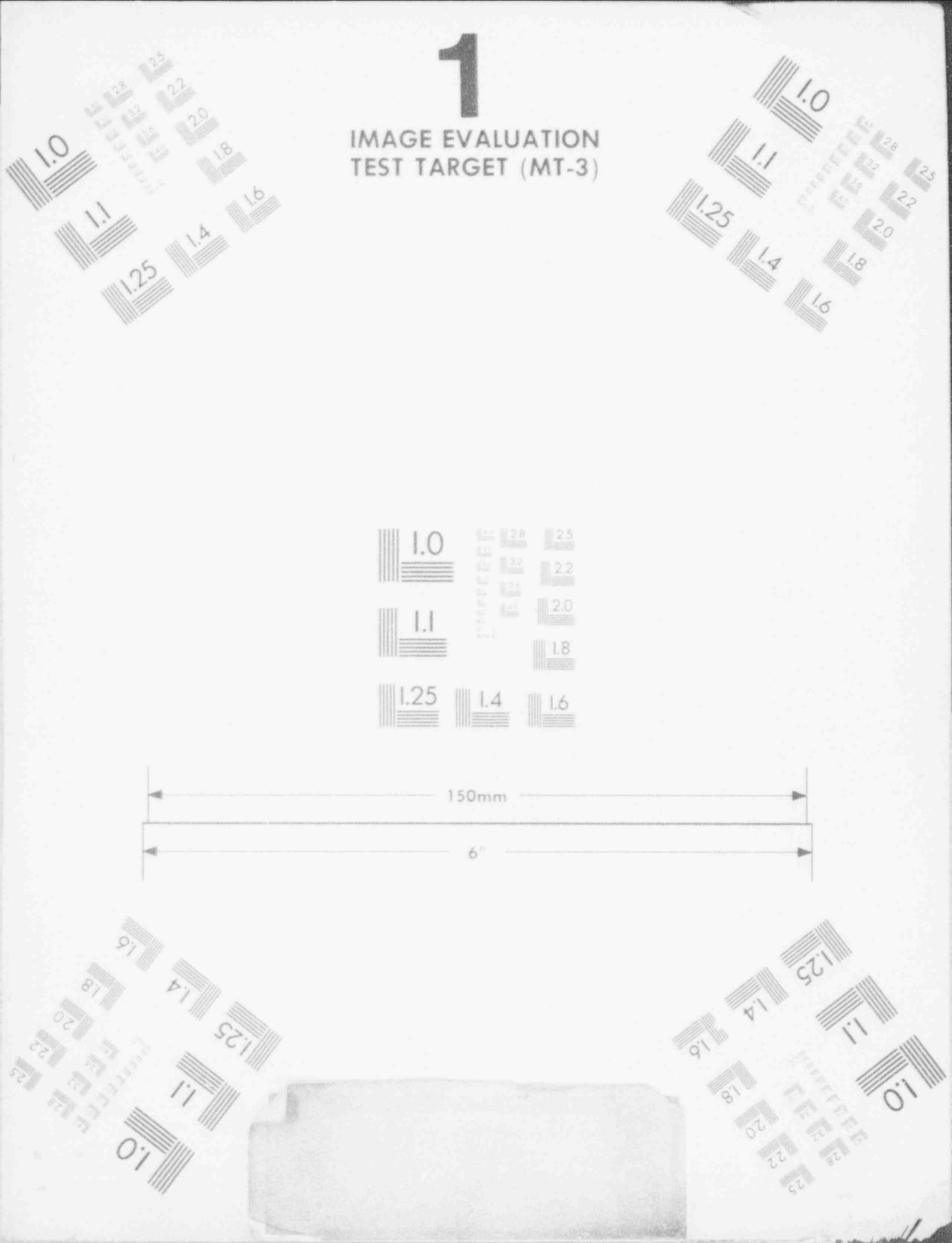
1
IMAGE EVALUATION
TEST TARGET (MT-3)
1.0
1.1
1.25
1.4
1.6
1.8
2.0
2.2
2.5
2.8
3.2
3.6
4.0
150mm
6"

1

IMAGE EVALUATION TEST TARGET (MT-3)

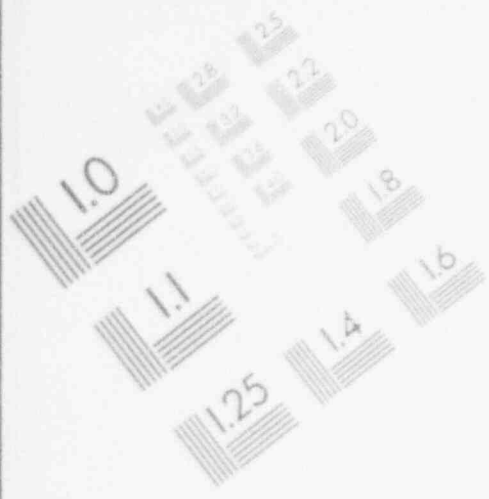

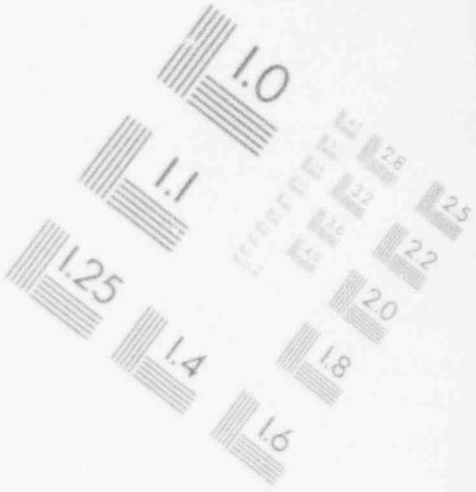

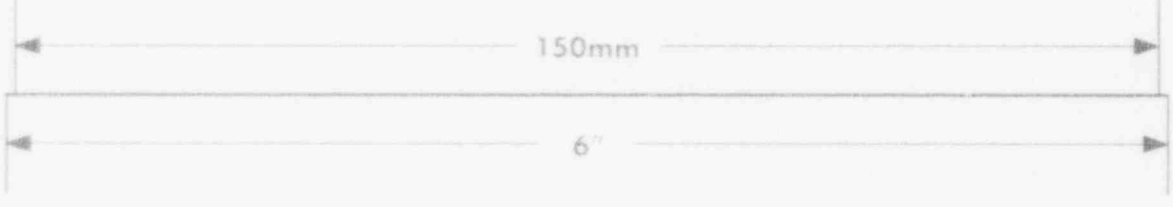

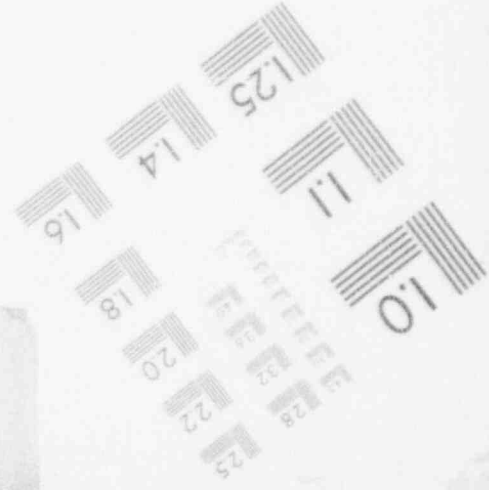

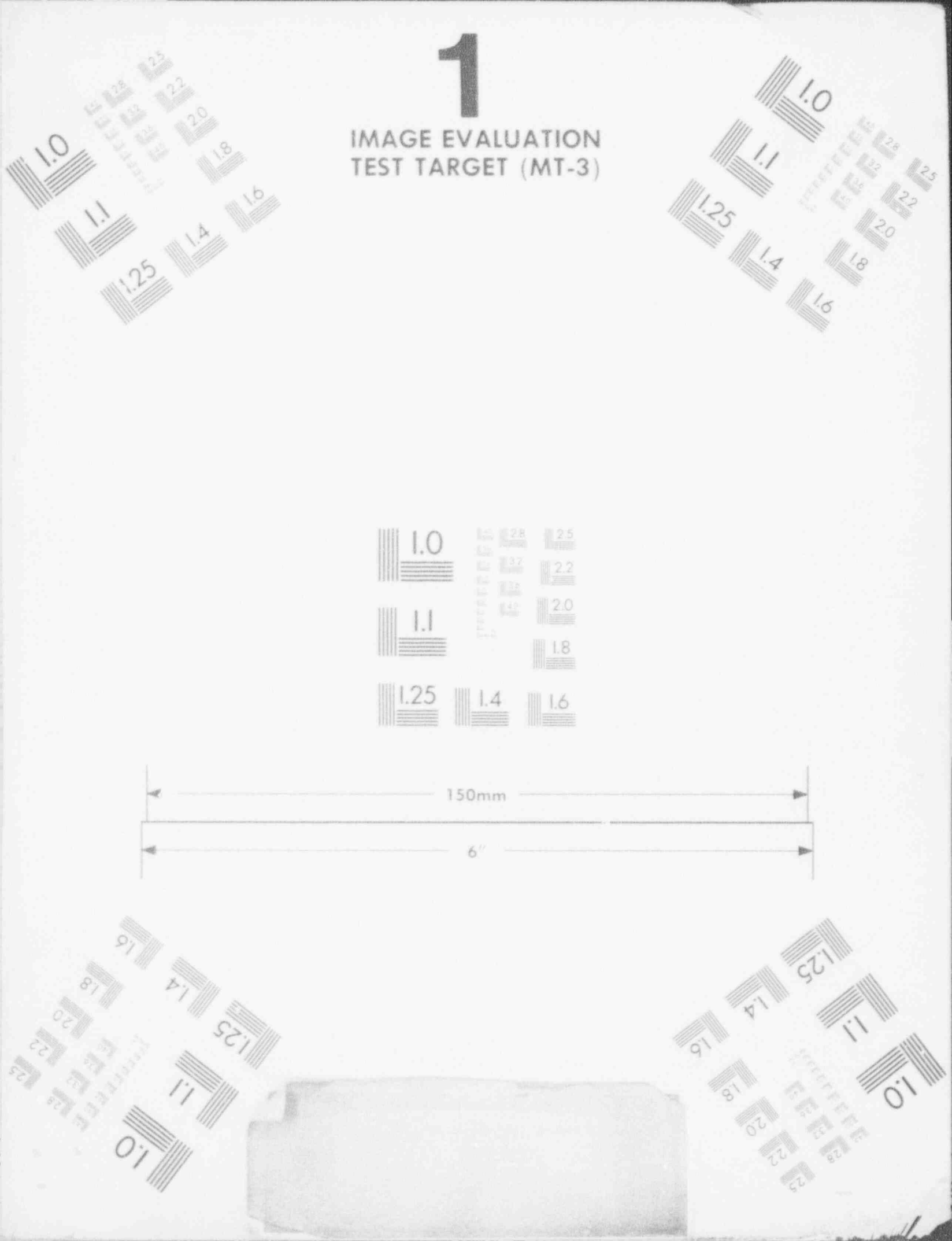
1
IMAGE EVALUATION
TEST TARGET (MT-3)
1.0
1.1
1.25
1.4
1.6
1.8
2.0
2.2
2.5
150mm
6"

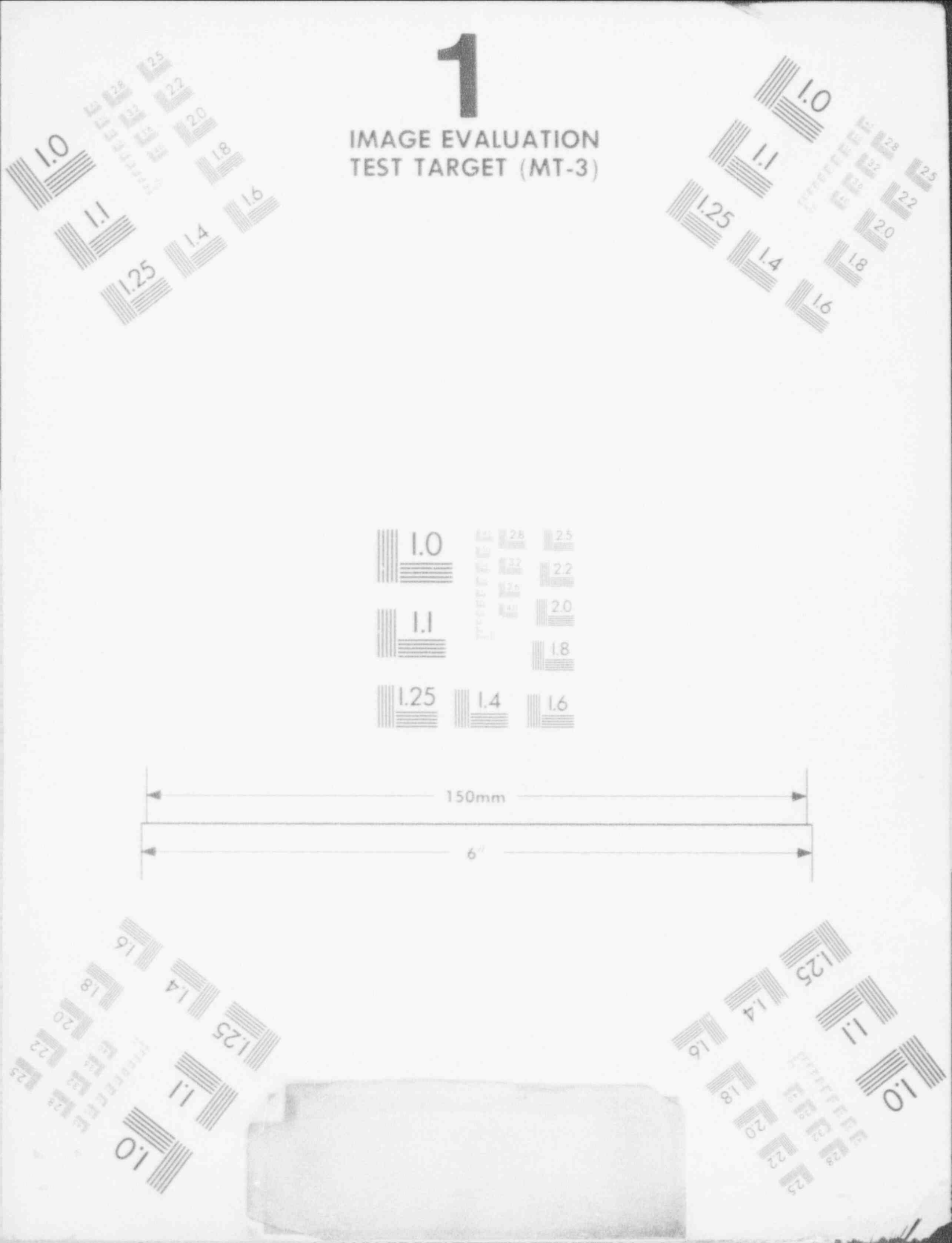
1
IMAGE EVALUATION
TEST TARGET (MT-3)
1.0
1.1
1.25
1.4
1.6
1.8
2.0
2.2
2.5
2.8
3.2
3.6
4.0
150mm
6"

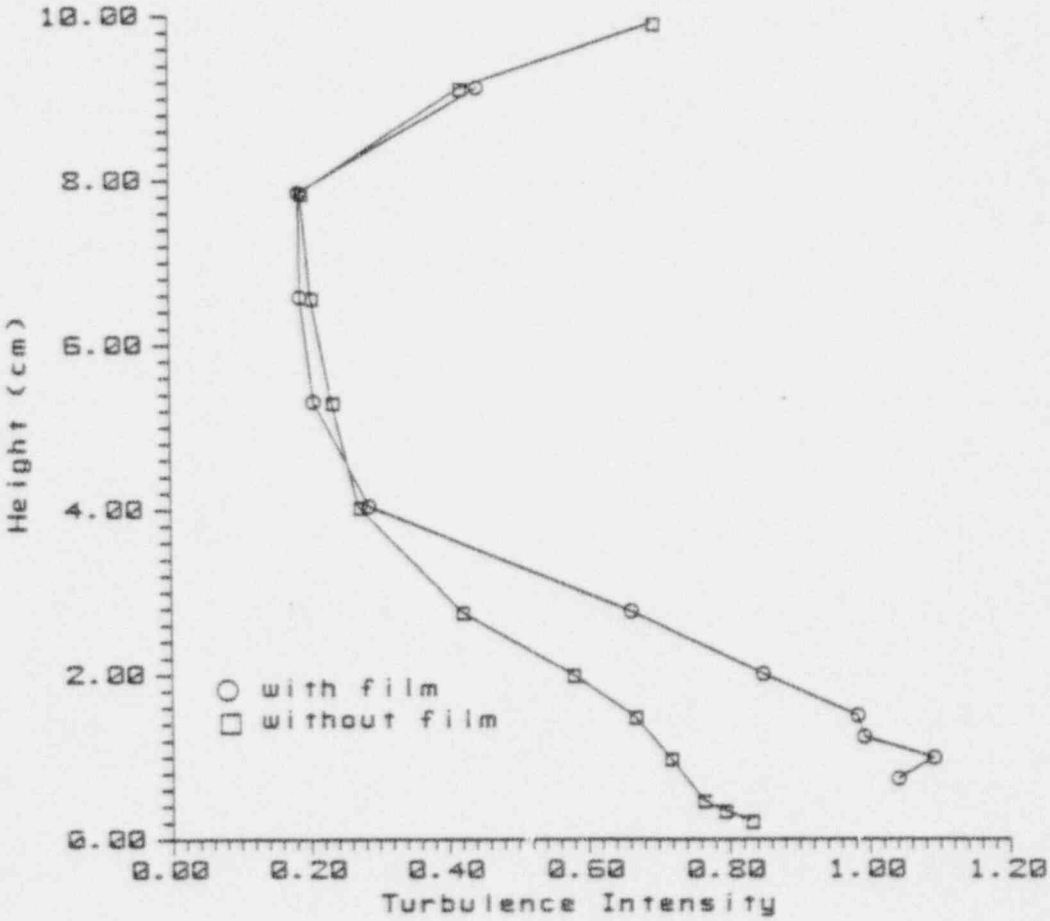

Figure 4.9 Turbulence Intensity Profile with Film

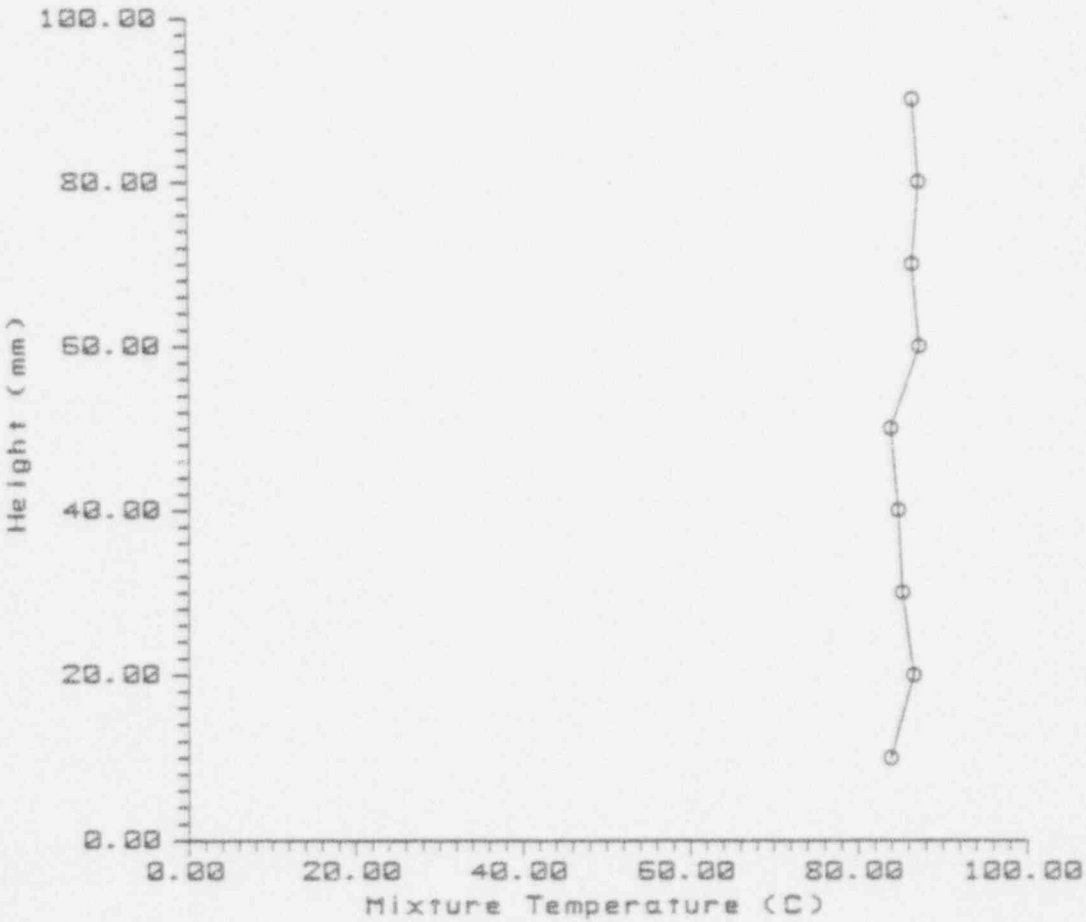

Figure 4.10 Test Section Gas Mixture Temperature Profile

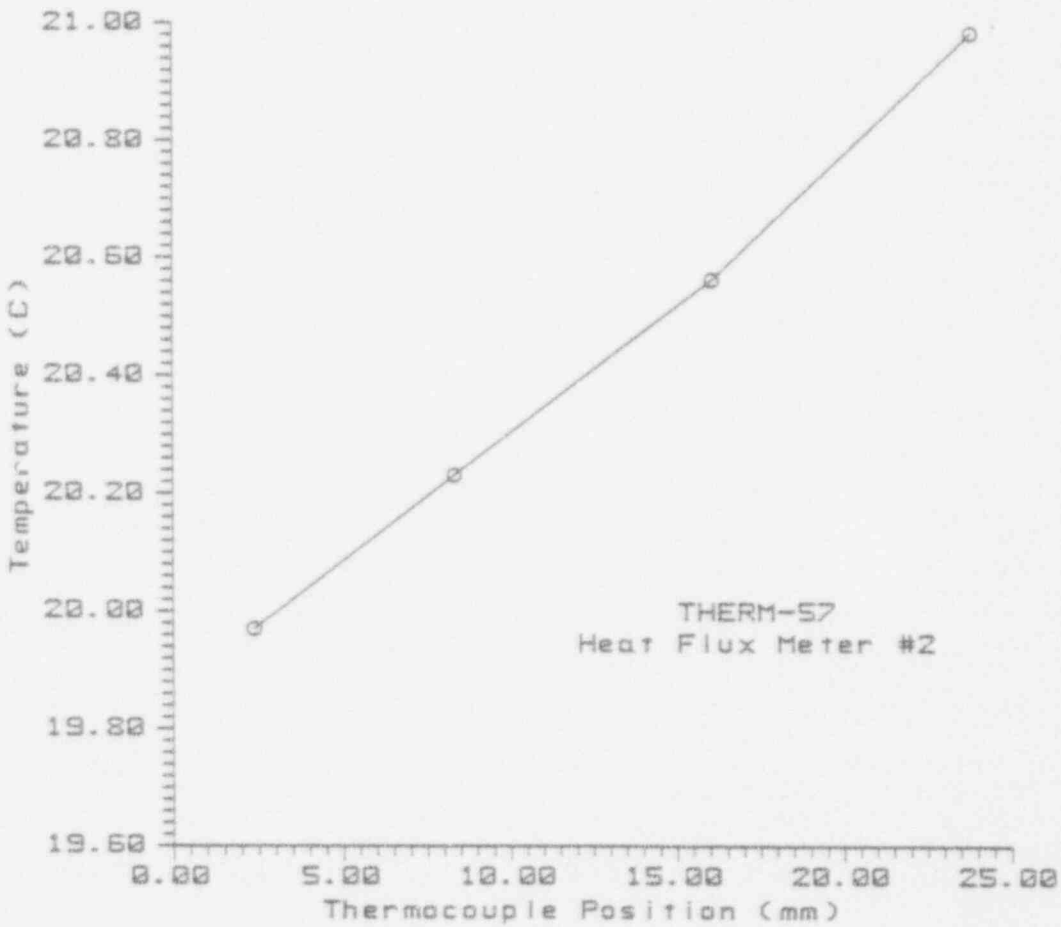

Figure 4.11 Typical Heat Flux Meter Temperature Profile

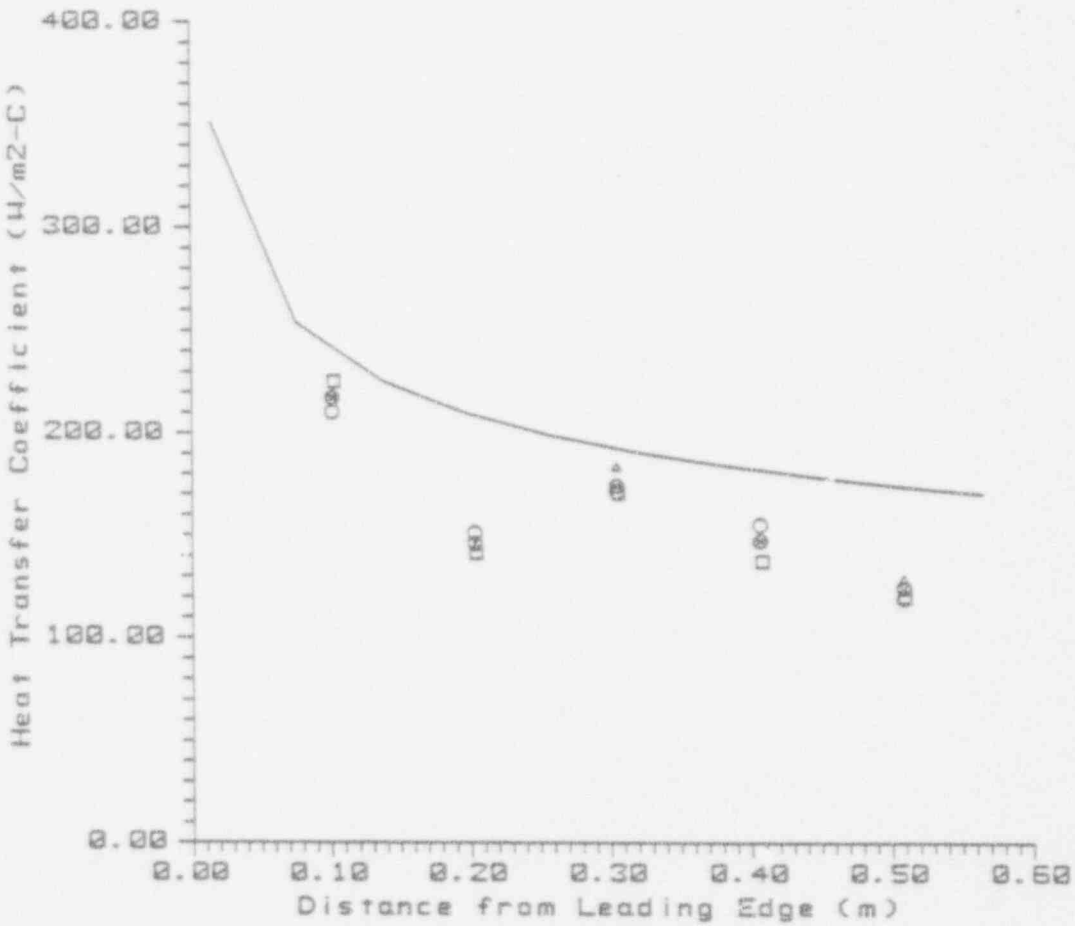

Figure 4.12 Heat Flux Meter Repeatability-Four Runs

(CWNG prediction shown as solid line)

5. ISOTHERMAL TEST SERIES

5.1 INTRODUCTION

The Isothermal Test Series served a number of purposes in the research program. One of its main purposes was to develop the measurement techniques that were to be used during the Air/Steam Test Series. There is a substantial body of data that has been acquired by previous researchers in isothermal air-water flows which was to be used for comparison. Such a validation was highly desirable because there is no comparable data available in condensation experiments.

Another purpose was to improve and extend the methods originally used by Akai and his co-workers [1]. Their use of a thermal anemometer in observing the properties of the interfacial waves was unique. The majority of other workers have used either light attenuation or conductivity cell methods. Although these methods are very useful in isothermal flows, they are not adaptable to heat transfer experiments in which the film must flow along a metallic heat transfer surface.

The work of Akai et al. was limited however. The primary result of their interfacial study was a map of the different interfacial wave regimes. Although the use of

the anemometer was an interesting way in which to develop the map, such maps had also been generated by simple visual observation many times previously.

Their technique was also only able to generate reliable values of wave parameters like frequency and celerity under the very restrictive conditions of two-dimensional flow. One of the motivations for the isothermal tests, then, was to develop a more advanced technique which would allow measurement of the wave parameters in the much more common three-dimensional flow regime.

The final goal of the test series was to generate a self-consistent set of parameters describing the wavy interface. The selection of descriptive parameters for a complex three-dimensional interface was not immediately obvious. Certain relationships were expected, but determination of the exact form of each parameter was necessary. It was hoped that choosing a set of parameters that gave a complete (to first-order) and self-consistent characterization of the interface would be particularly useful in development and evaluation of the heat transfer models for the heated experiments.

To accomplish these goals, three basic categories of experiments took place. The first group of experiments involved general development of the experimental methodology. This included design and optimization of

probe designs as well as generation of procedures and techniques. In some cases these experiments were quite brief and straightforward. In others, a great deal of time was spent in finding a solid, reliable method of acquiring and analyzing the data.

The second general category of experiments involved comparison of the results to those previously published in the literature. This comparison was useful as a guide in evaluating the possible descriptive parameters as well as in checking the accuracy and reliability of the measurement techniques. Two main sets of previous work could be referred to. In the work of Akai et al., comparison could be made to results obtained with a similar hot-wire/film anemometry technique. The extensive work of Hanratty and associates used a completely different measuring technique, light attenuation. Hence, a completely independent verification was possible.

The final set of experiments was done to complete a small isothermal test matrix. The independent variables in these experiments were the film flow rate (or Re_f), the velocity of the air (v_g), the angle of inclination of the test section (θ), and the measurement position (x) which was the distance from leading edge of plate. In these experiments, θ was fixed at 0 (horizontal) and the downstream measurement station ("calibration") was used

throughout. The test matrix consisted of the following conditions:

Air velocity (m/s)	-	6.3	
		9.0	
		11.9	
Film flow (lpm)	-	2	Re_f - 325
		3	488
		5	813

This test matrix was designed to provide data for comparison both to the Air/Steam Series and to future experiments in this laboratory or in others. The 6.3 m/s air velocity was selected because it was about the lowest velocity that sustained waves and that would also prevent the thick (5 lpm) films from backing up into the inlet duct. The high velocity was selected because it was the maximum velocity attainable. The film flow rates were selected because they covered the range that had been studied by previous workers. It should be noted that all of the experiments took place in the three-dimensional wave regime.

The following sections describe the measurement of each interfacial wave parameter in detail. The development of the measurement and analysis techniques is documented and the results of comparison to literature are

tabulated. Results for the isothermal test matrix are also given.

5.2 AMPLITUDE & FILM THICKNESS

The measurement of the amplitude and film thickness is important to quantify the properties of a wavy film. The amplitude of the waves has a strong effect on the shear stress and turbulence in the gas phase. The film thickness is probably the most important and basic property of the film. The film thickness is required in order to estimate important parameters such as the velocity of the film and the heat transfer resistance of the film.

The film thickness and amplitude were measured simultaneously in these experiments. A hot-wire or hot-film probe was used to traverse the interfacial area and generated a plot of film contact versus height. The film thickness and amplitude could be inferred from this plot. The original probes which were used for these measurements were the TSI 1212-60W and 1218-60W probes. Later, a home-made probe of similar configuration was used. A home-made probe is illustrated in Figure 5.1. All of the probes are of the horizontal sensor type and have supports which are swept in the upstream direction. For the purposes of the amplitude and film thickness measurements, the lower

frequency response of the TSI probes was not a concern. In addition, the film sensors were generally quite rugged. The home-made probes were preferred due to the availability of cheap, local repair and due to the smaller diameter of the wire sensor which was thought to suffer less from contact hysteresis.

The important first step in making the film thickness and amplitude measurements was to install the probe in the test section. The most important aspect of this was the determination of the traverse offset. This is defined as the reading on the traverse scale that corresponds to contact of the probe sensor with the bottom wall of the test section. The traverse offset is then used to calculate the position, y, of the sensor above the bottom wall. Measurement of the traverse offset directly by placing the sensor against the surface of the wall would usually break the sensor.

The traverse offset was measured by placing a 1 inch block in the test section next to the installed probe. The probe was then traversed until the sensor lined up visually with the top surface of the block. The traverse offset could then be computed by adding 1 inch to the reading on the traverse scale. This measurement of the traverse offset was estimated to be accurate to within 0.01 inches. With the traverse offset known, the experi-

ment could be run.

The probe was traversed beginning at a position just above the waves. At this point the signal would indicate single phase gas turbulence superimposed on a relatively low DC level (typically about 1 volt). The probe was then moved downward in 0.01 inch increments. At each stop, a data set was taken on the Nicolet digital oscilloscope, transferred to the computer, and then dumped to disk. Where waves contacted the sensor, the signal trace appeared as a set of uneven square waves with the width of the upper voltage level increasing in width as the probe traversed deeper into the waves. Eventually the signal became completely saturated at the higher voltage level corresponding to contact with the liquid phase (about 3 V) when the sensor was fully immersed. This completed the traverse.

The data was analyzed in terms of a quantity called the probability of contact.

$$P_C = \frac{\text{number of samples at high saturation}}{\text{total number of samples}} \qquad (5.1)$$

This quantity is easily computed for each data set in the traverse. A threshold voltage must be specified in order

to discriminate the samples at the high saturation voltage, then the number of data points above and below are simply counted. The P_c value exhibited little sensitivity to the threshold voltage parameter and V_{thresh} was normally set to be approximately 0.1 volts under the high saturation voltage. P_c was plotted as a function of the height of the sensor above the floor of the test section, y. A typical plot is shown in Figure 5.2.

The film thickness, δ, and the amplitude, A, are computed from the $P_c(y)$. The film thickness is defined as:

$$\delta = \int_0^\infty y \, P_c(y) \, dy \qquad (5.2)$$

The amplitude is defined in terms of the y values which correspond to P_c of the crest and trough.

$$A = y(P_{crest}) - y(P_{trough}) \qquad (5.3)$$

The definitions of the P_{crest} and P_{trough} are somewhat arbitrary but values of P_{crest} = 0.90-0.99 and P_{trough} = 0.01-0.10 were typically used. The entire procedure of calculating $P_c(y)$, δ, and A was coded into the FILM program.

In practice, there were a number of limitations on the film thickness and amplitude measurements. Due to the surface tension of the water, it tends to stick to the

sensor after initial contact, creating a contact hysteresis problem. This is much less a problem when the waves are large and the gas velocity is high than when one is trying to measure small waves with slow gas velocities. Another problem exists in the resolution of the traverse. The smallest increment is 0.01 inches or about 0.25 mm. Frequently, wave amplitudes are not much larger than this, hence the resolution is not very good. The strict definitions of P_{crest} and P_{trough} were somewhat superfluous due to the lack of resolution.

Neither of these limitations strongly affects the film thickness measurements. If the hysteresis effects are severe, the film thickness can be taken with little error as the height at which the sensor first contacts the interface. δ is also less affected by other errors because the integration process averages over several points. Therefore, although there are limitations in the method, the results for film thickness are generally fairly good. This is important because δ is used to compute other quantities.

Table 5.1 shows a comparison to some previously published data which shows good agreement, particularly in the film thicknesses. It should be noted that the previous experimenters listed, except for Akai et. al., utilized light transmission instrumentation. Akai used

thermal anemometry. It should also be mentioned that all of the previous work was done in two-dimensional duct geometries rather than in flat plate simulations. For comparison purposes, effective Reynolds numbers are given in the table.

The results of the film thickness and amplitude measurements for the isothermal test matrix are shown in Table 5.2.

5.3 FREQUENCY

The measurement of the wave frequency was undertaken for several purposes. One of the intentions of the isothermal tests was to quantify the wavelength in some way. The method used in this research required the measurement of the celerity and frequency of the waves and the computation of the wavelength from them. The frequency of the waves is also interesting for its effects on gas turbulence. A complete characterization of the wavy interface also requires a knowledge of the wave frequencies regardless of which method is used to determine the wavelengths.

The study of wave frequency began with the measurement of the frequency or power spectrum using thermal anemometry probes. Initially the probes were used to

generate square wave patterns similar to those used in the film thickness and amplitude measurements. A horizontal hot-wire or hot-film sensor was placed where waves would strike it. In later tests, the sensor was actually moved above the waves and sensed the frequency of the fluctuations induced in the gas phase. Finally, the method of using the same sensors and data sets as the celerity measurements was developed.

This final method had several advantages. One chief one was that the frequency and celerity data were taken simultaneously. In this way, it was assured that there was no change or drift in experimental conditions that might skew the data. Since the wavelength was to be computed from the celerity and frequency this was important. The double use of the data also lessened the amount of disk storage space that was required and reduced the amount of time required to run the tests and download the data from the digital oscilloscope to the computer. The one disadvantage to this method was that in order to achieve adequate resolution in the celerity measurement, the sampling rate was required to be somewhat larger than would be desirable for frequency measurements alone. As will be discussed shortly, this does limit the accuracy of the low frequency range.

The tool which was used to generate the frequency

spectra was the Fast Fourier Transform (FPT), so named because of the speedy algorithm it uses to compute the transform. As was discussed in the section on software, an FPT program was developed for these experiments.

In using FPT's to generate frequency spectra, there are several important considerations regarding the frequency range of interest. The low-frequency range of an FPT-generated power spectrum is generally not expected to be accurate. This is because the endpoints of the sampling interval must exactly define the period of the lowest frequency component. This is not possible with naturally occuring phenomena. At the high-frequency end, the user must be careful to avoid aliasing. This upper limit is called the Nyquist frequency and is twice the sampling frequency [126]. A low-pass filter is required to attentuate any high-frequency noise.

The following are the general recommendations which are made for setting up the sampling frequency and filters [127].

$$f_{sample} = 10\, f_{filter} \tag{5.4}$$

$$f_{filter} = 10\, f_{interest} \tag{5.5}$$

$$f_{low} = f_{sample}/N_s \tag{5.6}$$

$$f_{high} = f_{Nyquist} = f_{sample}/2 \qquad (5.7)$$

where f_{sample} - sampling frequency
f_{filter} - low-pass filter cutoff frequency
$f_{interest}$ - maximum frequency of interest
f_{low} - low frequency limit
f_{high} - high frequency limit
N_s - number of samples

Typical values of the parameters that occurred during the course of the experiments are listed below:

f_{sample} - 2 kHz
f_{filter} - 200 Hz
$f_{interest}$ - 20 Hz
f_{low} - 0.25 Hz
f_{high} - 1 kHz
N_s - 4096

One should note that f_{low} is somewhat higher than is desirable due to the simultaneous acquisition of celerity and frequency data. Note also that one requirement of the FFT algorithm that is normally fairly easily dealt with is the requirement that the number of data points to be transformed be a power of 2.

Two other important considerations were also encountered in the processing of the data with FFT's. Originally

only single data sets were processed and viewed. Repeatability from one to another was very poor. This was due to two reasons. The first was that the physical phenomenon do change slightly from one data set to another. The second, and more important reason, is that the standard deviation of a single transform is extremely large (approaching the magnitude of the transform). It is generally advisable to divide up a single data set into several smaller ones (if only one is available) and to average the results and accept the reduction in resolution [127]. For this reason, ten data sets were taken and averaged. The repeatability from one ten set average to another was very good. This is shown in Figure 5.3. All of the results shown later were obtained using ten set averages.

The other important consideration was much less important under the circumstances of this research, but would be vital in certain other applications. When one transforms a finite data set (as one must do with discrete data), it should be remembered that the real waveform continues on indefinitely, but that only a truncated portion is being transformed. The user is in reality transforming the convolution of the waveform and a rectangular window. The result is that the output transform has large sidelobes alongside the main frequency peak which

are due to the rectangular window. These sidelobes can be reduced by applying a taper to the data near the edges of the set. There are many such tapers or windows available depending on the amount of sidelobe reduction desired. One side effect of using a taper is that the main frequency peak is than spread out somewhat. Thus there is a tradeoff.

The Papoulis window was used throughout this research. It was recommended as having good general performance [127]. As was mentioned earlier, however, the taper was not critical to the current application. This is because the waves generate a more or less smooth spectrum. The presence of sidelobes does not really make too much of a difference. On the other hand, the spreading of the main peak doesn't make too much of a difference either. Several other tapers were tested along with the Papoulis window, but the effect was minimal. Under other circumstances where a specific frequency peak was desired, though, the choice of the best taper might be critical to good results.

In order to use the frequency spectrum results, some single or small group of parameters was needed to characterize the data. The value of the spectrum maximum was an obvious choice. There were several problems with this however. Firstly, it is fairly difficult to get a precise

value for the peak. Even after running the spectrum through the SMOOTH program, it was fairly rough, as can be seen in Figure 5.4 for example. Secondly, the uncertainty in the measurement of the peak is quite large due to the logarithmic scale. The most important reason, however, was that in trying to utilize the results to compute the wavelength, the peak frequencies generated wavelengths that were much larger than those which were observed visually.

In an effort to generate a more useful measure of the frequency spectrum, a simple average over the spectrum was taken using the program AVGFFT. These values were much larger than the peak frequencies and were useful in calculating wavelengths as will be discussed in that section. In comparing the frequency results to those of earlier researchers, it was found that they too had come up with two parameters describing their frequency spectra.

In the work of Cohen and Hanratty [97] and Lilleleht and Hanratty [93], they identified two frequencies: an f_{peak} and a number of waves per second or f_{wave}. The f_{peak} was defined as the maximum of the frequency spectrum. Good agreement was shown between their values and those of the current research as can be seen in Table 5.3. Interestingly, their f_{wave} parameter corresponded quite well with the values generated by spectrum

averaging. This can also be seen in the table. This then, appears to supply the physical interpretation of the spectrum average frequency as a measure of the number of waves per second. It should also be noted that the general shape of their frequency spectra were very similar to those measured here. Since the results of Cohen, Lilleleht, and Hanratty were obtained by analysis of film thickness traces generated by light transmission measurements, their work also represents an independent verification of the thermal anemometry technique developed here.

It should also be noted that the frequency measurement technique developed here was different and generally superior to that which was used previous by Akai et al. [1]. Although Akai used hot-wire anemometry to measure frequency, he and his co-workers analyzed the data much differently. The data were processed by a correlation and probability analyzer which generated the autocorrelation of the signal, $\rho(\tau)$. This is defined as:

$$\rho(\tau) = \int_0^\infty x(t)\, x(t+\tau)\, dt \qquad (5.8)$$

The period (hence frequency) of the waves was found by measuring the delay time between the waves. This technique is shown in Figure 5.5.

The primary problem with this technique is that it only works with two-dimensional waves. Two-dimensional

waves are very regular and periodic, but exist over only a very narrow range of parameters. Generally they are of little interest in practical applications. The autocorrelations may still be generated in the important three-dimensional wave regime, but the results are difficult or impossible to interpret. This is illustrated in Figure 5.5. The FFT technique developed in the present research is far more robust and can handle both two- and three-dimensional wave regimes.

Although the results of the frequency measurements compared well to those of the previous researchers, there is an additional consideration that must be dealt with. The true wave frequency is the frequency of the waves measured by an observer that is stationary in the medium. Due to the motion of the film (the medium), the frequency measured by the probe must be corrected. The correction is made by the standard Doppler shift formula.

$$f_{true} = f_{obs}(v_{rel}/(v_{rel} + v_{film})) \qquad (5.9)$$

where f_{true} - true wave frequency
f_{obs} - observed wave frequency
v_{rel} - wave speed relative to film
v_{film} - film velocity

If v_{rel} were much larger than v_{film}, the correction would

not be required, but this is not the case in the current research. This Doppler correction can be applied to either the peak or spectrum average frequency. The computation of the velocities is discussed in the next section (5.4).

The results of the frequency measurements for the isothermal test matrix are listed in Table 5.4. The data indicates a clear trend towards higher frequencies with thinner films. No formal error analysis was performed on the uncorrected frequency measurements, but repeatability tests indicated that the spectrum average frequency was good to a few hertz. The error analysis for the Doppler-corrected frequency is located in Appendix A. An error of 10% in the uncorrected values was assumed. The results of the error analysis are located in Table 5.4.

It is important to note that the frequency spectrum measured in the gas phase was very similar to that which was measured in the waves. The chief difference is that the high frequency end of the spectrum tailed off more slowly in the gas phase. This would be expected since the energy dissipation mechanisms in the film are much stronger than in the gas.

The similarity of the spectra indicates that in the vicinity of the interface the turbulence in the gas phase is driven strongly by the waves. This behavior was also

evident in the turbulence intensity profiles shown in section 4.2.1. The importance of this is that in modelling of a flow over a wavy film, the boundary condition at the interface is critical. A turbulence forcing function is needed. One method by which this effect can be included was used by Akai et al. [1]. In their work, a two-equation turbulence model (k-ϵ) was used. The boundary condition at the interface was modelled as a source of turbulent kinetic energy.

5.4 CELERITY

The celerity or wave speed is another important characteristic of a wavy film. In order to compute the wavelength indirectly, as was desired, the celerity must be measured. The measurement of celerity is somewhat more difficult than the measurement of amplitude, film thickness, or frequency. It cannot normally be measured using conductivity cell methods and is therefore not frequently measured.

The basic technique for celerity measurement was borrowed from Akai et al. [1]. The basic concept calls for using two thermal anemometer probes located a short distance apart in the interfacial region of the film. The probes are separated in the streamwise direction by a

known distance. They are also separated in the cross-stream direction so that the downstream probe is not affected by the upstream probe's wake. The time required for one wave to cross the known distance is then measured. This time is most easily measured by cross-correlating the two probes' signals. The basic method is illustrated in Figure 5.6.

Akai and his co-workers used two separate hot-film probes and processed the signals using a correlation and probability analyzer. Due to the rather wide separation distance necessitated by the use of two separate probes, their technique was best suited to two-dimensional waves as was also the case in the frequency measurements. With small three-dimensional waves, their technique was much less satisfactory.

In order to optimize this technique for the current research and to allow measurements in the three-dimensional wave regime, it became obvious that special probes would be required. The Celerity or C-series of probes were then designed with this purpose in mind. In order to allow a small separation distance, a single probe body was used to carry both sensors. The hot-wire sensors were vertically positioned with the lead (upstream) sensor located directly upstream of the probe body centerline and the trail (downstream) sensor located off to the side and

back several millimetres. The general design of the probe is shown in Figure 5.7.

The initial tests of the C-series probes indicated several areas for improvement. The first area involved the sensor separation distance in the streamwise direction. There were two time scales inherent in the operation of the probe. The first is simply determined by the wave speed and the separation of the sensors,

$$\Delta t = \Delta x / v_{app} \qquad (5.10)$$

where v_{app} = speed of the wave

Δx = separation distance of the probes

Δt = measured delay time

For adequate resolution, the sampling interval of the data acquisition system must be some small fraction of Δt, for instance 1%. Therefore,

$$\Delta t_{s1} = 0.01\ \Delta t \qquad (5.11)$$

where Δt_{s1} = required sampling interval

The second time scale is dependent on a different characteristic of the wavy interface, the number of waves per second. One would like to have the wave speed determined from an average over many waves. Unfortunately, as the data acquisition system is constrained in the total time over which it can sample due to its limited amount of

memory, another required sampling interval may be computed.

$$\Delta t_{s2} = N_w/(f_{wave}N_s) \qquad (5.12)$$

where Δt_{s2} - required sampling interval
N_w - desired number of waves per trace
N_s - number of samples
f_{wave} - wave frequency

Unfortunately, the situation is worse than this. The cross correlation of the signals is computed by the program CROSS which was briefly discussed in the Facilities section. The cross correlation is defined as:

$$\rho(\tau) = \int_0^\infty x(t)\, y(t + \tau)\, dt \qquad (5.13)$$

In calculating a discrete cross correlation, the maximum delay time (τ) should not exceed about 10% of the total sampling time ($\Delta t_s N_s$) [127]. In other words, the number of data points over which the cross correlation is calculated should not exceed 10% of the total number of data points. Therefore, the number of samples in the equation (5.12) should refer to the number of points in the cross correlation output, not to the total number of samples. The following is an illustration of the problem using typical values of the parameters:

v_{app} - 50 cm/s

Δx - 5 mm

Δt - 0.030 sec

N_s - 500 (793€ samples per channel)

f_{wave} - 25 hz

Δt_{s1} - 0.1 msec to get 1 % resolution

Δt_{s2} - 1.6 msec to get 20 waves

Clearly there is a tradeoff between resolution, number of waves per trace, and sensor separation distance. With a Δx of 5 mm which was used in the early versions, a reduction in resolution was required. In the later C-series probes Δx was boosted to about 12 mm. Five trials were also conducted for each run which effectively increased the total number of waves over which the value of Δt was averaged.

A second area of improvement in the C-series probes was in the length of the sensing wire. In the early probes the wires were about 5 mm in length. This worked quite well for relatively thick films with large waves, but was less satisfactory for thinner films. As such it was not really a defect in the probe, but a design parameter. Since thinner films corresponded to the more important applications of interest during the heated tests, the length of the sensing wires was later reduced

to about 3 mm.

With the development of the C-series probes, wave speed measurements could be made in three-dimensional waves. Initially the wave speed was calculated by the same method used by Akai et al. The delay time, Δt, was determined from the cross correlation. Using the known Δx, the speed could be computed.

$$c = \Delta x/\Delta t \tag{5.14}$$

These results were comparable with those of Akai and his co-workers. Prelimary results were in the range of 45-60 cm/s as compared to 50-62 cm/s for the limited data published by Akai et al.

As was the case in the frequency measurement, however, the important parameter was the wave speed relative to the medium (the film) rather than the apparent wave speed (relative to the probe). Using the values for the film thickness measured earlier, the average velocity of the film could be calculated,

$$v_{film} = Q_{film}/(W\delta) \tag{5.15}$$

where v_{film} = average velocity of the film

Q_{film} = volumetric flow rate of film

W = width of channel

The relative wave speed was then defined as,

$$c = v_{rel} = v_{app} - v_{film} \tag{5.16}$$

where v_{app} - apparent wave speed ($\Delta x/\Delta t$)

When the relative velocity was used to compute the wavelengths, the results were similar to those observed visually.

The wave speeds were also compared to those predicted by the hydrodynamic theory of Lamb [129]. Lamb's expression for the wave speed is:

$$c = (g\delta)^{0.5}(3(1 + A/\delta)^{0.5} - 2) \qquad (5.17)$$

where g - gravitational acceleration

Here there was no agreement with the apparent wave speed, but very good agreement with the relative speed. This is shown in Table 5.5.

The correct definition of celerity was thus determined to be the relative wave speed rather than the apparent wave speed used by Akai et al. The results of the wave speed measurements are listed in Table 5.5.

An error analysis was conducted for the celerity measurements and is detailed in Appendix A. The results of this analysis are shown in Table 5.7. The primary sources of the error were the traverse error in measuring δ, the accuracy of the flowmeter, and the error in determining Δt. The traverse error was due to the limited resolution of the traverse (0.01 inch). It was most

pronounced in the higher air velocity runs because of the reduction in film thickness. The flowmeter which was used in the isothermal series was the Dwyer VFC-151 rotameter which has a 2% of full scale error. Unfortunately these runs were conducted at the low end of the meter's scale where this translates to errors of 10-25%. This is the reason the flowmeter was later replaced with two smaller meters in parallel. The error in Δt was estimated based on the scatter of the data from the five runs taken at each flow condition. These were in the range from 3-15% and were generally larger than the resolution discussed previously (1.5-2.5%).

5.5 WAVELENGTH

One of the primary goals in these experiments was to be able to determine the wavelength from measurements of frequency and celerity. This was desirable for a number of reasons. First, wavelength could be measured independently by visual observation. Thus there was a check available on the results of the frequency and celerity determinations. The determination of wavelength by non-optical means is also useful. In many flows the optical access is limited or unavailable. This was also the case in the heated experiments in the current research.

Wavelength is also a valuable parameter because it is a length scale. Length scales are frequently very useful in modelling. An example of this is in turbulence modelling. Many of the popular turbulence models use a mixing length as a parameter. Finally, calculation of the wavelength and its subsequent verification completed the measurement of the basic set of parameters of the film in a robust and self-consistent way.

The visual observations were carried out in order to provide an independent measurement of the wavelength. The method used was quite simple. Markings were placed on the floor of the test section at one centimeter intervals. Slides were then taken taken of the flowing film using a 35mm SLR camera. The images were analyzed by projecting them and measuring by hand. Two slides were taken of most of the runs. Five measurements of different wave pairs were made on each slide. The measurements were then averaged and standard deviations computed. The results are given in Table 5.6. The standard deviations of the multiple measurements were typically about 10%.

As has been discussed previously, it was necessary to find the correct frequency and celerity parameters in order to compute wavelengths that were consistent with visual observations. The spectrum average frequency, which corresponds to the number of waves passing an obser-

vation point per second, was used as the frequency parameter. The speed of the waves relative to the bulk motion of the film was used as the celerity parameter. These parameters where found to generate the best wavelength values. The wavelength was calculated by the classic wave formula:

$$\lambda = c/f_{avg} \qquad (5.18)$$

where c - relative wave speed

f_{avg} - spectrum average frequency (Doppler-corrected)

It is also interesting to note that if one substitutes the expressions for the celerity and frequency in terms of the measured parameters (equations (5.9) and (5.16)) into equation (5.18) that the result is the following:

$$\lambda = v_{app}/f_{avg} \qquad (5.19)$$

where v_{app} - apparent wave speed

f_{avg} - spectrum average frequency (not Doppler-corrected)

Therefore, if one only wishes to calculate wavelength only, the simple apparent speed and uncorrected spectrum average frequency can be used. This is particularly valuable in those cases where the film velocity cannot be accurately estimated.

The results are shown in Table 5.6. Although the agreement of the calculated λ's with the measured values is only fair, it should be recalled that the three-dimensional waves which were studied here do not display a regular, periodic character. They can only be studied in terms of distributions or average values. The measured λ's represent an average over a relative small set and are somewhat suspect in that regard. The computed λ's also have generous error bars.

Another simple comparison can be made to the Taylor wavelength calculated from instability theory. The fastest growing Taylor wavelength is given as [35]:

$$\lambda_c = 2\pi\left(\frac{\sigma}{g(\rho_l - \rho_g)}\right)^{0.5} \qquad (5.20)$$

where σ = surface tension

g = gravitational acceleration

ρ_l = density of liquid

ρ_g = density of gas

Under the conditions of the experiments, λ_c was equal to 1.68 cm, which is of the order of the results listed in Table 5.6.

The analysis of error for the calculated λ values is contained in Appendix A. The results are summarized in Table 5.7. Since a detailed estimate of the error in the

(uncorrected) frequency parameter was not available, a value of 10% was used to compute the errors in λ. This is generally comparable to the error in determining the delay time in the apparent wave speed measurement. The errors in wavelength fall in the 10-20% range.

5.6 CONCLUSION

The Isothermal Test Series accomplished the major goals which were set for it. An experimental methodology was developed which used the hot-wire anemometer to characterize the interfacial waves. The methodology was shown to be reasonably reliable, robust, and capable of generating meaningful and useful results.

The measurements of film thickness, amplitude, and frequency were compared to the results of Hanratty and his co-workers and generally good agreement was shown. Film thickness was measured accurately and reliably under all of the conditions of interest. Amplitude was measured less reliably and with greater experimental error, but the problems associated with its measurement have been documented and may be amenable to improvement. The frequency measurements compared very well with those of the previous workers (without Doppler correction). The spectrum average frequency could be identified with the number of

waves per second from their work. Improved accuracy would be attained in the frequency measurements, however, if the sampling rate and correspondingly the low frequency limit were reduced slightly.

The results for the celerity measurements indicated a different interpretation was required than was used by Akai et al. Although the apparent wave speed agreed well with their work, it was the relative wave speed that was found to compare favorably to theoretical expressions. It was also the relative wave speed that was used to compute the most physically realistic values of the wavelength.

The work of Akai and associates was also improved and extended so that measurements could be taken in the three-dimensional wave regime rather than just in the more uncommon two-dimensional wave regime. Use of the FFT allowed a complete frequency distribution to be measured, while the development of the C-series probe enabled wave speed measurements in three-dimensional wave fields where the use of standard probes was unsatisfactory.

A self-consistent set of interfacial wave parameters was identified. Celerity and frequency parameters were defined based on readily measureable quantities. A wavelength was defined based on the celerity and the frequency parameters and was found to correspond to observed wavelengths.

Finally, a small test matrix of experiments was completed. The results include measurements of all of the interfacial wave parameters. These results and the methods used to obtain them are thus available for future use in studying and evaluating improved measurement techniques.

TABLE 5.1

FILM THICKNESS & WAVE AMPLITUDES

Comparison to Previous Work

Run	V_g(m/s)	Re_g(eff)	Q(lpm)	Re_f	δ (cm)	A (cm)
F-3	10.9	9100	3	490	0.278	0.076
F-4	11.0	9100	3	490	0.272	0.076
F-5	11.1	9100	3	490	0.293	0.076
F-7	11.2	9100	3	490	0.242	0.127
C & H [97]	11.2	--	-	483	0.270	0.088
Akai [1]	12.6	--	-	464	0.22	0.07
L & H [93]	--	10560	-	532	0.287	0.099
F-6	8.4	7000	3	490	0.355	0.076
C & H [97]	8.4	--	-	483	0.354	0.074
L & H [93]	--	7300	-	581	0.341	0.098

TABLE 5.2

FILM THICKNESS & WAVE AMPLITUDE

Isothermal Test Matrix

FILM THICKNESS δ (mm)

		Air Velocity (m/s)		
		6.3	9.0	11.9
Film	2	3.42	2.26	1.31
Flow	3	4.18	2.76	1.88
(lpm)	5	4.79	3.56	2.87

WAVE AMPLITUDE A (mm)

		Air Velocity (m/s)		
		6.3	9.0	11.9
Film	2	0.25	1.02	1.02
Flow	3	0.51	1.52	1.52
(lpm)	5	1.27	2.29	2.54

TABLE 5.3

WAVE FREQUENCIES

Comparison to Previous Work

Run	V_g(m/s)	Re_g(eff)	Q(lpm)	Re_f	f_{peak} (hz)	f_{avg}
AVG-F-1	8.4	7000	3	490	8.	22.4
AVG-F-2	8.4	7000	3	490	8.	22.7
AVG-F-3	8.4	7000	3	490	8.	34.5
C & H [97]	--	--	-	-	7-12*	
L & H [93]	--	7420	-	532	9.7	21.2
L & H [93]	--	7300	-	581	11.	22.2
AVG-F-4	11.2	9100	3	490	12.6	37.3
C & H [97]	--	--	-	-	7-12*	
L & H [93]	--	10560	-	532	12.	26.4
Akai [1]	12.6	--	-	464	-	27.

* Only a range given for all runs.

Note that no Doppler corrections were applied.

TABLE 5.4

WAVE FREQUENCIES

Isothermal Test Matrix

DOPPLER-CORRECTED

SPECTRUM AVERAGE FREQUENCY (hz)

		Air Velocity (m/s)		
		6.3	9.0	11.9
Film	2	15.4	23.1	10.7
Flow	3	16.2	16.7	11.9
(lpm)	5	12.2	10.5	11.5

ERRORS IN DOPPLER-CORRECTED

SPECTRUM AVERAGE FREQUENCY (%)

		Air Velocity (m/s)		
		6.3	9.0	11.9
Film	2	15.7	31.1	70.2
Flow	3	15.9	18.9	34.3
(lpm)	5	14.8	18.1	20.3

TABLE 5.5

CELERITY

Isothermal Test Matrix

Air Velocity (m/s)	Film Flow (lpm)	Apparent Speed	Film Speed	Relative Speed	Lamb's Th. Speed
			(cm/s)		
6.3	2	36.5	9.6	26.9	20.3
	3	37.5	11.7	25.8	23.9
	5	47.2	17.1	30.1	29.8
9.0	2	39.9	14.5	25.4	24.0
	3	41.8	17.8	24.0	28.7
	5	50.0	22.9	27.1	34.5
11.9	2	37.2	25.0	12.2	22.6
	3	46.0	26.1	19.9	27.7
	5	55.4	28.5	26.9	35.6

TABLE 5.6

WAVELENGTH

Isothermal Test Matrix

COMPUTED WAVELENGTHS (cm)

		Air Velocity (m/s)		
		6.3	9.0	11.9
Film	2	1.74	1.10	1.13
Flow	3	1.60	1.44	1.83
(lpm)	5	2.47	2.57	2.35

MEASURED WAVELENGTHS (cm)

		Air Velocity (m/s)		
		6.3	9.0	11.9
Film	2	0.99	0.86	0.72
Flow	3	1.11	1.18	0.79
(lpm)	5	1.47	1.32	1.03

TABLE 5.7

ERROR SUMMARY

ERROR IN CELERITY MEASUREMENT (%)

	Air Velocity (m/s)		
	6.3	9.0	11.9
Film 2	11.	26.	69.
Flow 3	11.	15.	32
(lpm) 5	9.8	14.	17.

ERROR IN MEASURED WAVELENGTHS (%)

	Air Velocity (m/s)		
	6.3	9.0	11.9
Film 2	11.2	17.1	12.9
Flow 3	11.5	11.3	12.4
(lpm) 5	11.1	11.5	11.0

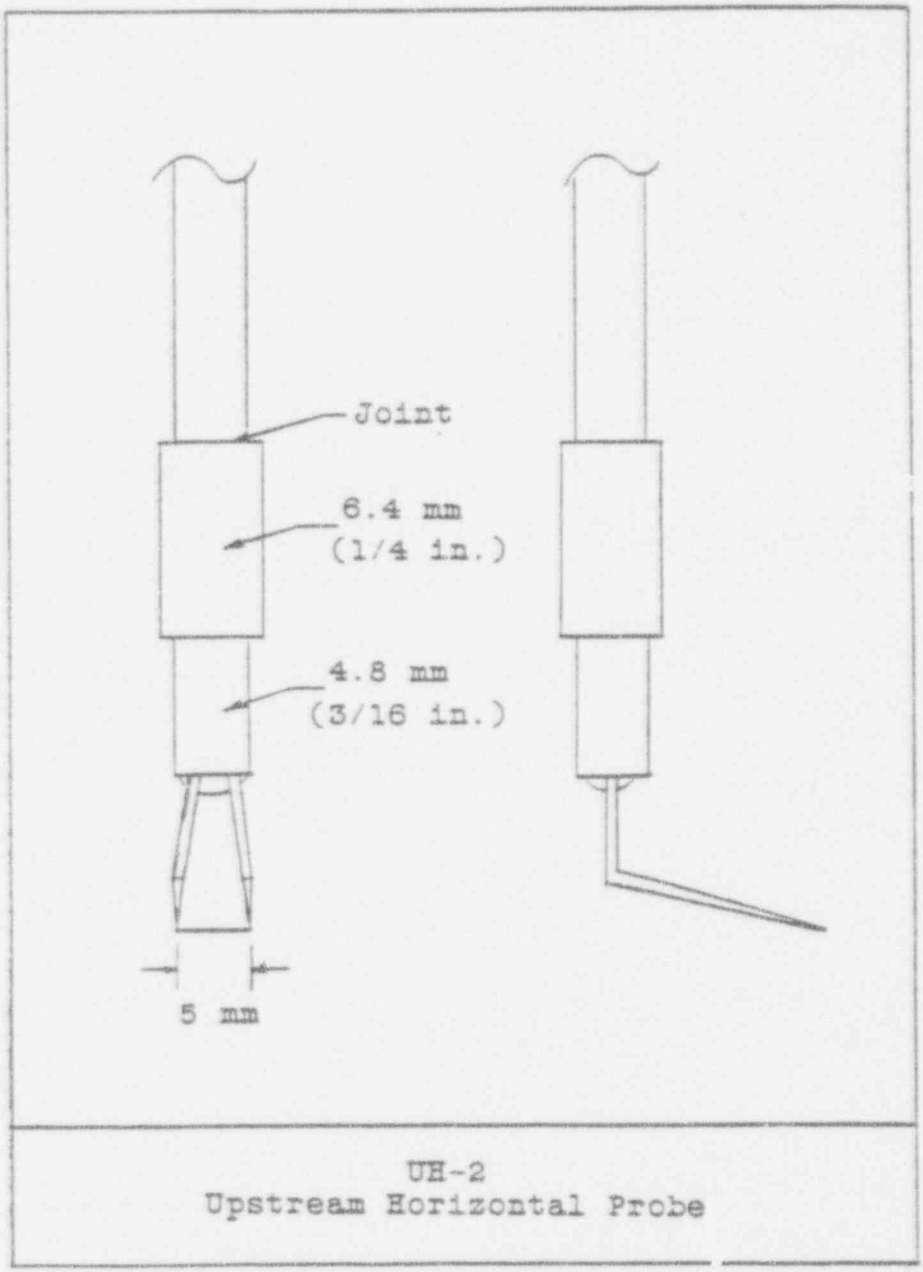

Figure 5.1 Upstream Probe for Film Measurements

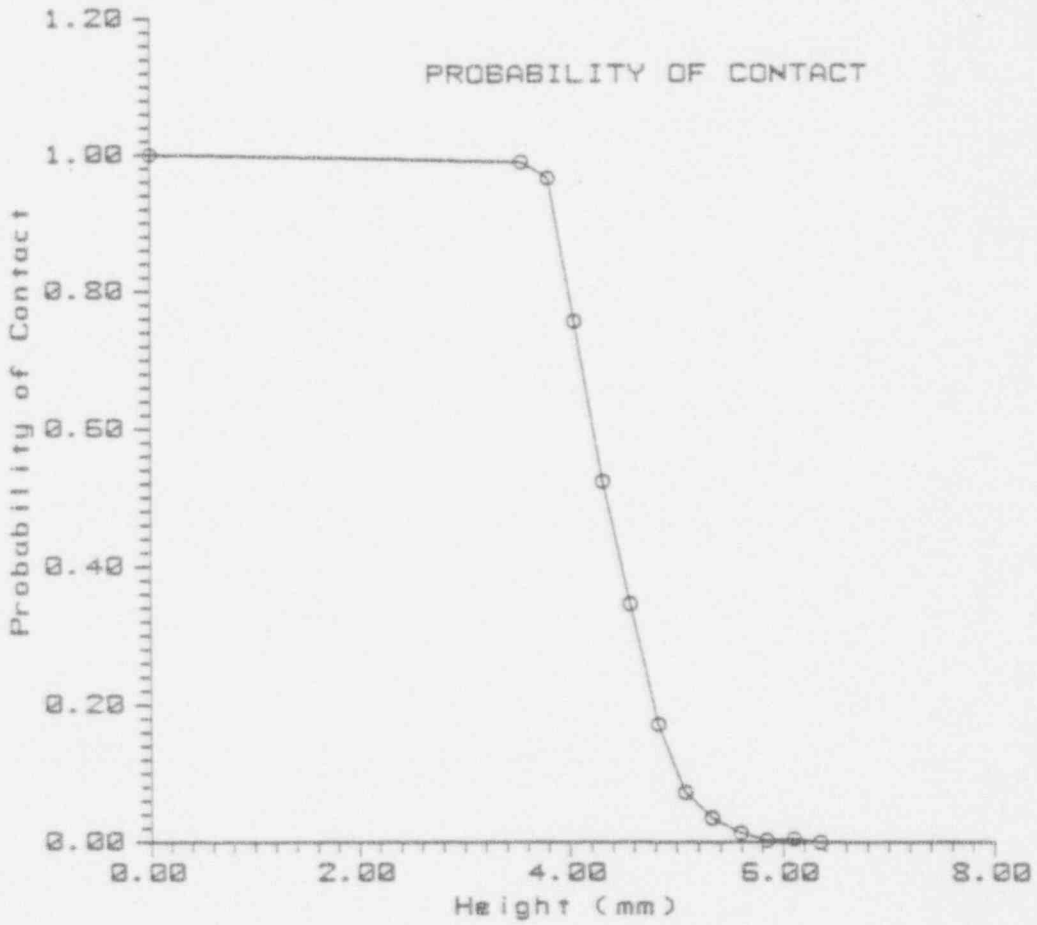

Figure 5.2 Typical P_c Plot

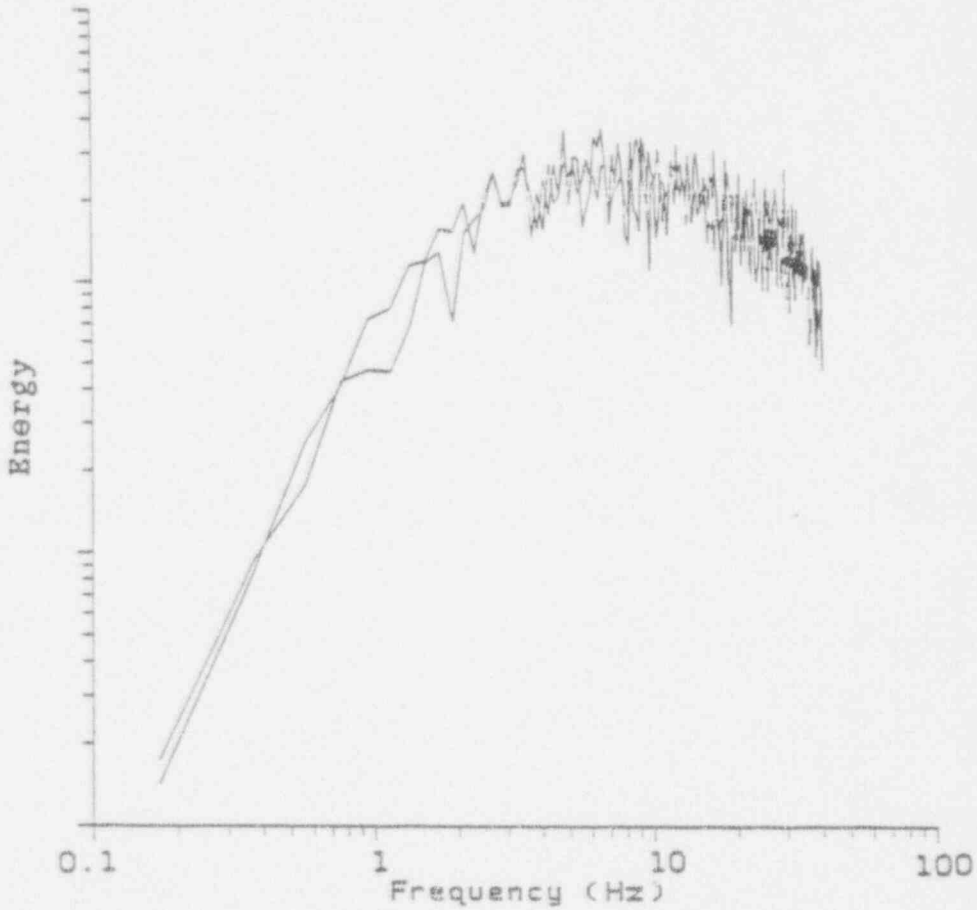

Figure 5.3 Frequency Spectra-Repeatability

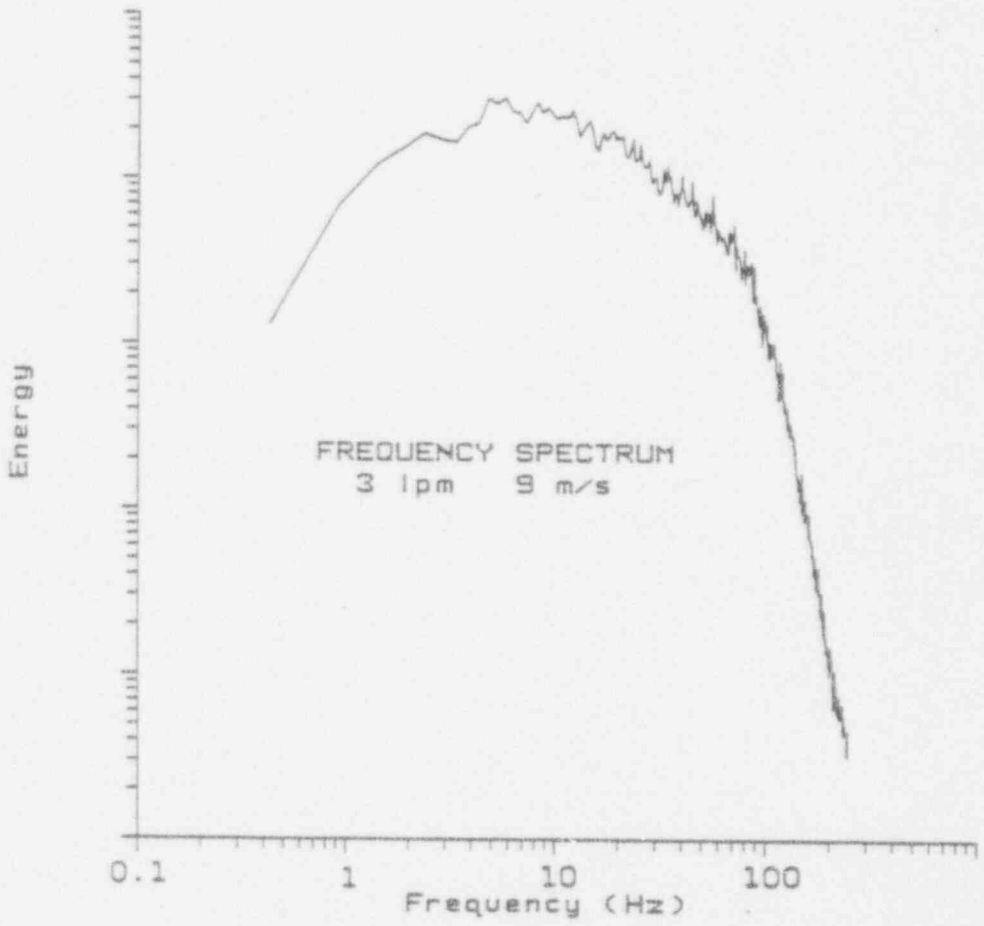

Figure 5.4 Typical Smoothed Frequency Spectrum

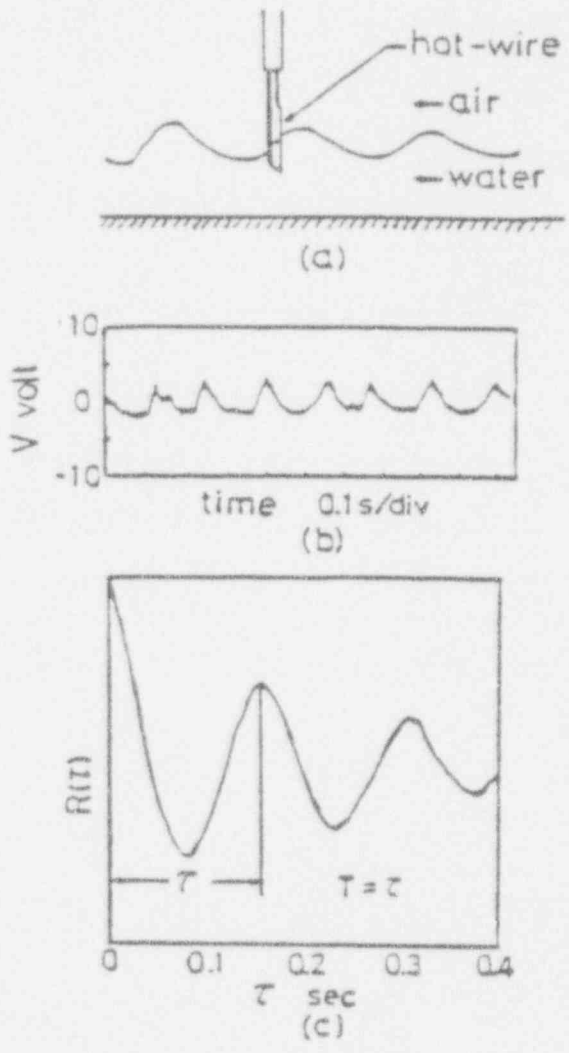

Figure 5.5 Frequency Measurement Technique of Akai et al [1]

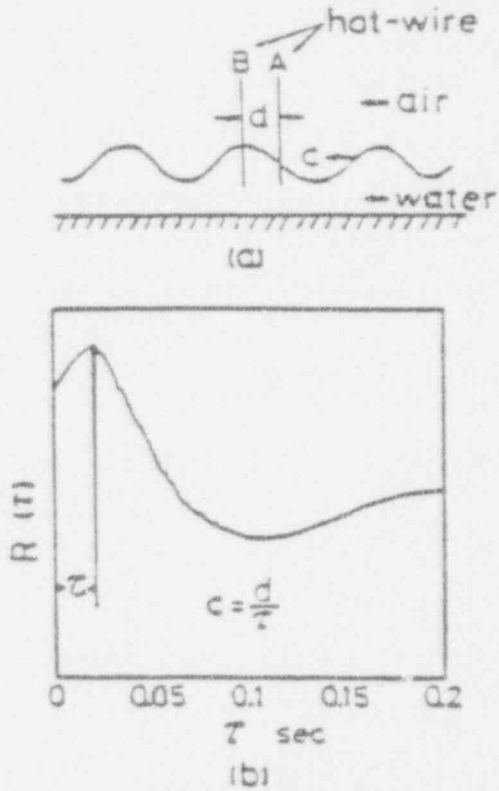

Figure 5.6 Wave Speed Measurement Technique

From Akai et al [1]

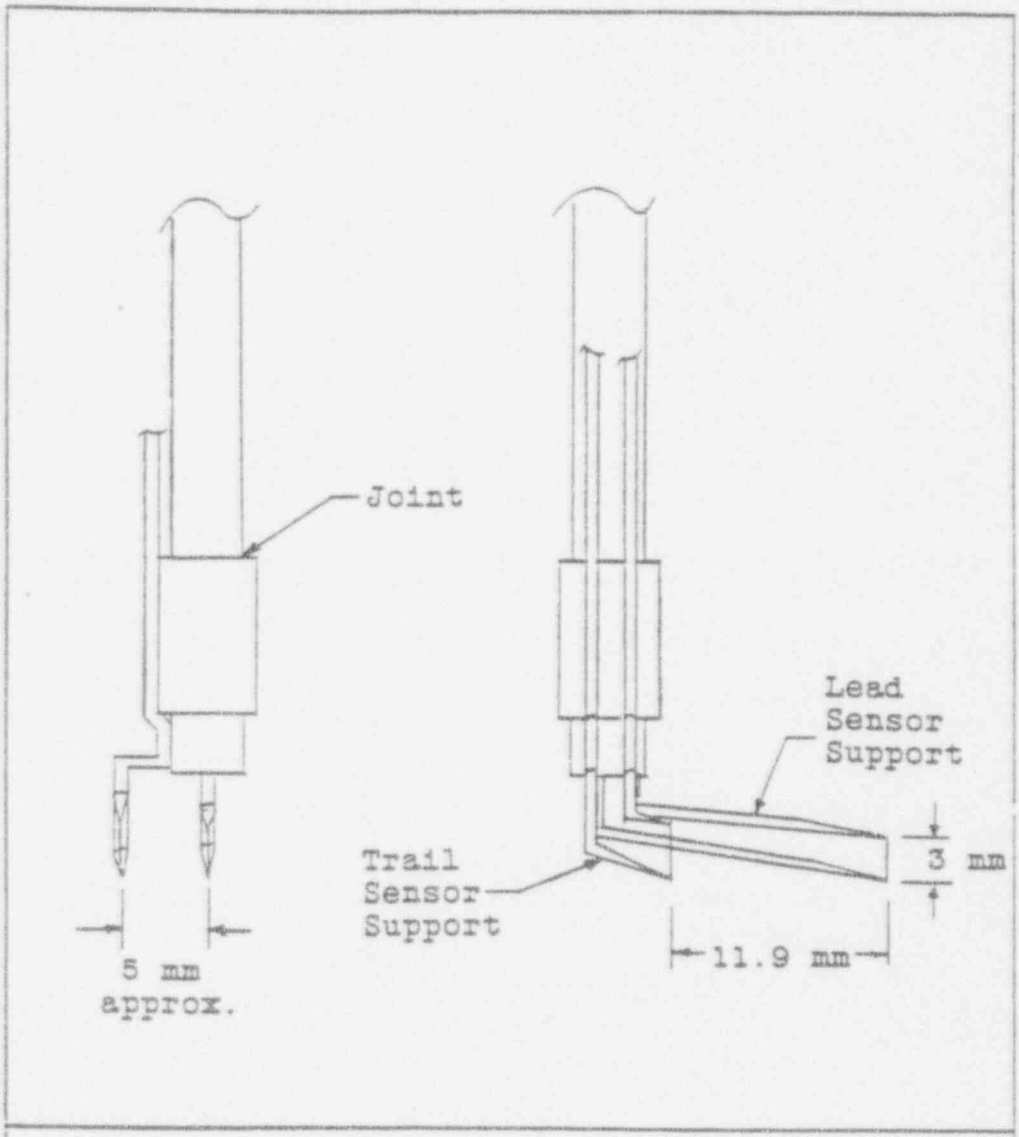

Figure 5.7 C-Series Probe

6. AIR/STEAM TEST SERIES

6.1 MEASUREMENT PROCEDURE

6.1.1 Data Acquisition.

There were several types of data which were taken during the course of the heated experiments. The readings from the three flowmeters, (coolant, film, and steam) used in these experiments were recorded manually on data sheets. The values of the differential pressure from the steam flowmeter varied cyclically with the boiler pressure. Although the attempt was made to reduce this behavior by using as large a boiler pressure as possible, it was still necessary to attempt to mentally average out the oscillations to get the final reading.

Wave data was taken in the heated tests with an injected film. The use of the hot-wire anemometer presented a slight complication due to the heated environment. For each new set of experimental conditions it was necessary to measure the "cold" resistance of the sensor since the cold resistance is dependent on the ambient temperature of the fluid. The overheat ratio was then used to calculate the operating resistance by the usual formula.

$$OHR = R_{op}/R_{cold} \qquad (6.1)$$

where OHR - overheat ratio

R_{op} - operating resistance

R_{cold} - cold (ambient temperature) resistance

An OHR of 1.05 was used. This is the value recommended by TSI for using wire sensors in liquids [130] and it seemed to work quite well. The wave data was taken using the Nicolet digital oscilloscope and transferred to the computer using the DATRAN program as was done in the isothermal runs.

Temperature data was taken using the DATAC program and the Keithley Series 500 Data Acquistion System described in the Facilities section. Due to the number of channels of temperature data which were acquired, two AIM-7 16-channel thermocouple input boards were used. This caused a complication. The design of the SOPT500 software precludes acquiring more than 16 channels at once if the internal temperature conversion routines are used. Therefore the acquisition of the temperature data was always done in two parts. The first part included the monitoring thermocouples and the first two heat flux meters. The second part was comprised of the remaining three heat flux meters.

Oscillations in the test section temperatures were present due to the differential pressure limitations of the boiler pressure controller discussed in the Equipment Testing section. These oscillations occurred on about a 1-2 minute period. It was necessary to average out these oscillations over time due to both the two-part nature of the temperature data acquisition and the differing heat capacities of the different system components. Data was therefore taken over a 10 minute interval at a rate of 1 sample every 5 seconds.

6.1.2 VEL Program.

The VEL program was written to compute test section gas mixture velocity, v_g, given the mixture temperature (T_{mix}), steam temperature at the orifice meter (T_{stm}), and the orifice meter differential pressure reading (Δp_{orif}) as well as the orifice flow meter design characteristics.

The first step in the calculation involves determination of the mass flow rate of steam through the orifice meter. The stand alone program FLOW was originally taken from the flowmeter design handbook [123] in BASIC. The algorithm was converted to FORTRAN and an equation-of-state package was added for steam. This then formed the basis for VEL. The details of the flow computation can be found in the aforementioned handbook, but the primary

equation is listed here.

$$m_s = \frac{C\epsilon\pi d^2 F_s (2\Delta p_{orif}\rho_{stm})^{0.5}}{4\,(1-\beta^4)^{0.5}} \qquad (6.2)$$

where C - $f(m_s)$ (curve fit given)

ϵ, F_s - correction factors

d - orifice diameter

D - diameter of pipe

β - d/D

ρ_{stm} - density of steam at T_{stm}

It should be noted that this is the correct form of the equation. As was mentioned earlier, the flowmeter handbook contained an error. The error was that Δp_{orif} was pulled out from under the square root. The velocity of the gas mixture can then be simply computed as follows:

$$\rho_s = \rho_g(T_{mix}) \quad \text{(EOS)}$$
$$v_g = m_s/(\rho_s A_{ts}) \qquad (6.3)$$

where ρ_s - steam density at T_{mix}

A_{ts} - area of test section

This completes the calculation of the velocity by the orifice meter.

The program also will calculate the velocity of the gas mixture based on a Pitot tube reading.

$$v_g = (2\Delta p_{pitot}\rho_{mix})^{0.5} \qquad (6.4)$$

where Δp_{pitot} = manometer reading

ρ_{mix} = density of the gas mixture

The gas mixture density is easily computed using the known value of T_{mix} and the EOS.

6.1.3 HTFLUX Program.

The HTFLUX program was written to do the reduction of the heat transfer data. This consists of computing the heat fluxes, heat transfer coefficients, and wall surface temperatures for each heat flux meter. The overall heat flux and heat transfer coefficient are computed from the coolant measurements.

The input for the program consists of the names of the setup file, the output file, T_{mix}, and Q_{cool}. The data file names are extracted from the setup file. The program then automatically opens the files and the mean and standard deviation are calculated for each thermocouple as needed.

A simple linear least square fit is applied to each meter in sequence using the temperatures previously calculated and the precise position of each thermocouple in each meter. These positions were measured prior to emplacement of the thermocouple strips in the heat transfer plate. This provides the temperature gradient and

T_{surf}. The temperature of the back surface of the heat transfer plate, T_{back}, is also computed.

The temperature gradient is then used to compute the heat flux in each meter. The overall heat flux is computed using the inlet and outlet coolant temperatures and the coolant flow rate. Next, the heat transfer coefficients are computed from the heat fluxes, the mixture temperature, and the surface temperatures. Finally, all of the results are output in a report format.

6.2 HEATED TESTS WITH INJECTED FILM

6.2.1 Introduction.

The heated tests which were conducted with the presence of an injected film were intended to address several areas of interest. The first area involved determination if the methods developed during the Isothermal Test Series would be applicable to experiments in condensation. The ability to use those techniques would provide a new capability for future research efforts. Another area of interest was in the effects of condensation heat transfer on the characteristics of the film. Change in the wave parameters of the film under the conditions of condensation was not unexpected. The final area of interest was in simultaneous measurement of wave

parameters and heat transfer coefficients. It was hoped that a knowledge of the wave parameters would aid the development or evaluation of an improved condensation heat transfer model.

The experimental test matrix which was selected was guided by these interests. The matrix was constrained, however, by the limitations in the capabilities of the experimental apparatus as discussed in the Equipment Testing section. Variation with T_{mix} and v_g was to be tested, along with runs which could be fairly directly compared with some in the Isothermal Test Series. Lower film flow rates were used so that the conditions would more properly reflect anticipated applications.

T_{mix}	v_g	Q_{film}
50 C	5.5 m/s	1 lpm
		2 lpm
60 C	5.5 m/s	1 lpm
		2 lpm
70 C	5.5 m/s	1 lpm
		2 lpm
50 C	6.5 m/s	1 lpm
		2 lpm
60 C	6.5 m/s	1 lpm
		2 lpm

The following sections discuss the measurements which were undertaken, the problems which were encountered, and the results that were obtained.

6.2.2 Film Thickness and Amplitude.

The measurement of film thickness and amplitude was made using the technique developed during the isothermal tests. A home-made upstream-type probe was installed and the traverse offset was determined. The experimental rig was then started up and a traverse was made through the interfacial region. The probability of contact with the liquid film (P_c) was then plotted and the film thickness, δ, and the amplitude, A, determined.

There were several difficulties which were encountered during these measurements, however. First the presence of the insulation on the test section made the operation of the traverse more clumsy. The primary effect here was to make the determination of traverse offset more difficult and slightly less accurate. The insulation also prevented direct visual observation of what was happening to the probe, although the oscilloscope display gave a fairly good indication.

A second more fundamental problem was that the test matrix was composed of fairly low velocity and low film flow rate runs. These types of runs do not generate very

large waves and the probes encounter a strong contact hysteresis effect. Therefore the P_C curve tends toward a perfect step function. This allows a reasonable estimate of film thickness to be made, but prevents any real information on the amplitude from being acquired.

The results of the film thickness and amplitude measurements are shown in Table 6.1. These results may be compared to those in Table 5.2 for the isothermal tests. It is readily apparent that in only one case was there a meaningful amplitude value to report.

A clear tendency towards substantially smaller film thicknesses in the heated tests is also observable. The reason for this tendency is not known. One would not expect the film thickness in the heated tests to be substantially larger than it was in the isothermal tests solely based on the increased mass flow rate due to condensation. The flow rate of condensate is probably negligible in comparison to the the flow rate of the injected film. One would not, however, expect to see a substantially smaller δ for the heated tests either.

There are several possible reasons for this. The additional errors in the determination of the traverse offset for the heated tests may have contributed. The gas velocity computed using the orifice meter steam flows may have underestimated the velocity. Another possibility is

that the use of the old (and much less accurate) film flowmeters for the isothermal runs caused those experiments to use an incorrect film flow rate. This should probably be considered less likely since the isothermal results compared well with those in the literature.

The lack of amplitude measurements itself may be indicative of one of the effects of condensation on the behavior of the film. This lack was probably due to the presence of very small wave amplitudes. If this is the case, then the expected damping effect of condensation may have been the culprit. It has been speculated that the flow of vapor to the interface may have a stabilizing effect on wave generation [3,17]. The results of the heated experiments tend to support this view, although additional work is needed before this effect can be shown conclusively.

6.2.3 Frequency.

The frequency measurements were made in exactly the same way as in the isothermal tests. The five data sets taken in the celerity measurements for both the lead and trail sensors were run through the FFT and averaging programs and yielded a spectrum average frequency value. The same sampling frequency, filter frequency, and number of data points were used. The probe which was used, which

will be discussed in the next section, was a modification of the same probe used in the isothermal measurements.

The frequency spectra exhibit a shape similar to those found in the isothermal series, although slightly different in detailed character, as can be seen in Figure 6.1. The Doppler-corrected spectrum average frequency, f_{avg}, results are listed in Table 6.2. Again the results seem similar to those which were found in the isothermal runs. Minor differences may be attributable to the probe modification.

6.2.4 Celerity.

The celerity measurements were also made utilizing the same procedure used in the isothermal test series. No serious problems were encountered and the measurement technique seemed quite amenable to use in the condensing environment.

Due to the selection of thinner 1 and 2 lpm films in the heated series, a slight modification to the C-5 probe used in the isothermal tests was required. With the use of shorter wire sensors in the C-6 probe, the results for the 2 lpm films were substantially better than they were for the isothermal tests using 2 lpm films. The 1 lpm films represented quite a challenge, even for the improved C-6 probe, but several of the tests yielded good results.

The tradeoff, of course, was that the C-6 probe would be unable to span the large wave amplitudes. Since the test matrix was limited however, no difficulty with this limitation was encountered.

The results of the celerity measurements are shown in Table 6.2. The apparent wave speeds seem to be somewhat reduced as compared to those measured in the corresponding isothermal runs, but due to the relatively large error bars such a conclusion is probably tenuous. The film velocities were higher in the heated tests. This is a direct result of the reduced film thicknesses which were measured. The relative wave speed or celerity figures are thus significantly lower than those which were measured in the isothermal tests due to the combined effects of the reduced apparent wave speed and the increased film velocity.

The celerity measurements were subject to much the same errors that were present during the isothermal tests with one exception. Since the film flowmeter was replaced with two lower capacity units, the error in the flow measurement was reduced to 7.5% for all of the heated runs. This ceased to be one of the main contributions. The traverse error again contributed substantially to the celerity error with much of the reason due simply to the fact that thinner (lower flow rate) films were selected.

The estimates of error in Δt (delay time) were generally improved over those of the isothermal tests for the 2 lpm films due to the improved C-6 probe, but Δt errors for the 1 lpm films were not nearly as good.

6.2.5 Wavelength.

Wavelengths were determined only by computation in the heated tests. The presence of insulation on the test section precluded visual observation. The computations were carried out in the same way as in the isothermal tests. Due to the possible uncertainty in the film thickness measurement which is used to compute v_{film}, the wavelength was calculated directly from the apparent wave speed and uncorrected spectrum average frequency (equation (5.19)).

The results of the wavelength computation are listed in Table 6.2. Several interesting points may be noted in comparison to the isothermal results in Table 5.6. The first observation is that the wavelengths are clearly reduced in the heated experiments. This again may be due to the damping effect of the flow of vapor towards the interface during condensation, but no mechanism for this effect has been identified. The data also exhibits the same trend toward larger wavelengths with thicker films that was noted in the isothermal results.

6.2.6 Heat Capacity Correction.

An important aspect of the measurement of the heat transfer coefficient in these experiments was the determination of the correction necessary to allow for the effects of the heat capacity of the injected film. The difficulty encountered in making this correction is the probable reason for the disappointing results in the heat transfer coefficient measurement.

The heat capacity correction is required due to the relatively large quantity of heat which is absorbed or released by the injected film. In the majority of cases in these experiments it was a release of heat to the cold wall that was important.

The water for film injection was taken from the constant head tank which is at approximately the same temperature as the water in the secondary condenser hotwell after the test rig has been run for some time. The temperature in the secondary condenser hotwell was a function of the temperature and flow rate of the incoming steam and film and the temperature and flow rate of the cooling water in the drain cooling coils and dehumidifier. As a practical matter, the temperature and flow rate of the cooling water (the ultimate heat sink) were essentially constant. Therefore the temperature in the hotwell and, by extension, in the film injection line was primarily a

function of the temperature and flow in the test section. Fortunately, this dependence worked in the correct direction. Under higher temperature conditions in the test section, the hotwell temperature was increased. Hence the injected film temperature was also increased which was basically the desired result. As no equipment was available for separate heating or cooling of the film prior to injection, this was indeed fortunate.

Nevertheless, a correction for the heat capacity of the film was required. Three film temperatures were measured during the course of the experimental series. These are shown in Figure 6.2. The inlet temperature was measured in the pipe leading into the film injection fitting. The traverse thermocouple probe was used to measure the film temperature at the leading edge of the heat transfer plate and the exhaust thermocouple probe was used to sense the film temperature at the trailing edge of the plate. A straightforward correction can be made by a simple energy balance:

$$q_{film} A_p = q A_p + m C_p \Delta T_{film} \qquad (6.5)$$

where q_{film} = heat flux (including film)

q = heat flux without film

A_p = area of the heat transfer plate

m = mass flow rate of the film

C_p - specific heat of film

ΔT_{film} - change in film temperature across plate

This equation can be easily rearranged to give:

$$q = q_{film} - m\, C_p \Delta T_{film} / A_p \qquad (6.6)$$

As all of the values are known or can be measured on the right-hand side, the corrected heat flux can be computed.

The difficulty comes in measuring the ΔT_{film} across the plate. As can readily be seen, the correct value to take for ΔT_{film} is the difference of the traverse and exhaust temperature readings since one doesn't really care what happens upstream of the plate. One simply wants to correct for the change in the bulk temperature of the film as it crosses the plate. Unfortunately, measuring the traverse and exhaust temperatures accurately was not easy. For the measurements taken in this series of experiments, the tip of the thermocouple probe was extended into the film. Due to conduction along the probe, the relative thinness of the film, and errors in positioning of the tip, the results were not very favorable.

Due to these measurement problems, the heat transfer correction was applied in two ways. In the first attempt, the traverse and exhaust temperatures were subtracted to give ΔT_{film}. The results were quite poor with the calcu-

lated q's often becoming nonsensically negative. Despite several attempts to reposition the probes, no reasonable correction could be achieved this way.

The second method utilized the inlet temperature instead of the traverse temperature. This method would not be expected to give particularly accurate results because the film may heat up somewhat in the entrance length of the test section before it reaches the heat transfer plate. Also, the exhaust temperature was still used as the outlet temperature despite the fact that it may have been as erroneous as the traverse temperature. Unfortunately no alternative sensor was available in this case.

An improved method of determination of ΔT_{film} is under study for future research. The exhaust temperature would seem to be the simpler of the two problems to fix. The use of an adiabatic mixing cup located just off the trailing edge of the plate seems promising. The measurement of temperature at the leading edge of the plate is still under study. It is more difficult to accomplish because it is important now to disturb the flow or wave pattern at a position just upstream of the plate.

One potential difficulty that correct measurement of the temperature change of the film will not address is that the heat capacity correction is linear. In other

words, the correction is made assuming that the film temperature changes linearly along the length of the heat transfer plate. If this were not the case the overall heat transfer coefficient would be properly corrected, but the values obtained from the individual heat flux meters would not. At this time, however, the linear assumption appears to be reasonable first assumption.

All of the heat transfer results for the heated runs with a film, including the heat transfer correction, are discussed in the following section.

6.2.7 Heat Transfer Coefficient.

One of the goals of the heated tests that were conducted with an injected film was to simultaneously measure both the wave parameters and the heat transfer coefficient. Although the wave parameters were determined reasonably successfully, the heat transfer coefficient results were much more suspect.

After taking and reducing the heat flux meter data, the heat transfer correction described in the previous section was applied. As was discussed there, the correction for the heat capacity of the film was made using the inlet and exhaust temperatures. As was also noted the results of this correction were not very satisfactory. One of the reasons being that the temperature measurement

was not believed to be very accurate. Another reason is that the heat capacity correction is a large fraction of the total heat flux. The results of therm-43 are a good example.

therm-36: T_{mix} - 68.0 m/s

T_{surf} - 32.4 C

v_g - 5.2 m/s

Q_{film} - 2 lpm

$q_{overall}$ - 29983 W/m^2 (uncorrected)

T_{inlet} - 41.0 C

$T_{exhaust}$ - 31.8 C

total heat transferred - $q_{overall} A_p$

- 1866 W

heat transferred to film - $mC_p \Delta T$

- 1276 W

Complete listings of the overall heat transfer coefficients for all of the runs with film are shown in Table 6.3. Several plots of heat transfer coefficient as a function of position on the plate are shown in Figures 6.3-6.5. Although the results do not look unreasonable, detailed analysis of them was not warranted because of the uncertainty.

Due to the indeterminate error which was introduced by

the heat capacity correction, no formal error analysis was conducted for the heat transfer coefficient in these runs. The error due to the thermocouple error and curve fit would generally be less than that which is reported for the heated tests without film injection. This is because the heat capacity of the film increases the heat flux through the plate.

6.2.8 Conclusion.

The heated tests made with an injected film were successful in addressing some of the areas of interest noted in the introduction. Need for further refinements in some of the techniques was also noted.

The wave parameter measurement techniques developed in the isothermal tests seemed to be quite applicable to the heated tests. Some problems were noted due to the thin films and low gas velocities, but these problems were expected and would surface in isothermal runs with thinner films and smaller velocities as well. The use of the home-made probes with wire sensors proved straightforward. No reliability problems were encountered and the performance matched or exceeded the performance which was obtained in the isothermal tests.

Some changes in the wave parameters in the heated tests as compared to the isothermal ones were noted. The

reduced film thicknesses were not readily explained and may be due to experimental error. These errors may also have effected the celerity results. The amplitude measurements do, however, point to some suppression in wave generation due to condensation. The wavelengths have also changed by a large amount and may indicate some effect. At this point the results are not considered conclusive and future studies should be undertaken to confirm these observations.

The heat transfer results were largely disappointing owing to the problems which occurred in trying to correct for the heat capacity of the film. Improvement in the measurement techniques for the film temperature would be expected to yield much better results.

6.3 HEATED TESTS WITHOUT INJECTED FILM

6.3.1 Introduction.

A series of heated tests were also conducted without film injection. Such a test series was of interest due to the high concentrations of noncondensable gas which could be used in the test section. As was discussed in the Literature Survey, previous condensation experiments utilized either pure vapor or vapor with low concentrations of noncondensable gas. Few experiments have ex-

amined condensation under the conditions of high noncondensable concentration which would be expected in certain accident conditions in reactor containment buildings. Hence this test series represented a unique opportunity for study of condensation for this application.

The test matrix was selected based on a desire to simulate a variety of conditions while remaining within the limitations of the experimental apparatus. Two independent variables were selected for study. The first was the air/steam mixture temperature (T_{mix}). Since the apparatus operates at constant (atmospheric) pressure, specification of T_{mix} is equivalent to choosing the mass ratio, R. Equation (4.4) demonstrates this dependence. The second independent variable selected was the gas mixture velocity, v_g. Both of these variables were varied throughout approximately their entire range in the test matrix as can be seen in Table 6.4. The limitations in these variables were discussed previously in the section on Equipment Testing.

The wall surface temperature, T_{surf}, was held at 25 C throughout the tests. This selection was made for several reasons. This was a very reasonable choice in terms of the intended application of the results (containment). In addition, selection of a T_{surf} very near to room temperature minimized any errors that could be caused by heat

losses to the room. Finally, this T_{surf} was one which could be maintained throughout the test matrix. Due to limitations of the refrigerated heat exchanger, T_{sink} and by extension T_{surf} were contrained to certain ranges depending on the heat flux.

The following sections describe the heat transfer measurements and visual observations which were made. These were not made simultaneously as it was necessary to remove insulation from the test section to obtain optical access.

6.3.2 Heat Transfer Coefficients.

Unlike the situation which existed in the heated tests with film injection, no correction for heat capacity of the film was required in this test series. For this reason the heat transfer results were much more satisfactory.

One problem which is more critical is in the accuracy of the heat flux meters. As was mentioned in the Equipment Testing section, the accuracy of the heat flux meters diminishes as the magnitude of the heat flux is reduced. This is due to the finite resolution of the thermocouple temperature measurement. In the heated tests with film injection, the heat capacity of the film resulted in much larger heat fluxes through the heat transfer plate. There-

fore, the accuracy of the heat flux meters was rarely a problem there. In some of the tests without an injected film, however, the heat flux is low enough that the accuracy of the heat flux meters becomes important. The detailed analysis of the error in heat flux measurement is given in Appendix A. Error estimates are also noted in the tables and figures.

The results of the heated tests with film injection are contained in Table 6.5 and Figures 6.6 - 6.12. Table 6.5 lists the overall heat transfer coefficient from coolant measurements for each of the runs in the test matrix. The average heat transfer coefficients calculated from the heat flux meters and the coefficients predicted by the CWNG program are also listed there. The agreement is generally quite good.

It may be observed in Table 6.5, that the overall heat transfer coefficients are consistently about 25% larger than those computed from the four heat flux meters. One reason for this may be that the thermal conductivity of the aluminum alloy in the heat transfer plate was not measured. The value was taken from average values for this alloy, but the suppliers warn that thermal properties may vary. This 25% difference is within the range of other similar alloys.

The heat transfer coefficients are plotted versus the

distance from the leading edge of the heat transfer plate in Figures 6.6-6.12. The effect of velocity is shown in Figures 6.6-6.9. The curves predicted by CWNG are also shown. One can see that the general shape and trends predicted by the code agree well with the data, but that the change in heat transfer coefficient with gas mixture velocity is not as well matched. The velocity of the gas mixture influences the heat transfer by increasing the mixing in the gas-vapor boundary layer. This mixing is enhanced by the increased waviness of the film as well. In addition, the increased sheer stress increases the turbulence (hence mixing) in the film.

The change in the heat transfer coefficient with the mass ratio (R) of air/steam is shown in Figure 6.10-6.12. The deleterious effect of the noncondensable gas is evident. The results of the CWNG predictions are also shown. One can see that again the CWNG results show very similar trends. The change of the heat transfer coefficient with mass ratio seems to be slightly better predicted by the code. One can see that despite the relatively large changes in mass ratio, both the code and the data show modest changes in the heat transfer coefficient. This is because of the forced convection which tends to sweep the noncondensable gas away from the interface. The enhanced mixing caused by the wavy interface also contributes to

the migitation of the noncondensable effect.

The CWNG model utilizes an analogy between heat and mass transfer to compute the condensation heat transfer coefficient. The velocity of the gas mixture is the most important factor in the CWNG model. The heat transfer coefficient is roughly proportional to $v_g^{0.8}$ [3]. One place where the model could be altered to improve agreement with the data is in this exponent. This may not be the best place however, since 0.8 is inherited from the well-established friction factor law by way of the analogy. There are several other possible places in the model where changes could be made.

There are several criteria for wave generation at the interface which are used in the code. The values used in the program are derived from isothermal air-water experiments. As was mentioned earlier, condensation may have a damping effect which might change these criteria.

Another possible area for improvement would be in the modelling of the effect of the interfacial waves on the gas mixture flow field. A rough wall correlation is used in CWNG. Rough wall representations have not been found to model the flow over a wavy film well [97]. This is thought to be due to the fact that the waves are a compliant rather than a rigid surface.

A detailed study of the damping effect of condensation

and of a better correlation for the friction factor over a wavy film would be beneficial in modifying the CWNG model to more properly predict the effect of changes in gas velocity. Investigation into the turbulent Prandtl and Schmidt number representations used in the code also might yield more proper results in both the velocity and mass ratio effects.

6.3.3 Visual Observations.

A limited set of visual observations were made of the condition of the condensate film. Because it was necessary to remove insulation in order to view the test section, it was not possible to make heat transfer measurements simultaneously. In addition, the polycarbonate wall of the test section had to be heated in order to prevent condensation on the inside surface from obscuring the view. This heating was accomplished with a hot air gun here, but for future use, the installation of an electrically heated viewing window might be worthwhile. The observations were made under the following conditions:

Run	T_{mix}	v_g
A	50 C	7 m/s
B	60 C	3 m/s
C	60 C	5.5 m/s
D	70 C	3 m/s

E 70 C 5.5 m/s

In reviewing the results described below, it should be kept in mind that even in an unwetted condition, some moisture appeared to be present on all areas of the heat transfer plate. Condensation therefore took place everywhere, but droplet agglomeration caused a discontinous film.

In Run A, there was no continuous film present. Instead, the condensate ran in rivulets. The appearance was quite similar to the description of dropwise condensation mentioned in the Literature Survey, except that the rivulets did not assume a droplet shape. The shape was more like that of a crescent. This result would be expected since the movement of droplets on a vertical surface depends mainly on gravitiational forces, while the movement of the rivulets here in horizontal flow is governed entirely by the force of the gas mixture drag. As one would expect the film became thicker and more continuous towards the exhaust end of the plate, but it never became a continuous film and the bulk motion of the condensate occurred in these crescent-shaped rivulets. Nothing identifiable as waves was visible.

A continuous film was present in Run B. The film appeared to be a few tenths of a millimetre thick and its

surface was completely smooth. The velocity of the gas mixture was apparently not adequate to disturb the surface. The film would have appeared stagnant except that a few dust particles could be observed moving. Their velocity was estimated at 0.5-1 cm/s.

Run C did not have a continuous film until at least 3/4 of the way along the plate. Prior to this there were some unwetted areas. The same crescent shape was again apparent in the flow of the condensate, but here it manifested itself as more of a disturbance in the surface of the film. These crescent-shaped "waves" of fluid passed through the film very slowly. Outside of these, however, the surface of the film appeared smooth and not wavy. In order to determine whether there would be a sizeable hysteresis effect, a 1 lpm film was run for a few minutes to completely wet the plate, then was turned off. The film returned to its previous discontinuous condition in a few minutes.

The results of Run D looked very similar to those of Run B. A thin smooth film was present over the entire plate. The film thickness appeared to be approximately 1 mm. There were no waves present.

Run E also displayed a continuous film. The top surface of the film looked fairly smooth and glassy, but a slight rippling in the reflection was present. This

looked extremely similar to the situation which was seen in isothermal flow just prior to wave formation. Therefore it would be expected that waves would appear if the velocity were boosted. The crescent-shaped rivulets did not appear during this run.

These visual observations point to several regimes in the film. In the first regime, a process similar to droplet condensation takes place in which individual crescent-shaped rivulets move down the surface of the plate. This would be expected to occur where the heat transfer coefficient was low enough that a continuous condensate film could not be supported. This process also requires substantial gas velocities.

The second regime takes place when lower gas velocities are present. Here a smooth continuous film is present and flows very slowly. No rivulets are seen. Due to the low shear stress, heat transfer coefficients need not be very large in order to supply adequate condensate to maintain the film.

In the third regime, the heat transfer coefficient is more substantial than that of the first regime, but due to the shear stress the film does not assume a smooth form but flows in crescent-shaped rivulets through the film. The film may be either partly or entirely continuous.

Finally, in the fourth regime both heat transfer

coefficient and gas velocity are large enough that a continous wavy film is formed. The size and appearance of the waves would, of course, depend on the gas velocity and film thickness.

6.3.4 Conclusion.

The heated tests without film injection were quite successful in their measurement of the heat transfer coefficient. The results of the heat flux meters appeared quite consistent with those of the overall coolant measurements. Comparison to predictions of the CWNG code indicated that some modifications to the code's models would be necessary to achieve good agreement. The general shape and trends of the CWNG results were quite good, but the magnitude of the results and the change with velocity and mass ratio could be improved. The visual observations illustrated the various regimes which can be identified for the film.

TABLE 6.1

FILM THICKNESS AND WAVE AMPLITUDE

Heated Tests with Injected Film

Nominal	Q_{film}(lpm)	δ (mm)	A (mm)
50 C	1	1.65	
5.5 m/s	2	3.43	
60 C	1	1.40	
5.5 m/s	2	2.92	
70 C	1	1.40	
5.5 m/s	2	2.79	
50 C	1	1.14	
6.5 m/s	2	2.15	0.76
60 C	1	1.14	
6.5 m/s	2	2.41	

TABLE 6.2

SPECTRUM AVERAGE FREQUENCY, CELERITY,
AND WAVELENGTH
Heated Tests with Injected Film

Nominal	Q_{film}(lpm)	f^{*}_{avg}(hz)	v_{film}(cm/s)	c (cm/s)	λ (mm)
50 C	1	23.3	9.9	20.2	0.86
5.5 m/s	2	16.8	9.5	20.3	1.21
60 C	1	16.8	11.7	12.9	0.76
5.5 m/s	2	17.2	11.2	23.0	1.34
70 C	1	21.8	11.7	19.4	0.90
5.5 m/s	2	16.1	11.7	20.4	1.27
50 C	1	16.7	14.3	14.7	0.89
6.5 m/s	2	14.2	15.2	16.4	1.16
60 C	1	20.7	14.3	14.1	0.68
6.5 m/s	2	21.6	13.6	17.7	0.81

* Doppler-corrected.

TABLE 6.3

OVERALL HEAT TRANSFER COEFFICIENTS

Heated Tests with Injected Film

		(W/m^2-C)	
		raw	corrected
Nominal	Q_{film}(lpm)	$h_{overall}$	$h_{overall}$
50 C	1	326	388
5.5 m/s	2	305	408
60 C	1	546	323
5.5 m/s	2	145	366
70 C	1	531	246
5.5 m/s	2	843	266
50 C	1	378	492
6.5 m/s	2	533	437
60 C	1	655	450
6.5 m/s	2	977	578

TABLE 6.4

TEST MATRIX

Heated Tests without Injected Film

	v_g (m/s)				
T_{mix}	2	3	5.5	6.5	8
50 C	(1)		therm-45	therm-46	therm-47
60 C		therm-48	therm-49	therm-50	
70 C	therm-51	therm-52	therm-53		
80 C	therm-54	therm-55		(2)	
90 C	therm-56				

Note: Test matrix limited by:

(1) pressure gauge and boiler pressure control

(2) boiler capacity

See Chapter 4 for details.

TABLE 6.5

OVERALL HEAT TRANSFER COEFFICIENT

Heated Tests without Injected Film

				HF Meters	CWNG	
Run	T_{mix} (C)	v_g (m/s)	$h_{overall}$	h_{mean} (W/m2-C)	h_{avg}	σ_h
therm-45	52.6	5.0	205	160	173	32
therm-46	51.3	6.3	233	165	197	32
therm-47	51.3	6.9	288	227	212	34
therm-48	62.0	2.9	147	110	149	23
therm-49	60.4	5.5	299	241	234	30
therm-50	60.4	6.3	325	270	260	31
therm-51	70.1	2.2	130	89	156	19
therm-52	72.2	2.8	218	170	209	22
therm-53	70.9	4.9	334	278	308	33
therm-54	78.4	2.1	248	206	216	25
therm-55	81.2	2.9	260	213	315	27
therm-56	88.2	1.9	318	255	330	37

table continued on next page

Table 6.5 continued

therm-57	70.4	3.1	201	159	209	22
therm-58	72.4	2.9	203	157	215	22
therm-59	71.7	3.0	206	160	215	22
therm-60	72.4	2.9	208	159	216	22

Note: σ_h represents the experimental error in $h_{overall}$.

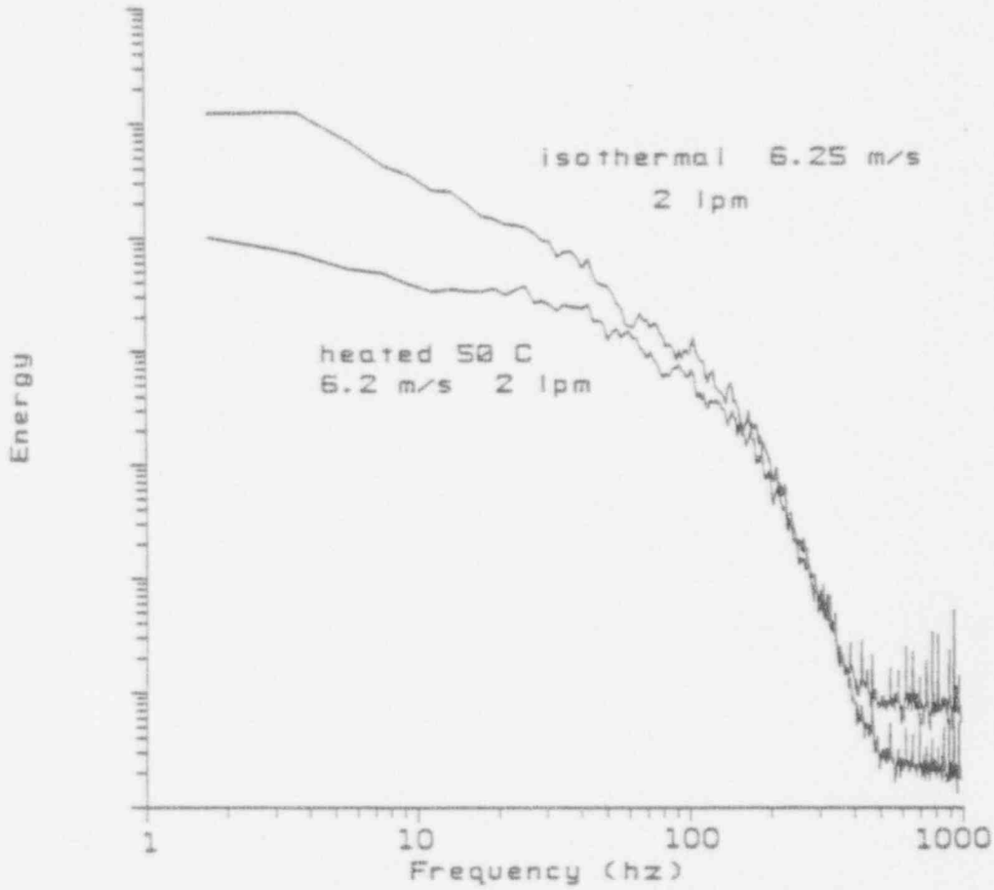

Figure 6.1 Comparison of Isothermal and Heated Frequency Spectra

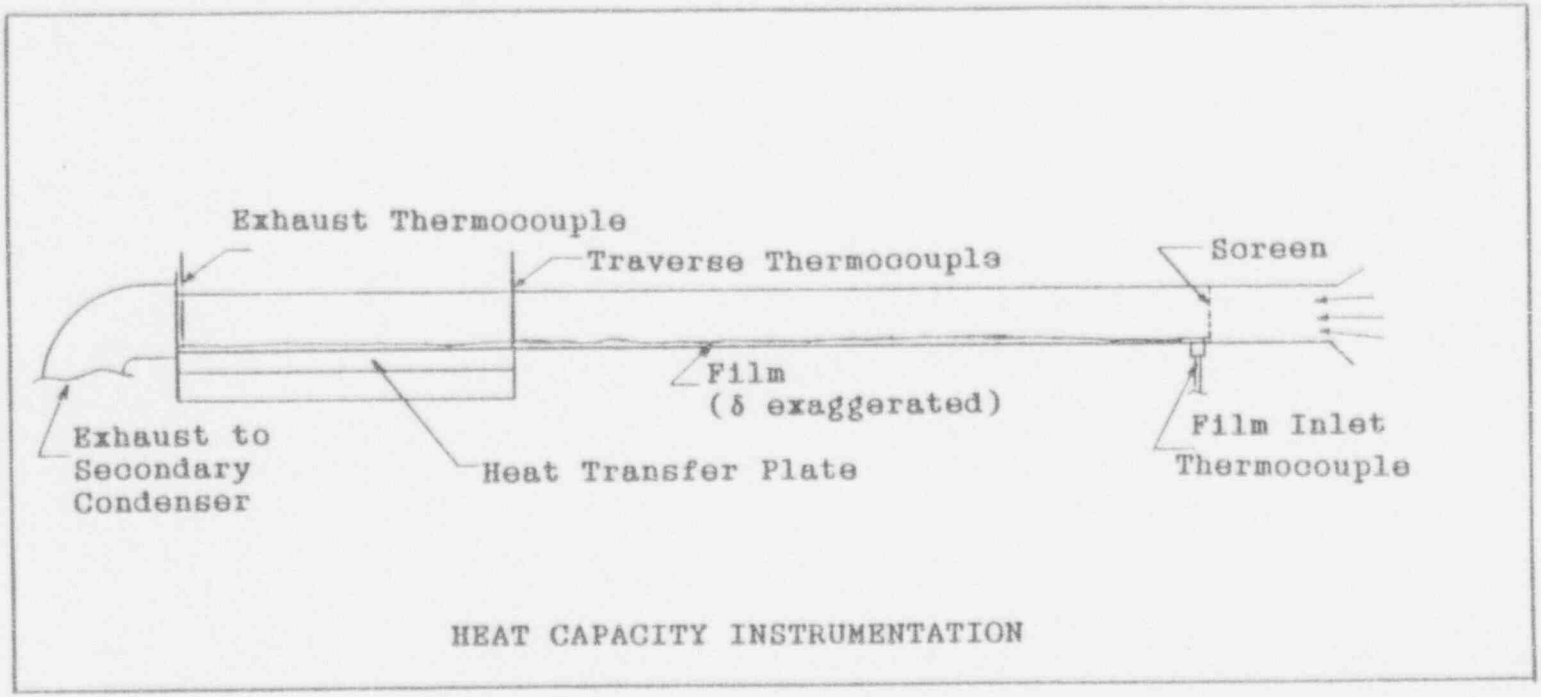

Figure 6.2 Heat Capacity Correction-Position of Thermocouples

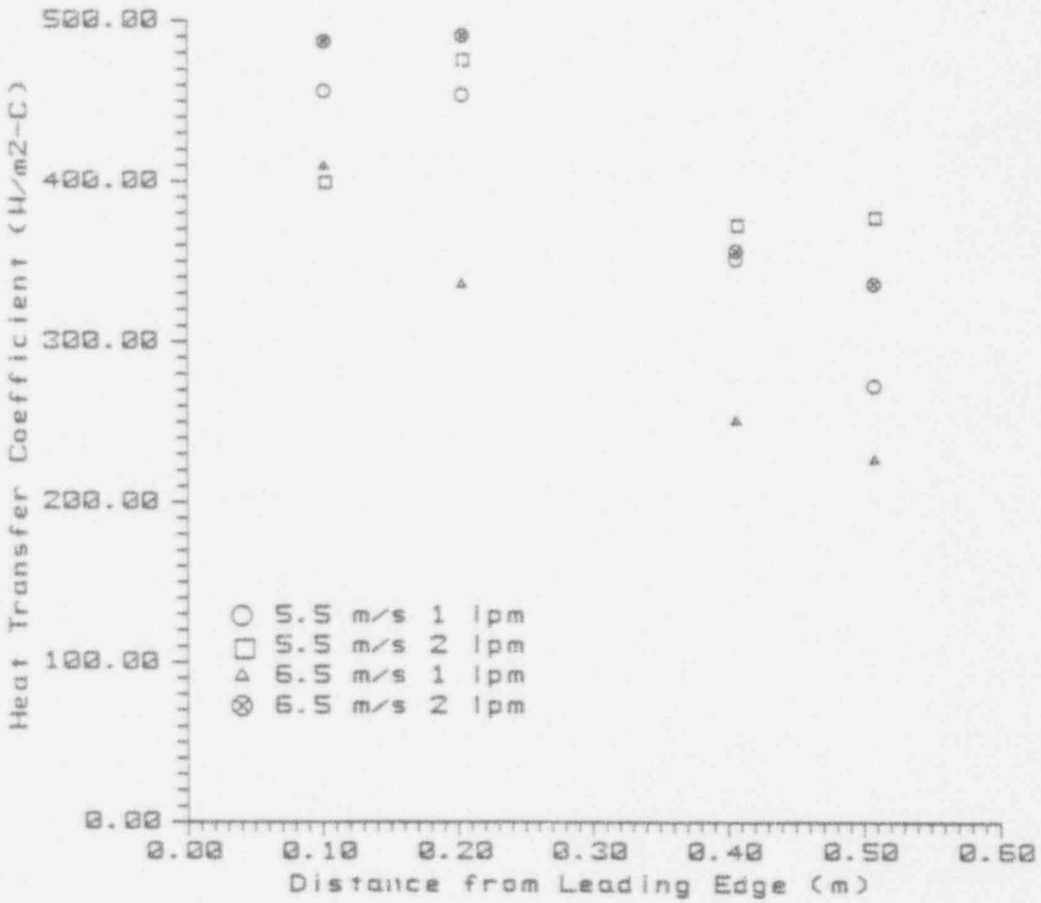

Figure 6.3 Heat Transfer Coefficient vs. Length:

50 C with Film

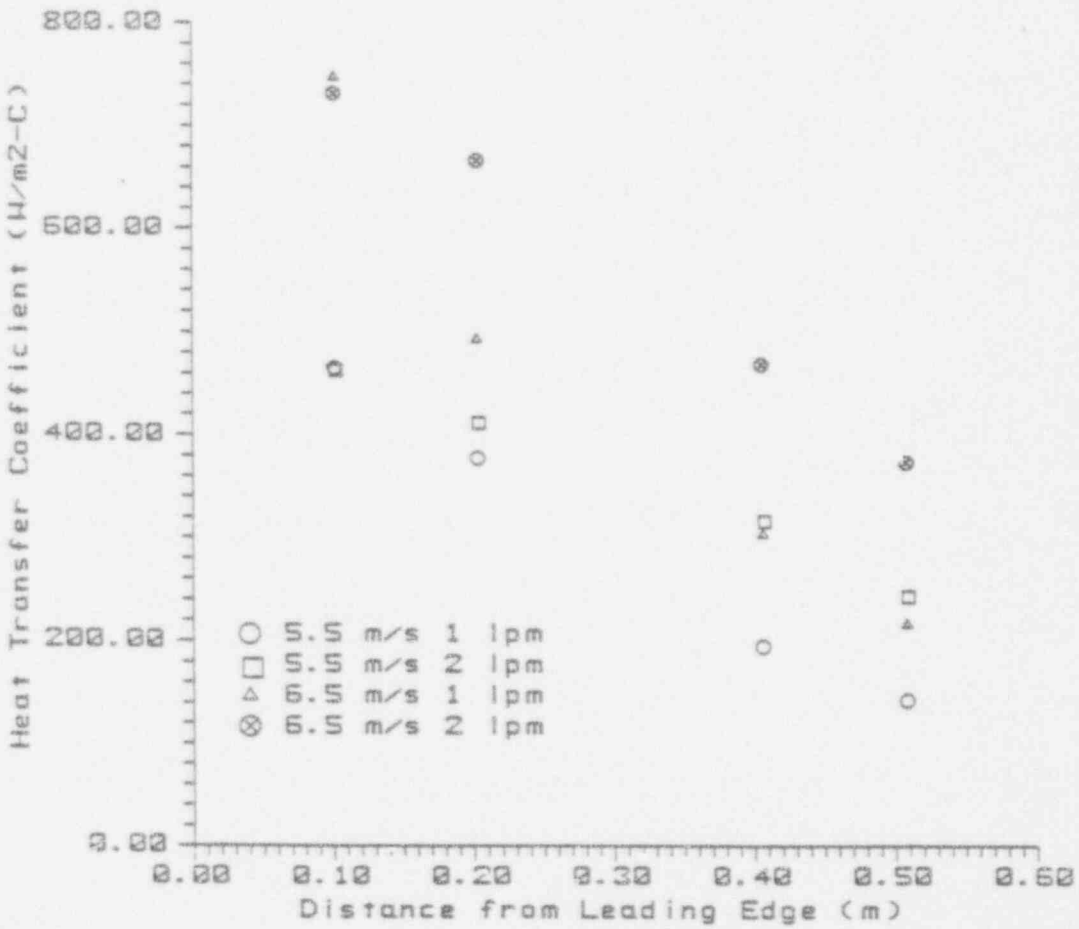

Figure 6.4 Heat Transfer Coefficient vs. Length:

60 C with Film

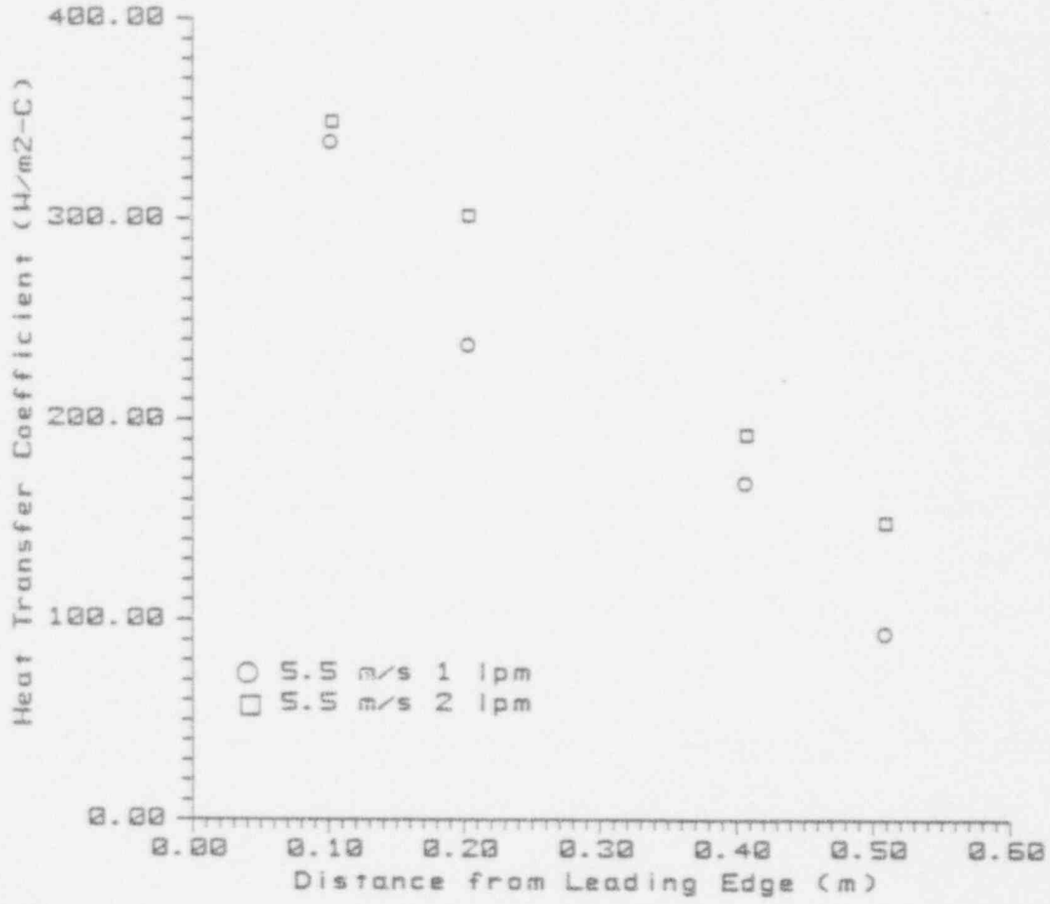

Figure 6.5 Heat Transfer Coefficient vs. Length:

70 C with Film

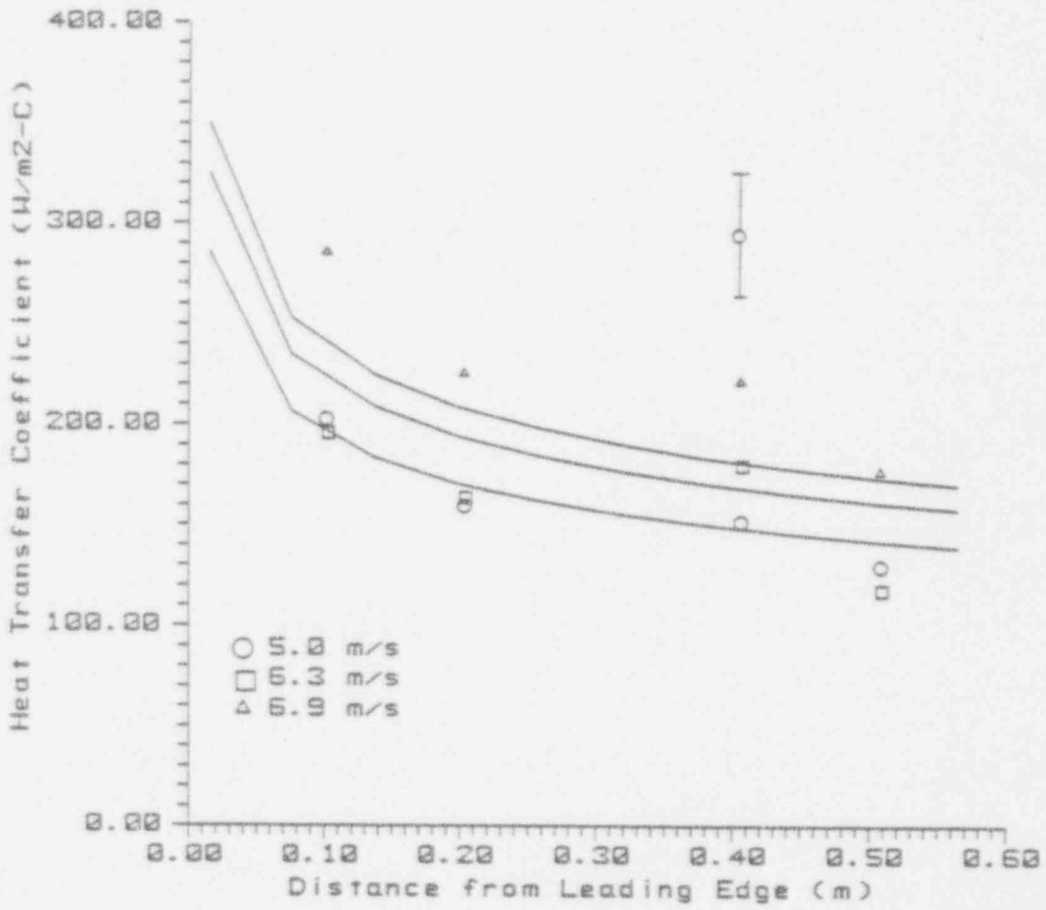

Figure 6.6 Heat Transfer Coefficient vs. Length:

50 C without Film

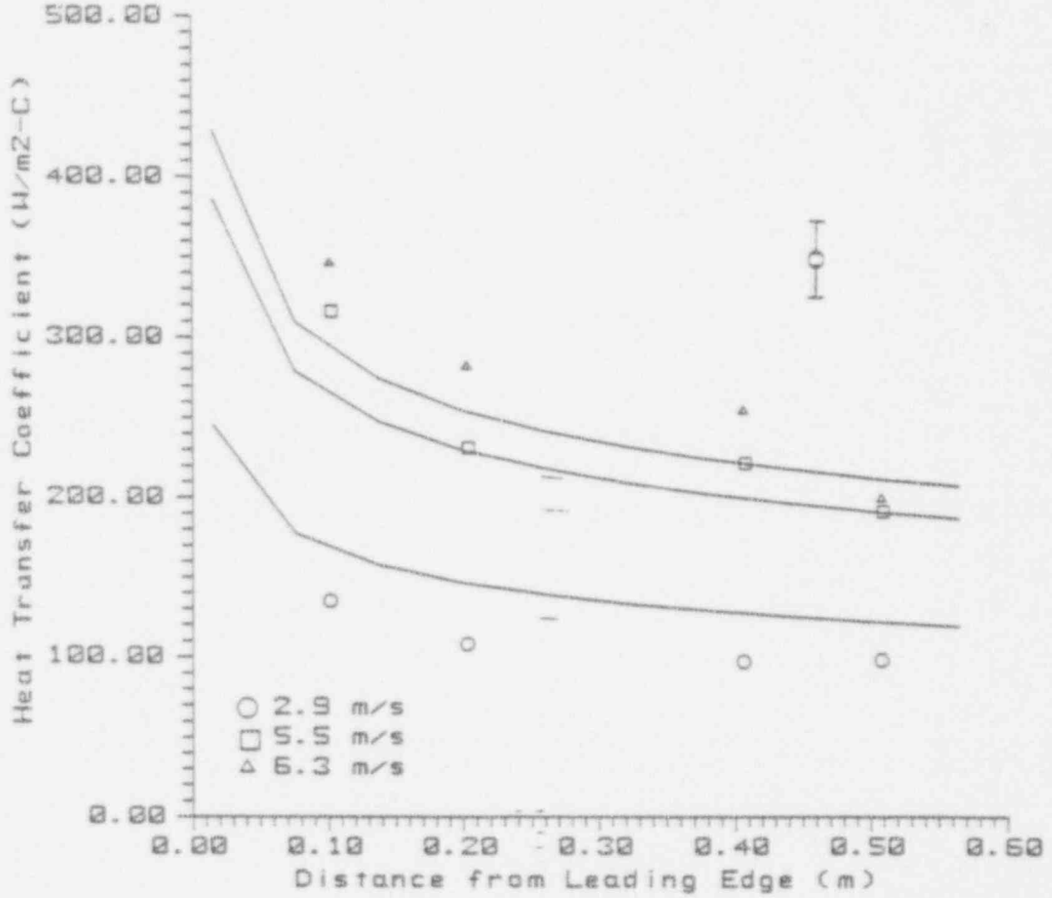

Figure 6.7 Heat Transfer Coefficient vs. Length:

60 C without Film

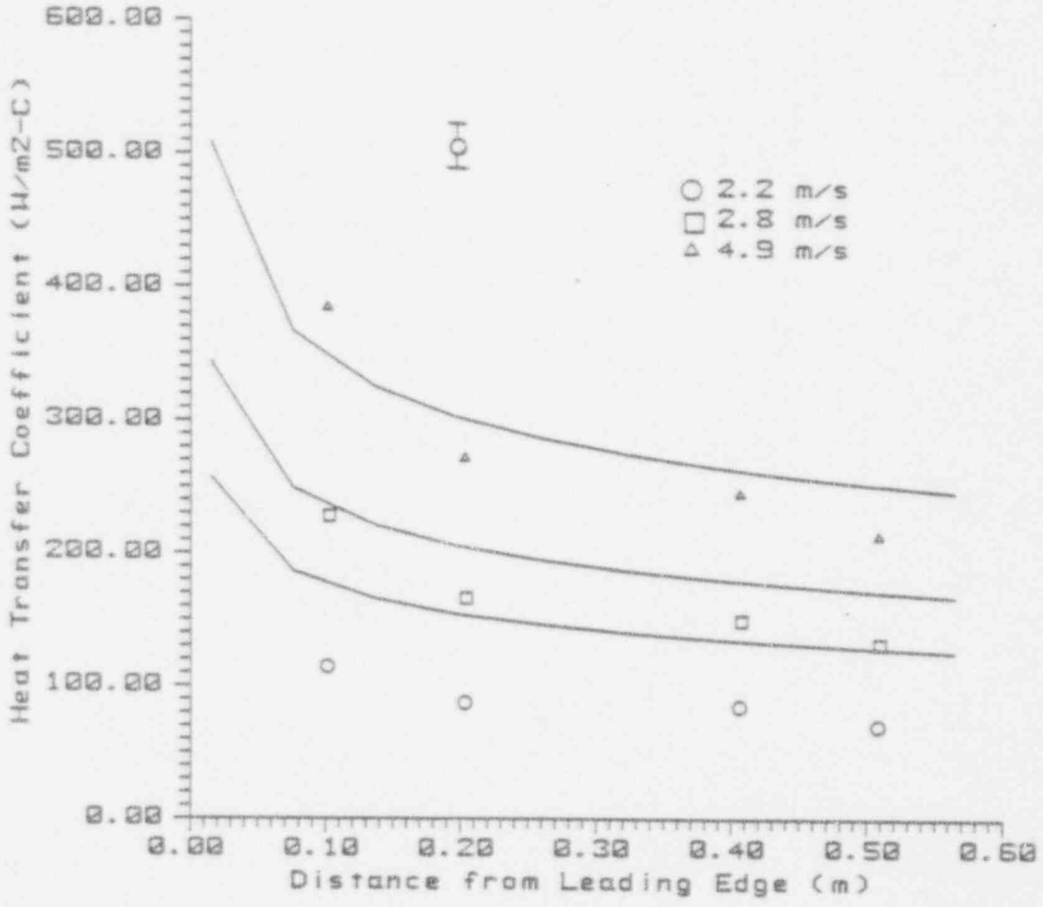

Figure 6.8 Heat Transfer Coefficient vs. Length:

70 C without Film

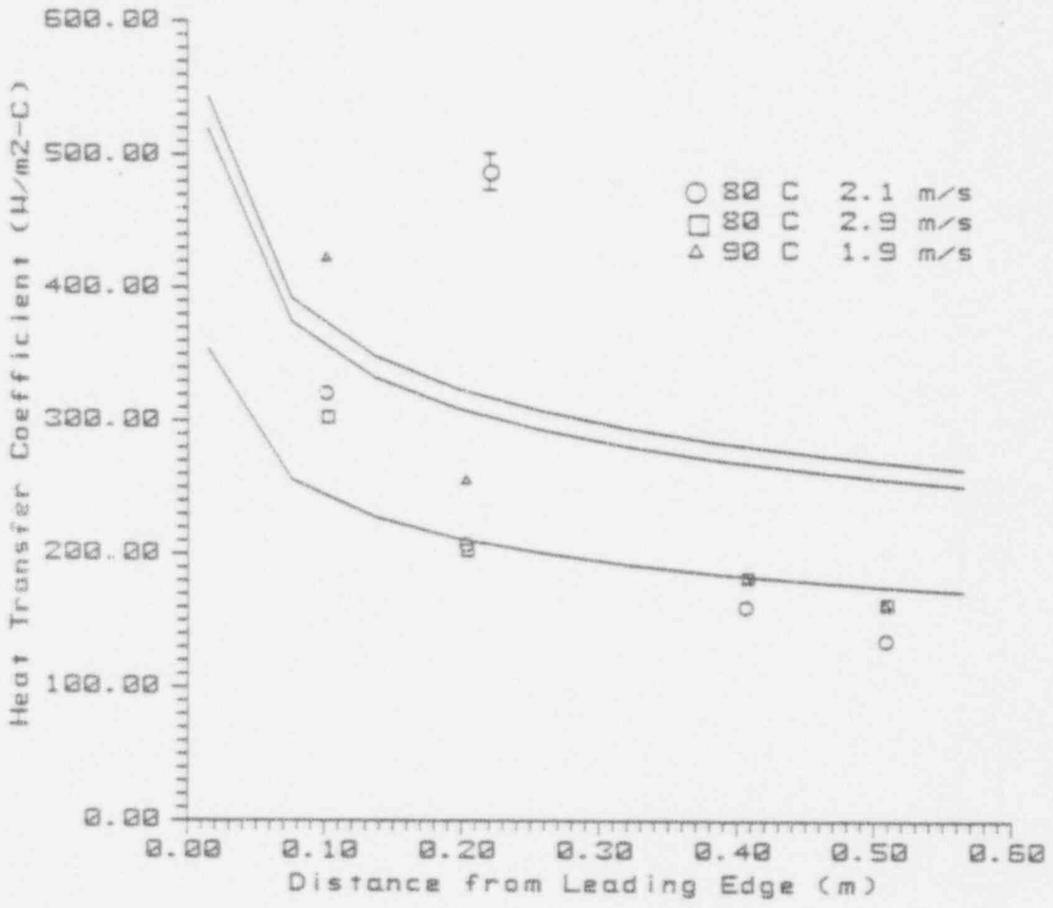

Figure 6.9 Heat Transfer Coefficient vs. Length:

80 & 90 C without Film

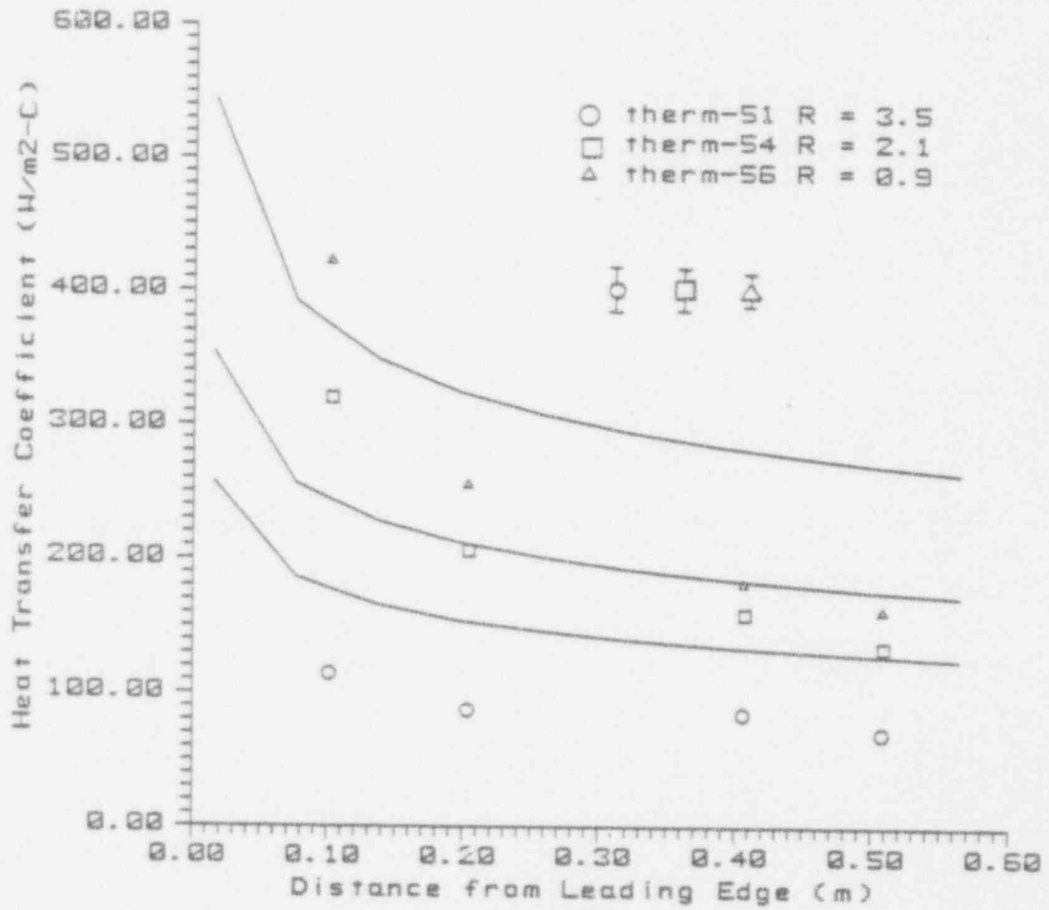

Figure 6.10 Heat Transfer Coefficient vs. Length:
Gas Mixture Velocity = 2 m/s
(without film)

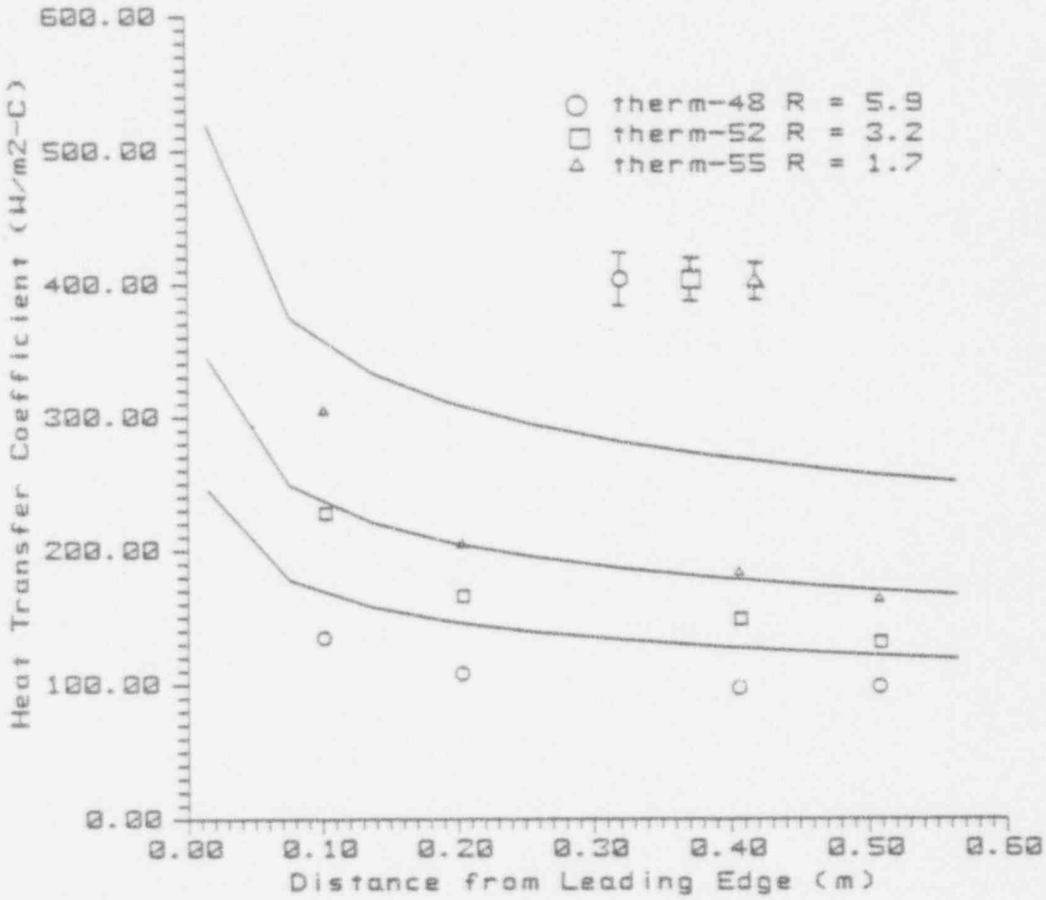

Figure 6.11 Heat Transfer Coefficient vs. Length:
Gas Mixture Velocity = 3 m/s
(without film)

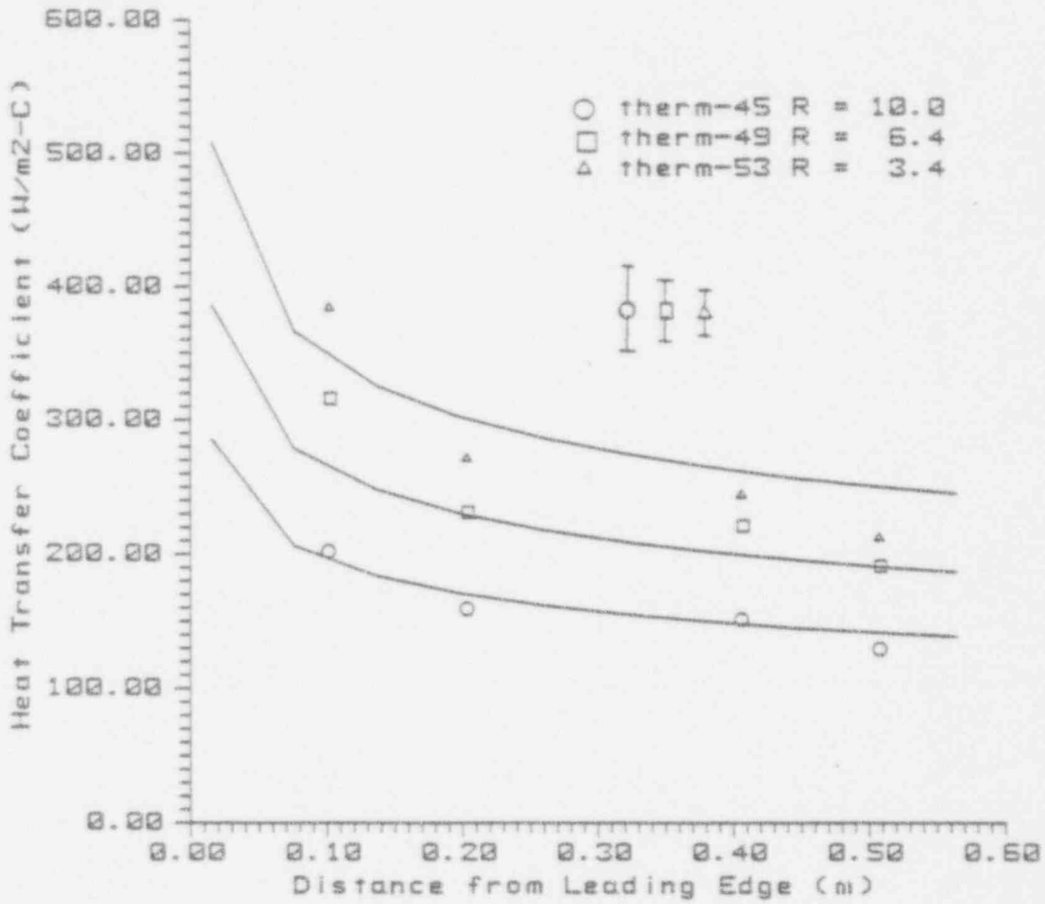

Figure 6.12 Heat Transfer Coefficient vs. Length:
Gas Mixture Velocity - 5 m/s
(without film)

7. CONCLUSION AND RECOMMENDATIONS

An experimental program was undertaken to study the effect of interfacial structure on film condensation heat transfer in the presence of a noncondensable gas. In order to accomplish this a fairly large and sophisticated experimental facility was built. Numerous features were designed into the apparatus to allow study under a variety of conditions. The facilities were then tested to assure that the proper set of experimental conditions could be achieved and a full set of operating procedures were drafted.

A set of isothermal experiments were conducted in which air was blown over a flowing film of water. Experimental techniques were developed in order to quantify the wave behavior of the interface. The film thickness and wave amplitude were measured. A frequency parameter was identified from wave spectra. A celerity parameter was defined as well. These were used to calculate a wavelength which was found to correspond well to visual observations.

The next set of experiments was conducted in air/steam flows with an injected film. The wave parameters were measured using the techniques developed in the isothermal

test series. The results of these measurements indicated that condensation might be acting to suppress the formation of waves. In addition, heat transfer measurements were made. Corrections for the heat capacity of the film were necessary, however. Due to problems in measuring the film temperatures, these corrections were not reliable enough. Hence the heat transfer coefficients obtained in these tests were suspect.

The final set of experiments were conducted in air/steam without film injection. In this case the heat transfer measurements were not subject to the heat transfer correction. The heat transfer coefficients obtained from these runs were compared with the predictions of the CWNG computer code [3]. The results agreed well in general shape and trends. Some areas for improvement of the CWNG model were suggested however. Visual observation of the condensate film suggested several flow regime classifications.

The conclusions and accomplishments of the experimental program can be listed as follows:

1) A complete experimental facility has been constructed and tested. This includes the test section and support equipment as well as the instrumention, data acquisition system, and software.

2) A new set of wave parameters were defined. The film thickness and wave amplitude were defined based on the probability of contact curve. The wave frequency was indentified as the spectrum average frequency. The celerity was defined as the wave speed relative to the film. The wavelength calculated from these definitions was comparable to that observed visually.

3) The methods of Akai et al. for use of thermal anemometry in determining wave characteristics were extended from the two-dimensional wave regime to the three-dimensional regime with good results. The resulting techniques were more robust and required less interpretation on the part of the user.

4) Hot-wire probes were designed and built for celerity and other measurements. These probes yielded good results in both isothermal and heated tests.

5) The measurement of interfacial waves was carried out in condensing flows. The methods were found to work well in a steam environment. The condensation process seemed to have a damping effect on the wave formation.

6) Measurement of heat transfer in the heated tests

with film injection encountered difficulty in getting good results, but the problems with the heat capacity correction were identified and solutions were suggested.

7) Very good results were obtained in the heat transfer measurements without injected film. The CWNG code was found to predict the general trends well. Suggestions were also made for improvement in the model.

8) Visual observation suggested some initial flow film regimes and identified at which point a film became present in the experiments.

As with most research efforts, the current one has led to a plethora of new questions and ideas. The following recommendations are made for improvement in the facilities and experimental methods for the benefit of future research:

1) The boiler pressure controller should be upgraded to reduce the differential pressure band. This would serve to reduce the oscillations in test section temperature. This would also enable extension of the operating envelope of the test rig to lower mixture temperature and mixture velocity combinations.

2) The film temperatures at both upstream and downstream ends of the heat transfer plate should be measured more accurately. An adiabatic mixing cup should probably work at the exhaust end. The temperature at the leading edge will be more challenging to measure.
3) Each individual cooling circuit in the plate should be instrumented. This would require inlet and outlet coolant thermocouples for each. This would be relatively simple. Measurement of the flow in each circuit would also be desirable, but more difficult to accomplish. This would allow a redundant measurement of the heat transfer coefficient along the plate.
4) Alternate measurement technologies such as laser doppler velocimetry should be investigated. These might obviate some of the problems which occurred in this research or provide new capabilities. An LDV, for instance, might be able to map the gas mixture flow field which would be very difficult with thermal anemometry.
5) Improvement in the design of hot-wire probes should be continued. The C-series probes should be further optimized for use in thinner films, for example.
6) Separate measurement of the wave frequency spectrum should be considered. The resolution restriction

for the celerity measurements forces the sampling rate to be higher than is optimal for the frequency measurements. Although preferred, measurement simultaneous with celerity should not be continued unless an improved C-series probe is developed which relaxes the resolution restriction.

6) Installation of a heated window in the test section should be investigated. This would allow direct observation of the flow at all times.

7) The condensation models of CWNG should be reviewed for improvement in light of the experimental results.

8) The experimental matrix should be extended to include other variables, particularly angle of inclination. In addition, more runs should be made within the current test matrices.

9) The heat transfer plate could be remachined with slightly deeper slots. This would allow thermocouple strips with wider spacing to be installed and would increase the accuracy of low heat flux measurements.

10) The thermal conductivity of the heat transfer plate aluminum alloy should be measured to determine a more accurate value.

APPENDIX A. ERROR ANALYSIS

A.1 WAVE DATA

Sources of Error:

Traverse error		0.01 in.
Sensor separation (Δx)		1/64 in.
Resolution in delay time (Δt)		varies
Deviation in delay time (Δt)		varies
Spectrum average frequency		unknown
		estimate 10%
Film flow rate	isothermal	0.45 lpm
	heated	7.5%

Results and Propagation of Error:

Amplitude 0.01 in. = 0.25 mm

Film Thickness $\delta = \text{offset} - y$

$$\sigma_\delta^2 = \sigma_{offset}^2 + \sigma_y^2$$

$$\sigma_\delta = 0.28 \text{ mm}$$

Apparent Wave Speed $\Delta x/\Delta t$

Δx component = (1/64)/(30/64)

= 3.33 %

Δt component = computed for each run

Celerity $c = \Delta x/\Delta t - v_{film}$

$$\sigma_c^2 = [(\sigma_{\Delta x}/\Delta x)^2 + (\sigma_{\Delta t}/\Delta t)^2](\Delta x/\Delta t)^2 + [(\sigma_{Qfilm}/Q_{film})^2 + (\sigma_\delta/\delta)^2](v_{film})^2$$

Frequency $f_{true} = f_{obs}(c/v_{app})$

$$(\sigma_{ftrue}/f_{true})^2 = (\sigma_{fobs}/f_{obs})^2 + (\sigma_c/c)^2 + (\sigma_{\delta t}/\delta t)^2 + (\sigma_{\delta x}/\delta x)^2$$

Wavelength $\lambda = v_{app}/f_{obs}$

$$(\sigma_\lambda/\lambda)^2 = (\sigma_{vapp}/v_{app})^2 + (\sigma_{fobs}/f_{obs})^2$$

example: Therm-33 60 C

6.5 m/s

2 lpm

σ_δ/δ = 11.6%

$\sigma_{\Delta x}/\Delta x$ = 3.33%

$\sigma_{\Delta t}/\Delta t$ = 10.5%

σ_{Qfilm}/Q_{film} = 7.5%

σ_c/c = 22%

σ_{ftrue}/f_{true} = 27%

σ_λ/λ = 15%

A.2 HEAT FLUX METER DATA

Sources of Error:

Thermocouple temperature	0.08 C
Position of thermocouples in strip	1/64 in.

Results and Propagation of Error:

Error propagation in least square fits ref [131].

$Y = MX + B$ n = number of pairs

$$\sigma_M^2 = \Sigma w_{ii}/d$$

$$\sigma_B^2 = \Sigma w_{ii} X_i^2/d$$

where $w_{ii} = 1/\sigma_{Yi}^2$

$$d = (\Sigma w_{ii} X_i^2)(\Sigma w_{ii}) - (\Sigma w_{ii} X_i)^2$$

Here, σ_{Yi} = const = 0.08 C

therefore w_{ii} = const

The above formulas reduce to:

$$\sigma_M^2 = n\sigma_Y^2/[n(\Sigma X_i^2) - (\Sigma X_i)^2]$$

$$\sigma_B^2 = \sigma_Y^2 \Sigma X_i^2/[n(\Sigma X_i^2) - (\Sigma X_i)^2]$$

Results:	Strip	σ_M (C/mm)	σ_B (C)
	#1	5.02E-03	0.073
	#2	4.96E-03	0.074
	#3	9.20E-03	0.158
	#4	5.10E-03	0.077
	#5	5.10E-03	0.078

Note: These results only depend on the errors in temperature measurement. Due to the calculation procedure they apply to all of the runs.

The procedure can be used to compute the effect of errors in the X (t/c position) measurement. The temperature and position are switched in the above equations. The computation is much more cumbersome however, because it then becomes specific to each run. The following results are given as an example:

therm-50	Strip	(slope) (C/mm)	(intercept) (C)
	#1	2.02E-03	0.76
	#3	2.91E-03	1.14
	#5	8.84E-04	0.55

Due to the difficulty of computing these latter error

estimates for each run, those errors were not included in the final analysis. The errors in the intercept (which affected T_{surf} most) were not found to be large enough to warrant carrying through the calculation either. Hence the error in the heat transfer coefficient determined by the heat flux meters was taken as the error in M as listed in the table above.

example: Therm-50

Strip	dT/dx	σ_M	%Error
#1	0.077	5.02E-03	6.5%
#2	0.067	4.96E-03	7.4%
#3	0.069	9.20E-03	13.3%
#4	0.061	5.10E-03	8.4%
#5	0.047	5.10E-03	10.9%

A.3 OVERALL HEAT FLUX DATA

Sources of Error:

Thermocouple temperature	0.08 C
Cooling water flow rate	0.4 lpm

Results and Propagation of Error:

$$h = m C_p \Delta T / A$$
$$\approx Q_{cool}(T_{out} - T_{in})$$

$$(\sigma_h/h)^2 = (\sigma_{Qcool}/Q_{cool})^2 + [(\sigma^2_{Tout} + \sigma^2_{Tin})/\Delta T^2]$$
$$= (\sigma_{Qcool}/Q_{cool})^2 + 2(\sigma_T/\Delta T)^2$$

example: Therm-50 60 C
6.5 m/s

$Q_{cool} = 6.8$ lpm
$\Delta T = 15.30 - 13.79 = 1.51$ C

$\sigma_{Qcool}/Q_{cool} = 5.9\%$
$\sigma_T/\Delta T = 5.3\%$
$\sigma_h/h = 9.5\%$

R E F E R E N C E S

1. Akai, M., A. Inoue, and S. Aoki, "Structure of a Co-Current Stratified Two-Phase Flow with Wavy Interface," Theo. Appl. Mech., Vol. 25, pp. 445-456, (1977).

2. Akai, M., A. Inoue, S. Aoki, and K. Endo, "A Co-Current Stratified Air-Mercury Flow with Wavy Interface," Int. J. Multiphase Flow, Vol. 6, pp. 173-190, (1980).

3. Kim, M. H., "Modelling of Condensation Heat Transfer in a Reactor Containment," PhD Thesis, University of Wisconsin-Madison, (1986).

4. McAdams, W. H., Heat Transmission, 3rd ed., McGraw-Hill, (1954).

5. Mills, A. F. and R. A. Seban, "The Condensation Coefficient of Water," Int. J. Heat Mass Transfer, Vol. 10, pp. 1815-1827, (1967).

6. Slegers, L. and R. A. Seban, "Laminar Film Condensation of Steam Containing Small Concentrations of Air," Int. J. Heat Mass Transfer, Vol. 13, pp. 1941-1947, (1970).

7. Al-Diwany, H. K. and J. W. Rose, "Free Convection Film Condensation of Steam in the Presence of Non-Condensing Gases," Int. J. Heat Mass Transfer, Vol. 16, pp. 1359-1369, (1973).

8. Othmer, D. F., "The Condensation of Steam," Ind. and Eng. Chem., Vol. 21, No. 6, (1929).

9. Rauscher, J. W., A. F. Mills, and V. E. Denny, "Experimental Study of Film Condensation from Steam-Air Mixtures Flowing Downward over a Horizontal Tube," J. of Heat Transfer, Vol. 96, pp. 83-88, (1974).

10. Kutateladze, S. S. and I. I. Gogonin, "Heat Transfer in Film Condensation of Slowly Moving Vapour," Int. J. Heat Mass Transfer, Vol. 22, pp. 1593-1599, (1979).

11. Lee, W. C. and J. W. Rose, "Forced Convection Film

Condensation on a Horizontal Tube with and without Non-Condensing Gases," Int. J. Heat Mass Transfer, Vol. 27, pp. 519-528, (1984).

12. Rosson, H. F. and J. A. Myers, "Point Values of Condensing Film Coefficients inside a Horizontal Pipe," Chem. Engr. Progress Symp. Series, No. 59, Vol. 61, (1965).

13. Goodykoontz, J. H. and R. G. Dorsch, "Local Heat Transfer Coefficients for Condensation of Steam in Vertical Down Flow within a 5/8 inch Diameter Tube," NASA TN D-3326, (1966).

14. Goodykoontz, J. H. and R. G. Dorsch, "Local Heat Transfer Coefficients and Static Pressures for Condensation of High-Velocity Steam within a Tube," NASA TN D-3953, (1967).

15. Mayhew, Y. R., D. J. Griffiths, and J. W. Phillips, "Effect of Vapour Drag on Laminar Film Condensation on a Vertical Surface," Proc. Instn. Mech. Engrs., Vol. 180, (1965-66).

16. Mayhew, Y. R., "Comments on the Paper 'Theoretical Study of Laminar Film Condensation of Flowing Vapor' (by I. G. Shekriladze and V. I. Gomelauri)," Int. J. Heat Mass Transfer, Vol. 10, pp. 107-108, ((1967).

17. Mayhew, Y. R. and J. K. Aggarwal, "Laminar Film Condensation with Vapour Drag on a Flat Surface," Int. J. Heat Mass Transfer, Vol. 16, pp. 1944-1949, (1973).

18. Asano, K., Y. Nakano, and M. Inaba, "Forced Convection Film Condensation of Vapors in the Presence of Noncondensable Gas on a Small Vertical Flat Plate," J. of Chem. Engr. of Japan, Vol. 12, No. 3, (1979)

19. Choi, H. Y., "Electrohydrodynamic Condensation Heat Transfer," J. of Heat Transfer, pp. 98-102, (1968).

20. Linehan, J. H., M. Petrick, and M. M. El-Wakil, "On the Interface Shear Stress in Annular Flow Condensation," J. of Heat Transfer, Vol. 91, pp. 450-452, (1969).

21. Lim, I. S., R. S. Tankin, and M. C. Yuen, "Condensa-